RUBBER MODIFIED ASPHALT PAVEMENT LAYER FOR NOISE AND VIBRATION ABSORPTION

Dissertation

submitted to and approved by the

Faculty of Architecture, Civil Engineering and Environmental Sciences

University of Braunschweig

and the

Department of Civil and Environmental Engineering

University of Florence

in candidacy for the degree of a

Doktor-Ingenieur (Dr.-Ing.) /

Dottore di Ricerca in Civil and Environmental Engineering[*)]

by

Jiandong Huang

born (28/12/1990)

from (Linyi), (China)

Submitted on	20 August 2019
Oral examination on	06 November 2019
Professorial advisors	Prof. Massimo Losa
	Prof. Michael P. Wistuba

2019

Acknowledgments

I would like to express my greatest gratitude to the people and institutions without who and which this thesis would have been impossible.

To my supervisors, Prof. Massimo Losa (University of Pisa) and Prof. Michael P. Wistuba (TU Braunschweig) for your continuous support, guidance, advice, and encouragement.

To my advisors, Prof. Pietro Leandri for your expertise without which this thesis would not exist.

To my family and friends, for everything.

To My Beloved Mother Country,

China

Abstract

Nowadays, a complex transportation network has been a symbol of urbanization development. Convenient transportation enriches people's life. However, on one hand, traffic noise and vibrations from the transportation network are around everyone in the city, which affect the living condition of urban residents and could result in sleeping disorder. The induced vibration may cause some fatigue damage of surrounding (historic) buildings as well; on the other hand, the indirect impact of the more convenient transportation network is the recycling problem of end-of-life tires from increasing numbers of vehicles. In order to solve the above problems, this study is trying to refine and optimize a new noise and vibration absorbing system for road pavements while complying with the requirement of sustainability by the use of crumb rubber from end-of-life tires. This noise and vibration absorbing system is composed of a gap graded asphalt surface layer, containing a certain amount of crumb rubber, and a lower vibration-absorbing layer with higher damping property. The main objectivities of this study are to study the noise reduction mechanism of the surface layer, to design and evaluate the asphalt mixtures for the damping layer based on the mechanical and damping properties, and to optimize the pavement structure based on the functional and mechanical characteristics.

As far as the surface layer, two experimental gap graded asphalt mixtures with a high content of crumb rubber by the different adding process (wet process and dry process) are designed and analyzed based on the test data of the previous "Leopoldo" project, with a comparison of two conventional asphalt mixtures commonly used as low noise pavements (LNPs) in Europe. By comparing the texture depth, sound absorption coefficient, stiffness modulus and other factors that affect the noise level, the mechanism of gap-graded asphalt mixture with crumb rubber to reduce tire/pavement noise is inferred, as the main research output of the surface layer.

As far as the damping layer, the damping effect is evaluated firstly in order to verify whether it makes sense to lay a damping (vibration-absorbing) layer in the pavement structure. The methods commonly used in the field of road engineering to characterize damping property are reviewed, and the shortcomings of these methods when applied in this study are summarized. In order to overcome these weaknesses, a more accurate and reasonable method to characterize the damping effect in the field of road engineering is proposed and it is proved to be applicable not only to roads composed of materials with close damping properties but also to the ones composed of materials with large different damping (E.g., a road structure with a

special damping layer). Rubberized and non-rubberized road pavements are used to verify the accuracy of the method by comparing the simulation results obtained by the proposed method to the field measurement results. After the proposed method is verified, this study evaluates the effects of laying a damping layer on vibration reduction of the road pavements and surrounding environments. Additionally, a parametric study of the damping layer is performed, including different damping layer locations, thicknesses, and damping ratios. Based on this parametric study, an optimized pavement structure is proposed.

Considering the paving materials specifically for the damping layer, this study designs the asphalt mixtures with high binder content as well as high crumb rubber content in order to improve the damping property. The basic mechanical properties, as well as the damping properties, are evaluated in the laboratory to assess if the designed asphalt mixtures can meet the requirements. In addition, considering that the asphalt mixture's damping capacity and anti-rutting ability are typically opposite, this study designs a special Hamburg wheel tracking (HWT) test, where the damping layer acts as the interlayer in the pavement structure, in order to evaluate the rutting resistance. At the same time, an experimental road with a damping layer is carried out in the field to verify the construction feasibility of the asphalt mixture.

By comparing the factors that affect the noise level, the mechanisms of enhanced low noise ability by adding crumb rubber in asphalt mixtures by the wet process and dry process are referred to as reducing the tire/pavement vibration and reducing the aerodynamic noise, respectively. Therefore, adding crumb rubber to gap graded asphalt mixture by wet process, can not only reduce noise to achieve anti-noise pavements but also can reduce the generation of tire/pavement vibration waves and realize the design of the anti-vibration pavements. Therefore, this asphalt mixture will be used as the surface layer of the designed "vibration and noise absorbing system".

Based on the idealized shear beam model, a more reasonable and accurate method to calculate natural frequencies of different layers of pavement is proposed, by which the damping matrix of the pavement system can be layered assembly. By comparing the results of the finite element (FE) model and in-situ field tests, good agreements are achieved between simulation and field measurement results demonstrating the accuracy of the proposed model. Confirmed by the FE model based on the proposed method, when a damping layer is laid in the pavement structure, the vibration at 10 m away from the pavement can be reduced by about 20% and the one at 30 m away from the pavement can be reduced by about 15%. Through a parametric study of the damping layer, the optimal damping layer position is determined as the middle of the asphalt layer, and the optimal thickness is 3 cm. The asphalt mixtures designed to work as

a damping layer, are verified by laboratory tests and proved to have sufficient strength to meet the requirements of the specification and much higher damping capacity than conventional asphalt mixtures. It can also work together well with the upper and lower asphalt layers as well as providing enough ability to resist rutting according to the results of the special HWT tests. The mixing, laying and rolling processes of the experimental road with the damping layer show that the mineral materials are embedded and stabilized, and the asphalt is evenly distributed, demonstrating that the designed asphalt mixture has the good working ability and compaction performance similar to traditional asphalt mixture. By laying a damping layer in the road structure, the deflection can be reduced by almost 50% at the loading center position, while the deflection can be reduced by about 20% at the 1.9m position around the road, demonstrating the effectiveness of the damping layer. Finally, according to the above results, a theoretical and practical procedure for characterizing and modeling the "low-noise + low-vibration + vibration-absorbing" system for pavement structure is proposed.

CONTENTS

LIST OF FIGURES

LIST OF TABLES

Chapter 1: Introduction

1.1 Background

1.1.1 Traffic-induced noise

Today, complex transportation networks have become a symbol of urbanization. The convenient transportation has enriched people's lives. However, traffic noise from traffic networks is around everyone in the city, which affect the living conditions of urban residents and can lead to sleep disorders, and is becoming more and more serious.

Traffic noise pollution has the characteristics of continuous interference and great harm. Many people complain that traffic noise has the most direct impact on their lives (Milne 2006). With the increase of highway traffic mileage, traffic flow and vehicle traffic speed, the extent of road traffic noise interference to the normal living, working, learning and rest environment of residents along the line are also intensifying and expanding. The hazards brought by traffic noise pollution to urban residents are as follows:

(1) Traffic-induced noise can damage people's health

Traffic-induced noise can cause great damage to human hearing (Daniel 2007). In the normal activities such as production and living in areas with serious noise pollution, such as traffic trunks, the human ear is stimulated and impacted by external noise, which is vulnerable to damage and thus causes hearing loss: higher the noise intensity, greater the damage. If people live in a strong noise environment for a long time, the human ear may cause a qualitative lesion to form noise deafness (Miller 1974).

(2) Traffic-induced noise can affect people's normal life and rest

When the human brain is fully rested, it can relieve fatigue and restore physical strength. Adequate sleep is a prerequisite for the human brain to fully rest. Ample sleep can only be achieved in a quiet environment. Residents living on both sides of roads with serious traffic noise pollution, under the long-term interference of noise, their sleep quality is not guaranteed for a long time, resulting in dizziness, tinnitus and other adverse

symptoms, which in turn cause diseases such as the nervous system, greatly affecting people's work, life and physical and mental health (Frei et al. 2014).

1.1.2 Traffic-induced vibration

Traffic-induced vibration is another relevant issue in some European cities where heavy traffic is running close to buildings; the problem is particularly relevant when pavement surfaces are uneven like in the case of stone pavements or artificial bumps. Discrete, periodic and random irregularities on the road surface and defects in the vehicle itself lead to dynamic interaction forces between the vehicle and the road, which can be characterized by a source-path-receiver scenario (See Figure 1.1). These forces create stress waves in the supporting soil, which in turn causes vibrations in adjacent buildings (Al-Hunaidi 1996).
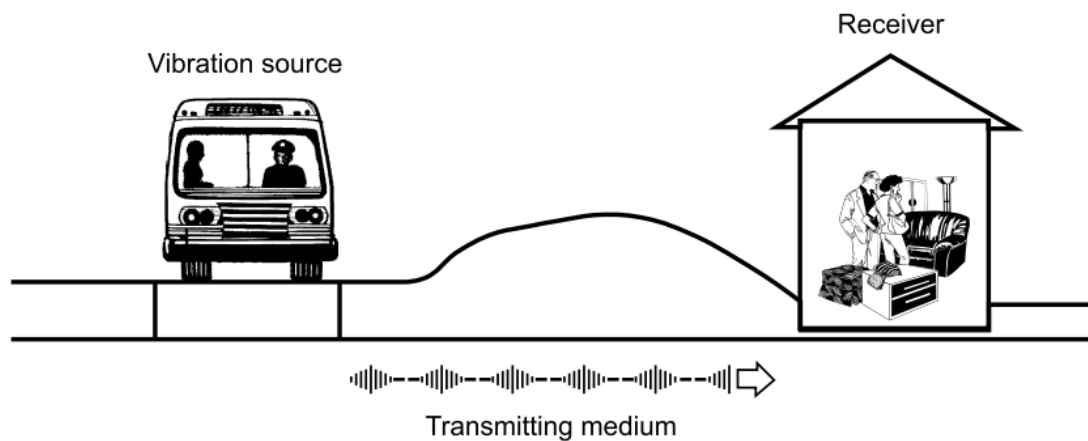
Figure 1.1 Traffic vibrations can be characterized by a source-path-receiver scenario

Table 1.1 Vibration levels induced by a bus and a truck [mm/s^2] (Hunaidi 2000)

Location	25km/h		50km/h	
	Bus	Truck	Bus	Truck
Ground in front of house	20.5	19.9	64.5	33.2
External foundation wall	11.2	10.1	30.9	15.7
Midpoint of floor in 1st storey	20.3	20.8	62.9	30.1
Midpoint of floor in 2nd storey	35.0	37.3	96.2	46.7

The dominant frequency and amplitude of vibration depend on many factors, including road conditions, vehicle weight, speed & suspension system, soil type & stratification,

seasons of the year, distance from the road and building type (Hunaidi 2000). E.g., Table 1.1 is a comparison of vibration levels [mm/s^2, root mean square (RMS)] induced by a bus and a truck, to demonstrate the effect of different suspension systems at different speeds. The impacts of vibration caused by traffic mainly reflect on the following aspects:

(1) Effect of vibrations on people's health

Vibrations induced by road traffic are not health and safety issues; they are more of an annoying problem. Due to the human body's annoying physical sensation, interference with activities such as sleep and conversation, the snoring of window panes and loose objects, and the fear of damage to buildings and their contents caused by vibration may not be accepted for occupants. Experience has shown that if the vibration level is only slightly above the perceptual threshold, people living in the home may complain, and the main concern is that the building or its contents are damaged (Hunaidi 2000). This kind of concern may be a contributory factor to stress-related diseases (Royal Commission on environmental pollution 1994).

(2) Effect of vibrations on the surrounding environment

Homeowners may complain about damage caused by traffic vibrations, such as cracks in walls and ceilings, separation of masonry blocks, and cracks in foundations. However, the level of vibration is rarely high enough to cause direct damage to these damages, although they may cause deterioration processes due to other causes. Building components often produce residual strain due to uneven soil movement, humidity and temperature cycling, poor maintenance or past renovations and repairs. Therefore, small vibration levels caused by road traffic may cause damage by "supplementing" residual strain. It is therefore difficult to establish a level of vibration that can cause damage to the building, so the controversy still revolves around this problem. In some cases, when the building is subjected to vibration for many years, if the induced stress in the building is sufficiently high, fatigue damage (i.e., caused by repeated loading) may occur. In the case of historic buildings, especially those in a weak condition (e.g., the wall cracking of Villa Farnesina in Roma caused by traffic-induced vibrations), traffic-induced vibration is of concern regarding its long-term effect (Hunaidi et al. 1997). The vibration also may disturb sensitive operations, as for example in hospital operating theatres, scientific research labs, and high-tech industries (Hao et al. 2001).

Figure 1.2 Wall cracking of Villa Farnesina caused by traffic vibration (Feiden 2007)

1.1.3 Recycled crumb rubber

Scrap tires constitute an important part of the world's solid waste management issues, and market groups predict that used tires will increase in the coming years. Globally, the number of used polymer products has increased year by year: most of them are used in automotive tires. According to the report of the largest tire and rubber producer association, the annual global tire production is about 1.4 billion, equivalent to an estimated 17 million tons of used tires each year (European Tire and Rubber Manufacturers' Association 2011; Sienkiewicz 2012). The dynamic growth of the number of used tires is well reflected in the EU, with production increasing from 2.1 million tons in 1994 to 3.3 million tons in 2010, and annual processing costs in EU countries are close to 600 million euros (European tire & Rubber Manufacturers' Association 2010a).

An important channel for recycling scrap tires is through the production of crumb rubber modifiers (CRM) and its main advantage of using in the production of asphalt mixtures is the environmental sustainability of the pavement associated with the opportunity to recycle scrap tires. In addition, the rubber asphalt composition can improve the quality of the pavement, making it thermally stable and resistant to aging. The addition of abrasive rubber to the asphalt also improves the flexibility of the asphalt binder and reduces the surface susceptibility to rutting. By modifying the mineral with rubber particles, the asphalt mixture improves its resistance to slip and wear, reduces

tire surface noise, and improves tire grip in wet and cold weather (Lee et al. 2008; Paje et al. 2010; Kök et al. 2011; Liu et al. 2012).

1.2 Research problem

1. Large numbers of low noise pavements (LNPs) have been constructed using modified mixtures for surface layers, particularly in Europe (Ohiduzzaman et al. 2016). However, very limited research work (Taniguchi et al. 1979; Hanazato et al. 1991) can consider the combined response of vibration and noise, as well as the effects of traffic-induced vibrations on people's life and surrounding environment close to the roads.

2. In terms of functional characteristics, the low noise performance of rubberized asphalt mixtures has been fully confirmed (Biligiri 2013; Vázquez et al. 2016). However, the noise reduction mechanism of rubberized asphalt mixtures (dry process and wet process) is not yet clear and lacking in effective evidence to be inferred.

3. In many studies about dynamics analysis of pavements, as a basic parameter for determining the damping capacity of different structural members, the damping ratio of the road structure has been defined without being ignored (Ling & Newcomb 1991; Zeng et al. 2005; Al-Qadi et al. 2008; Wang et al. 2009; Uddin et al. 2010; Tang et al. 2013; Xu 2014). According to the literature, different methods have been applied, but there was still no uniform and persuasive method to characterize the damping properties in road engineering. In addition, when the damping was characterized, most studies used the natural frequencies of the road structure from empirical values or reference values (Wang et al. 2009; Uddin et al. 2010) instead of the true values calculated from the field, resulting in imprecise dynamic analysis results.

4. Damping effect has been extensively used in the design process of large structural members, especially in civil engineering, such as embankments and bridges, to distinguish between two different vibration attenuation capacities. However, the damping effect was rarely applied in pavement structures (Dondi et al. 2005; Grandi

2008; Huang et al. 2018) and the literature focus on verifying such damping effect has rarely been found (Hanazato et al. 1991).

5. The rubberized asphalt mixtures were confirmed particularly effective in absorbing vibrations and were designed and adopted as roads' base layer and railways' sub-basalt layer in some studies (Zeng et al. 2001; Wang et al. 2005; Soto et al. 2017). However, according to the literature knowledge known to the author, no research has been focused on the design and test of asphalt mixtures specifically for damping layers in road engineering.

1.3 Research objective

The main aim of this study is to refine and optimize a new noise and vibration absorbing system for road pavements while complying with the requirement of sustainability by the use of crumb rubber from end-of-life tires. The noise and vibration absorbing system is composed of a gap graded asphalt surface layer, containing a certain amount of crumb rubber, and a lower vibration-absorbing layer. The schematic diagram of such noise and vibration absorbing system is shown in Figure 1.3.
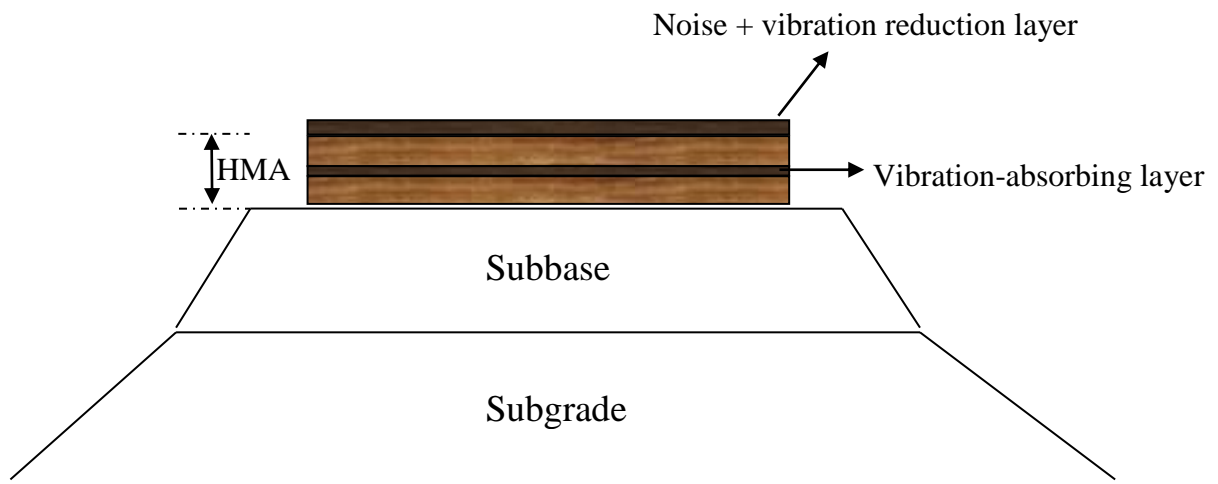
Figure 1.3 Schematic diagram of the noise and vibration absorbing system

The asphalt mixture of the surface layer will be determined with regard to laboratory mechanical performance and in-situ performance. The vibration-absorbing layer will be designed to achieve a specific target in terms of high damping and evaluated with regard to mechanical and damping properties.

The objectives of the study are shown as follows:

1) To study the noise reduction mechanism of the rubberized asphalt mixtures and to determine the most suitable asphalt mixture, which can be used as a surface layer for noise and vibration reduction;

2) To propose a uniform method that can be applied to the road structure to characterize the damping property and verify its effectiveness by comparing to field experiments;

3) To establish a finite element (FE) model to accurately simulate the effect of the damping layer on traffic-induced vibration;

4) To design and evaluate the asphalt mixtures for the damping layer based on the mechanical properties and damping properties.

1.4 Research approach and plans

According to the aims of this research project, the main research approaches and plans can be divided into the following parts:

1) A literature review of the tire/pavement noise generating mechanism as well as the conventional types of LNPs. Literature about the state of arts of recycled crumb rubber (CR), as well as asphalt mixtures with crumb rubber by the dry process (DP) and wet process (WP), will also be reviewed. Through these literature reviews, directions can be provided for the design of noise reduction and vibration absorption system for road pavements.

2) Review the commonly used damping characterization model applied in road engineering, summarize and verify the accuracy and applicability of existing research methods. In addition, commonly used methods and software for pavement structural analysis as well as the image analysis software will be reviewed in order to provide ideas and methods for characterizing the damping and mechanical properties of road structures.

3) According to the literature review about the mechanism of tire/road noise generation and the noise reduction of LNPs, The laboratory and in-situ experimental data of the

"Leopoldo" project will be analyzed. According to the results drawn from the analysis, this study will infer the noise reduction mechanism of adding crumb rubber particles by DP and WP, and according to this mechanism, this study will determine the most suitable asphalt mixture, which can be used as surface layer for noise and vibration reduction.

4) Regarding the commonly used damping characterization model applied in road engineering, a more accurate and scientific method that can be applied to the road structure will be modified and proposed. Its accuracy and effectiveness will be verified by the comparison with field experiment results. Based on the proposed method, a finite element (FE) model will be established to accurately simulate the effect of the damping layer on traffic-induced vibration. Besides, the effect of the damping layer on mechanical response and pavement performance will also be evaluated. Based on the above response analysis, a refined and optimized pavement structure used for noise and vibration absorbing will be designed.

5) The vibration-reducing layer will be designed to achieve a specific target in terms of damping by adding a large amount of asphalt rubber (AR) and evaluated with regard to mechanical property (volumetric properties, indirect tensile strength, water sensitive, rutting resistance, dynamic modulus, etc.) and damping property (viscoelasticity and phase angle). Since rutting resistance and damping property are generally opposite, while the damping performance of the asphalt mixture is improved, the anti-rutting ability will be strictly tested by the newly designed test to verify the feasibility of the damping layer in actual construction and application.

The research approach and plans are also shown in Figure 1.4 as the form of a flow chart.
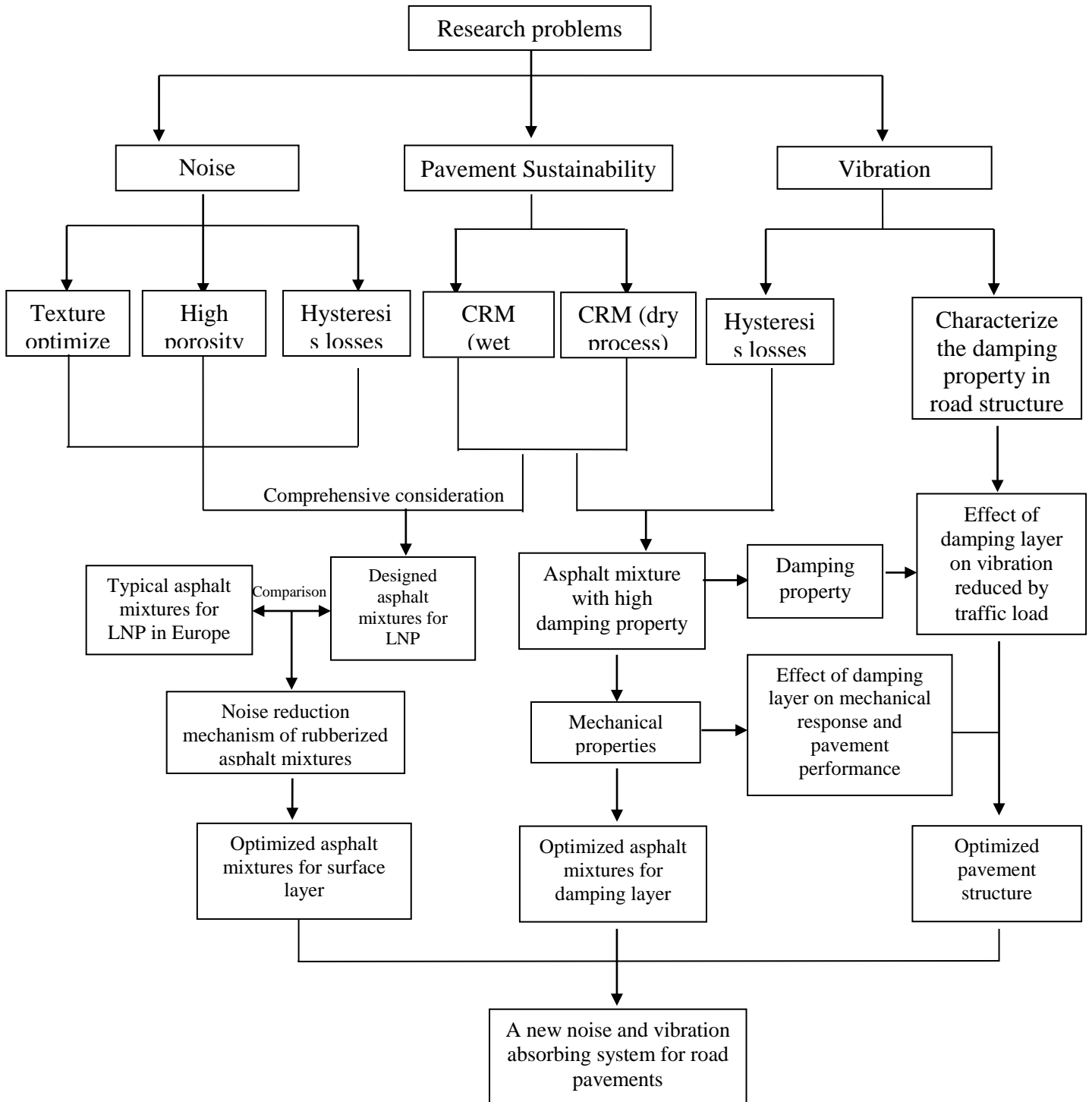
Figure 1.4 The methodology used in this study

1.5 Organization of the study

The study is organized into seven chapters including this one, which introduces the background, as well as research problem, objective and methodology of the research project.

The second chapter gives a literature overview of tire-pavement noise generation mechanisms, conventional low noise and vibration pavements, recycled crumb rubber, asphalt mixtures with crumb rubber by DP and WP, commonly used methods and software for pavement structural analysis and dynamics of pavement structure as well as several image analysis software and methods for infrastructure materials.

The third chapter has a focus on the noise reduction mechanism of rubberized asphalt mixture.

The fourth chapter highlights a novel model to determine Rayleigh damping coefficients for the FE analysis in the pavement as well as the verification process compared to in-situ experimental results.

The fifth chapter introduces a parametric study of the effect of the damping layer on vibration response of pavement and the surrounding environment, as well as the mechanical response and pavement performance.

The sixth chapter has a focus on the designing and testing of asphalt mixtures for the damping layer.

Finally, the last chapter summarizes the conclusions and future work of the research study.

Chapter 2: Literature review

2.1 Tire-pavement noise generation mechanisms

Since the 1970s, tire/pavement noise generation mechanisms have been studied. Tire/pavement noise and propagation mechanisms created by interactions tire and road are complex. Therefore, it is necessary to have a deep understanding of the noise generation mechanism in order to design a low noise road surface. Some mechanisms generate energy as sound radiation when the tire impacts the road; while other mechanisms amplify the sound is generated from the generation mechanism (Sandberg et al. 2002; Bernhard et al. 2005; Ruhala et al. 1999). Most researchers agreed with the theory of noise generation mechanisms but disputed the relative importance of them in generating tire-pavement noise (Sandberg et al. 2002). This is because the noise depends on the properties of the tire and the road surface as well as the complex interaction between these two parameters. In general, the noise generation mechanism can be divided into two modes: structure-borne, which is directly related to the mechanical vibration of the tire and is referred to as source generation mechanism, and air pumping, related to aerodynamic phenomena and referred to as sound enhancement mechanism (Bernhard et al. 2005). However, as the tire rolls on the road, many mechanisms work together to create noise. The tire-pavement noise generation mechanism is described in the following sections.

2.1.1 Tread Impact

The first sound mechanism occurs when the tire tread block hits the road surface causing the tire carcass to vibrate, as shown in Figure 2.1. When the rolling tire treads travel circumferentially with the tire, they individually impact the contact surface of the road for a hundred times in a second, if not a thousand times (Rasmussen et al. 2007, Bernhard et al. 2005). This vibration is radiated as acoustic energy and may be the main source of tire/pavement noise. This is similar to a small rubber hammer hitting the pavement thousands of times in a second. Tread impact vibrations can exist in the radial, tangential or axial directions and typically affect noise below 1000 Hz (Nilsson et al. 1980). Tire tread vibration is mainly affected by surface macrotexture.
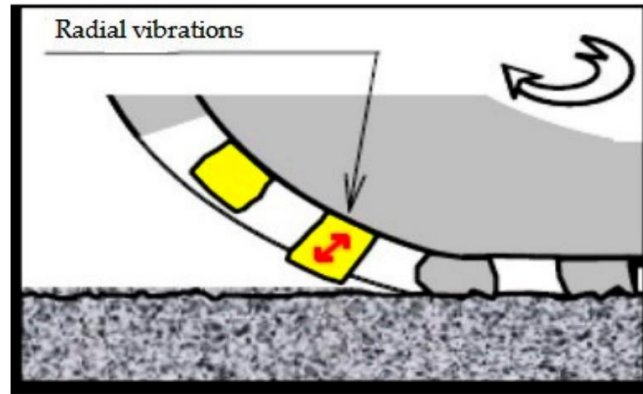
Figure 2.1 Tire tread block/pavement interaction

2.1.2 Air Pumping

When air pumping or compressing air is at the interface between the tire and the road surface, an air pumping mechanism occurs, as shown in Figure 2.2. Due to the passages and grooves in the tread pattern of the tire, significant void spaces can be created at the contact faces. When the vehicle is traveling on the sidewalk, the gap space between the passage and the groove in the tire is continuously distorted and deformed. The entrapped air in the void spaces compresses and is pumped out as the tire loses contact with the pavement. Therefore, aerodynamics produces sound due to air compression and pumping effects. This is similar to clap your hands with both hands, the air being compressed and squeezed at the edge of the hand, which creates a part sound of the applause (Ruhala et al. 1999; Sandberg et al. 2002; Bernhard et al. 2005). Whistling is another example where the air is forced to pass outward through a small opening. The air pumping mechanism is affected by the porosity and macrotexture of the pavement; therefore, it is one of the main sources of tire-road noise referred to in various research reports. The study (Nilsson et al. 1980) showed that the air pumping mechanism is more prominent at frequencies above 1000 Hz.
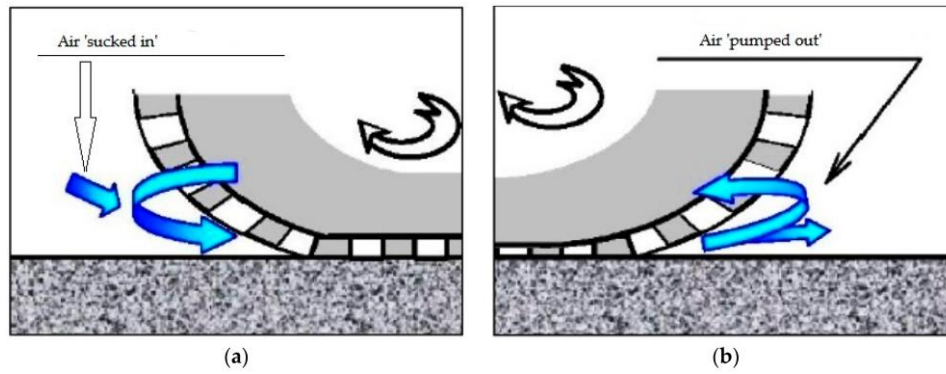
Figure 2.2 Air pumping mechanism (a) entrance; the (b) exit of the contact patch
(Sandberg & Ejsmont 2002)

2.1.3 Stick-Slip

The tread blocks of a tire at the contact patch experience a considerable amount of horizontal forces due to distortion of the tire carcass while rotating on the surface of pavements. These horizontal forces of the tire tread are transmitted to the road surface during acceleration or braking. If these horizontal forces are greater than the friction of the road surface, the tire tread blocks will temporarily slide before re-adhering to the road surface (Ruhala et al. 1999; Sandberg et al. 2002; Bernhard et al. 2005). These events of sliding and re-adhesion under each tread block occur thousands of times per second, producing high-frequency sound. This is similar to the sound of sneakers squeaking in a gym or basketball court. The stick-slip mechanism is shown in Figure 2.3. The stick-slip mechanism causes noise during and above the frequency range (1000 Hz - 2500 Hz) (Plotkin et al. 1980; Wozniak et al. 2001). Whether the surface texture is positive or negative, this noise mechanism is affected by all wavelength textures. Temperature also has a large effect on this noise mechanism since the friction of tire rubber changes with temperature. (Dare et al. 2014)
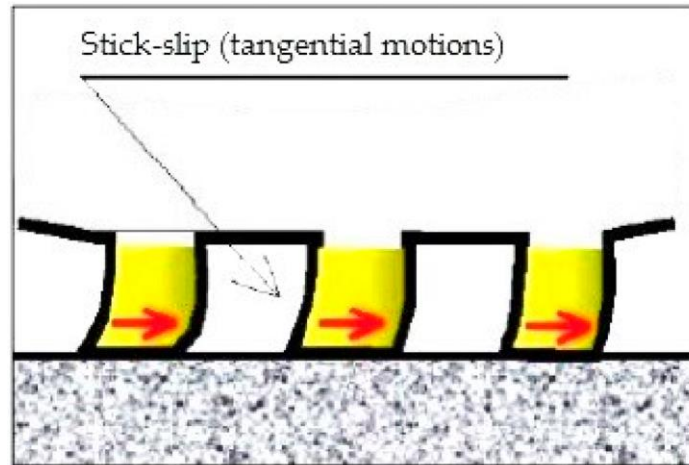
Figure 2.3 Slip-stick mechanisms of sound under tread blocks

2.1.4 Stick-Snap

The sound from the stick-snap mechanism occurs due to the adhesion between the tire tread block and the road surface, as shown in Figure 2.4. The sticking tread block is released at the trailing edge of the contact area to generate vibration which radiated as sound energy. This phenomenon is similar to a suction cup stick to a smooth surface (Sandberg et al. 2002; Ruhala et al. 1999). The stick-snap mechanism at the trailing edge is shown to affect noise at a frequency above 1000 Hz. This noise mechanism is influenced by both microtextures of surface and temperature (Nilsson et al. 1980; Kroger et al. 2004). The adhesion mechanism is reduced under wet conditions but increases under dry conditions. (Kroger et al. 2004)
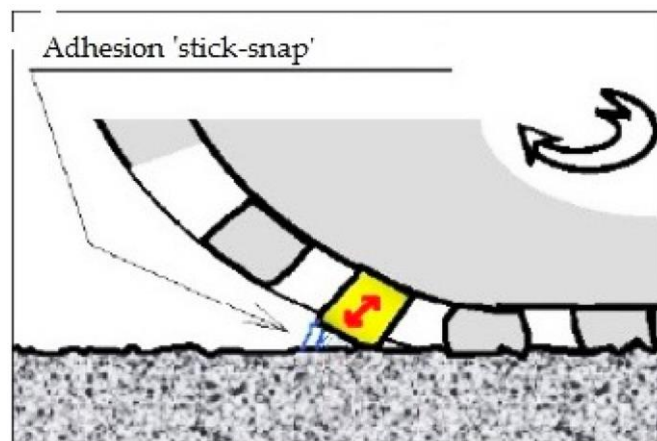
Figure 2.4 Stick-snap mechanism of sound under tread blocks

2.2 Conventional low noise and vibration pavements

2.2.1 Porous asphalt surface

Porous mixtures have been used in the asphalt pavement industry since the 1960s. This is because porous asphalt increases slip resistance under wet conditions and enhance fatigue and rutting resistance (Sandberg et al. 2002). In addition, the porous surface effectively discharges rainwater, thereby reducing splashes and sprays behind the car (Crocker et al. 2004). The noise-beneficial properties of porous asphalt were discovered in the mid-1980s. Researchers have observed that porosity plays an important role in the generation and propagation of road noise, especially for asphalt pavements. Generally, dense-graded asphalt (DGA) and porous asphalt are distinguished by porosity. If the porosity of the asphalt pavement is less than 10%, it is referred to as the DGA surface. However, the commonly used porous surface, known as the open-graded friction course (OGFC) must have more than 15% air voids. In addition, European authorities recommend that porous roads with more than 20% of air voids are beneficial for noise reduction (Donavan et al. 2005). Many researchers (Sandberg et al. 2002; Hanson et al. 2004) indicate that OGFC can significantly reduce noise (3 dB to 5 dB) compared to DGA surfaces. The air trapped between the tire and the road surface moves into the available void space in the porous surface, thereby reducing the "horn effect" of noise amplification. In addition, it provides enhanced sound absorption to reduce noise.

2.2.2 Double layer porous surface

In Europe, the concept of two layers of drainage pavement was introduced to solve the problem of clogging in the porous pavement (Faure et al. 2000). In such a pavement system, the top layer is filled with a finer mixture (maximum aggregate size of 2 mm) and the bottom layer is filled with a thick, highly porous mixture (maximum aggregate size of 20 mm) for sound absorption (Sandberg et al. 2009). Sandberg et al. (2009) demonstrated the initial noise reduction of newly constructed double-layer porous is up to 6–7 dB compared to a DGA or stone mastic asphalt (SMA) surface (maximum aggregate size of 11 mm) for the mixed traffic. The noise reduction of the double-layered porous surface is due to the combination of the two mechanisms. First, the small aggregate of the top layer produces a smooth surface that minimizes the texture effects of the tire. Second, the lower layer consists of coarse aggregate, which has a higher void content, thus increasing sound absorption. Therefore, when air can pass through the

interconnected spaces in the road surface, the air under the tire is pumped and suppressed. In addition, the top surface filters out clogged particles; hence, acoustic performance can be maintained for a longer period of time (Goubert et al. 2005, Bendtsen et al. 2001).

2.2.3 Thin asphalt Layer

The thin asphalt layer (TAL) is a gap-graded, high-quality aggregate asphalt mixture with layer thicknesses ranging from 10 mm to 30 mm, depending on the nominal maximum size of the aggregate (approximately 12 mm or smaller) (EAPA 2007; Sandberg et al. 2001). In these mixtures, a moderate percentage of sand and modified polymer binders are also added. The air void content of these mixtures varies between 15% and 25%. The initial noise reduction of the TAL surface of the passenger car varies between 0.9 and 6.9 dB depending on the maximum aggregate size and surface type. For multi-axle trucks, the initial noise reduction of the TAL surface is small compared to passenger cars. In addition, TAL has low road maintenance costs and low initial construction costs; therefore, it is widely used in Europe's busy roads. However, as observed for other porous surfaces, the noise benefit of the TAL surface decreases with age. Recently, SPB and CPX noise tests were performed by Vuye et al. (2016) on various TAL sections of Belgium at different road aging times. For the SPB and CPX methods, the noise benefits of these TAL pavements were reduced at a rate of 0.02-0.14 dB/month and 0.05-0.20 dB/month, respectively. In the case of heavy traffic, the noise benefits of these TAL surfaces are diminished due to the raveling of aggregates. Therefore, it is very difficult to use these TAL surfaces where heavy vehicles exert high shear forces on the surface layers.

2.2.4 Stone mastic asphalt

Stone mastic asphalt (SMA) is a gap graded asphalt mixture with an aggregate skeleton of relatively coarse aggregate filled with asphalt mastic, filler and fine aggregate (EAPA 2007). The layer thickness varies according to the nominal aggregate size and typically varies between 15 mm (SMA 0/6 mm) and 45 mm (SMA 0/16 mm). The SMA surface was originally developed in Germany in the mid-1960s to provide high resistance to inlaid tires. It was later discovered that these surfaces have many other benefits and are therefore used in busy roads in Europe. These surfaces offer high durability, excellent rutting resistance, and comfortable riding characteristics. In addition, a European study (EAPA 2008) showed a 2-3 dB noise reduction in SMA pavement with a maximum

aggregate size of 11 mm (0/11 mm) or less (0/6 mm) compared to the DGA surface. This is because SMA has a relatively open surface texture that reduces the air pumping mechanism and thus reduces noise (Bendtsen et al. 2005). Studies conducted in Finland have shown that SMA surfaces with a 5 mm aggregate size show initial noise reduction of 3 dB and 5 dB at 50 km/h and 80 km/h, respectively, compared to the original pavement (Valtonen et al. 2002). However, after one year, the noise increased significantly due to the wear of the SMA surface. SMA surfaces are generally more expensive than conventional DGA surfaces due to higher binder content and high-quality aggregates.

2.2.5 Asphalt rubber friction course

The asphalt rubber friction course (ARFC) surface was originally developed in Arizona to resist cracking and is now also used to reduce traffic noise. In this surface, the binder is mixed with granulated rubber (particles 0.5-2.0 mm). The proportion of crumb rubber is 10% weight of the total binder content, typically twice the amounts of the polymer modifier used in the porous asphalt surface (Sandberg et al. 2001). Mixing the crumb rubber with the asphalt is carried out by WP instead of DP. The Arizona Department of Transportation (ADOT) placed an ARFC surface on the existing Portland cement concrete (PCC) surface and conducted noise studies using the OBSI test method (Aspro 2005). The test results showed that the noise reduction of the ARFC surface is 7 dB compared to the existing PCC surface. Sandberg (2001) explained that the noise reduction of the ARFC surface is due to a combination of factors. First, the surface texture of ARFC has a negative profile due to the small maximum aggregate size as Bendtsen et al. (2008) demonstrated negative pavement texture generates low noise due to minimum tire tread vibration. Secondly, due to the excessive binder and rubber content, the ARFC surface has a lower stiffness, so the impact between the tire tread and the road surface becomes smaller, thereby reducing noise. In addition, Sotil et al. (2006) demonstrated the hysteresis loss due to the vibration of the viscoelastic material, that is, the asphalt rubber mixture reduces noise. Furthermore, Ripke et al. (2005) stated that the open texture of an ARFC surface developed from the mix of aggregate size reduces the air pumping noise mechanism. Recently, Tehrani (2014) reviewed the surface of rubberized Hot Mix Asphalt (HMA) for noise reduction technology and concluded that adding rubber can reduce the noise level by about 2 to 3 dB compared to the surface of the HMA and 4.5 to 6 dB compared to the PCC surface. The researchers

explained that adding rubber to the pavement mixture tends to reduce the noise frequency to a lower frequency which is close to the tire noise. Therefore, the rubber does not resonate at high frequencies, thus limiting the amplification of the noise mechanism which in turn generates less low noise. However, as observed for other modified surfaces or mixtures, the noise benefits of crumb rubber asphalt mixture are also diminished with time (Ripke et al. 2005; Tehrani et al. 2014).

2.2.6 Poroelastic road surface

Poroelastic road surface (PERS) is a wearing course made of rubber granulates combined with binder. According to the EU-sponsored SILVIA (2006) project, many PERS surfaces have been constructed and noise data were collected using the CPX method. The noise reduction mechanism of PERS is due to the combination of a number of factors. The results showed that using the PERS surface can significantly reduce noise. A well-constructed PERS has a very smooth surface texture with less impact on the tire. In addition, PERS typically has a very high air void content (30% - 35%) which effectively minimizes the air pumping mechanism. Due to the high air void content, PERS also absorbs a large part of the noise (Sandberg et al. 2011). This idea was adopted by Japanese researchers and used for street paving. OBSI noise testing was performed on these pavements and the results showed an initial reduction of 7-9 dB compared to the conventional DGA (0/16 mm) surface (Morgen et al. 2008). The temperature has a large effect on the acoustic performance of the PERS surface. The test results showed that for every 1 °C decrease in temperature, the noise increases by 0.142 dB, which indicated that due to joint expansion, colder weather can cause a nosier PERS (Morgan et al. 2008). PERS has been developed in Sweden a long time ago, but these surfaces have not gained popularity due to durability issues and high construction costs.

2.3 Anti-vibration paving

Road traffic generates vibration due to the engine, air resistance, tire movement, and braking. In addition, due to the laying procedure, the use of technology and the presence of surface damage, other noise is generated due to irregular paving surfaces. These irregularities result in oscillating motion in the vehicle, disturbing people in the vehicle, and the energy waves from the road surface are transmitted to the structures and people therein (Venturini et al. 2016).

It is possible to reduce vibration pollution thanks to periodic monitoring of surface damage and taking corrective measures (road maintenance) to ensure a suitable road surface, with the aim of reducing the generation of vibrational waves. Otherwise, it is possible to take action against the propagation between source and receiver, studying the design phase. Further solutions, which allow the reduction of vibrations, are "anti-vibration" pavements using innovative technology. This technological solution avoids the production of excessive vibration and contains the propagation (Venturini et al. 2016).

The first attempt of anti-vibration pavements in the world was carried out in 1970. In order to preserve an ancient building (the Villa Farnesina in Roma) against traffic-induced vibrations, an anti-vibration system was developed under the near Lungotevere road. The anti-vibration system was composed of a concrete grid supported by rubber pads. A preliminary experimental investigation was carried out in order to define the size and the number of rubber bearings to be used. A steel square plate was located on the road foundation supported by means of different kinds of rubber bearing. Different kinds of input were considered. An oscillography recorded the vibrations in the basement of the building. According to the obtained results, this system determined a reduction of the acceleration values of about 80%. The results were highly satisfactory. Massari, responsible for Villa Farnesina, wrote: ''This is the first time, in Europe and in the world, that a road has been repaired in order to protect a monument against traffic-induced vibrations''. Similar solutions have also been used for new constructions in Piazzetta S. Paolo, Milan and Via Parigi, Rome (Clemente et al. 1998).

In the following time, with the development of technology, based on the modern paving techniques and materials, anti-vibration pavement was still being tried. In 2008, a new anti-vibration pavement was designed by the University of Bologna (Dondi et al. 2005; Grandi 2008), as shown in Figure 2.5. The advantages of this anti-vibration pavement have been confirmed as follows (Dondi et al. 2005):

1. The reducing stiffness of the vibration-absorbing layer will not reduce the stiffness of the whole pavement systems as a consequent advantage in terms of using life;

2. Increasing the elastic absorption capacity of the vibrations caused by surface irregularities near the source with a consequent increase in the effectiveness of the intervention;

3. An environmental advantage produced by re-using the material coming from the crumb rubber of heavy vehicle tires.

(E= elastic modulus, v= Poisson's ratio)

0.10 (m) — Surface layer (E=4500 MPa, v=0.35)

0.15 (m) — Base layer (E=3500 MPa, v=0.35)

0.25 (m) — Cement stabilizing layer (E=1800 MPa, v=0.35)

0.03 (m) — Anti-vibration pad (E=0.2 MPa, v=0.35)

0.30 (m) — Unbound graded base (E=200 MPa, v=0.35)

Subgrade (soil) (E=90 MPa, v=0.35)
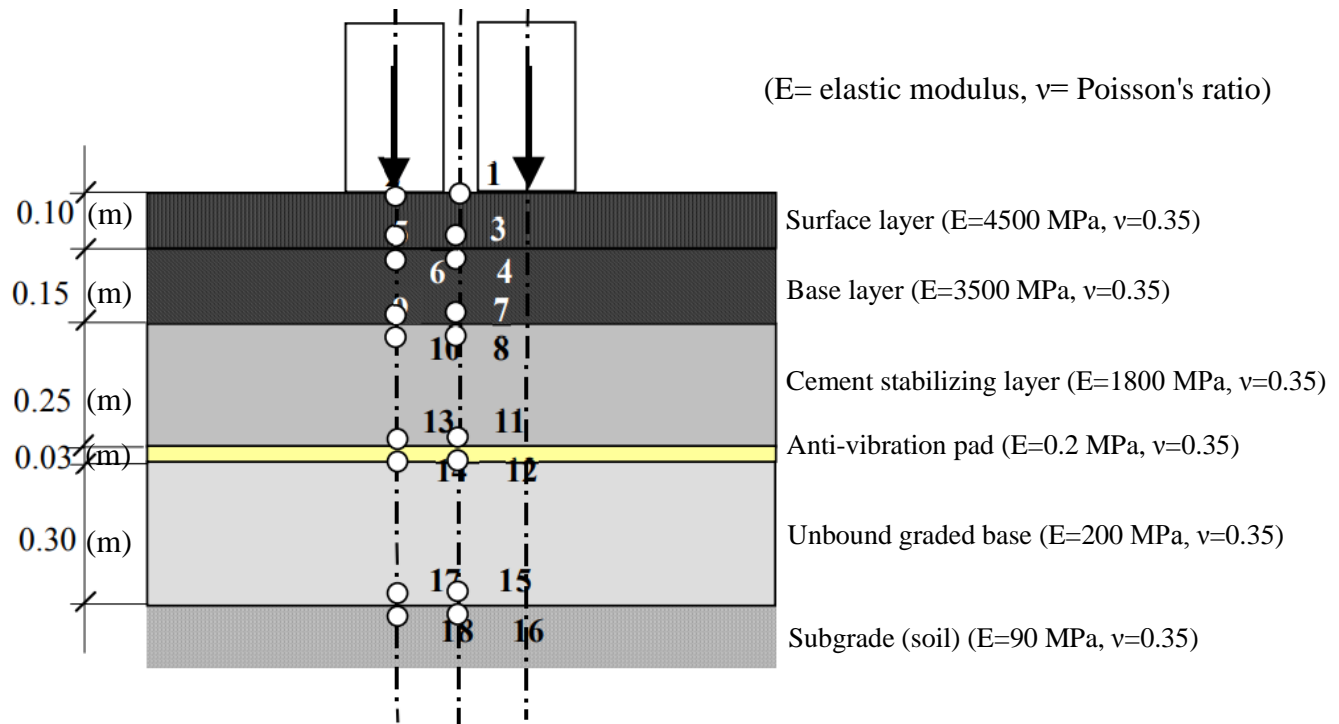
Figure 2.5 Anti-vibration pavement designed by the University of Bologna

Later in 2016, dependent on the new production technologies, another anti-vibration pavement was constructed for the Municipality of Novara, Italy. The new technology was focused on two key issues (Venturini et al. 2016):

1. The optimized surface texture, depending on the particular grading curve designed;

2. The coefficient of vibration absorption of the pavement, optimized by the presence of rubber particles.

The verification of the newly developed technology was conducted by in-situ experimental tests. The test involved the analysis of the data detected by the transit vehicle of reference, on a stretch of anti-vibration pavement and on one reference, and showed the anti-vibration level reaches.

2.4 Recycled crumb rubber (CR)

In Europe, the use of CR from reclaimed tires in pavement construction has increased over the past few years. This use may contribute to sustainable development and environmental protection as it involves the appreciation of waste materials, provides solutions to waste management problems, and implies reducing the use of natural resources in road construction (Huang et al. 2007).

According to different production processes, the crumb rubber is mainly added to the asphalt mixture in two ways: DP and WP (Ongel & Harvey 2010; Losa et al. 2012). The WP technology is based on the process invented by Charles McDonald for asphalt rubber (AR) production. In this case, the rubber is added to the conventional asphalt and used as a modifier. The melting and mixing process of CR and binder is given by a mechanical agitation operating system in the range of 190 °C and 218 °C between 45 and 60 minutes (Presti 2013). According to this method, the rheological properties of the asphalt are improved in terms of rutting resistance, fatigue and thermal cracking, which are confirmed by specific research and application (Xiao et al. 2007). In contrast, in the DP, CR is added directly to the asphalt mixture as additional aggregates. Therefore, there is no substantial interaction between the rubber and the asphalt so that the binder can be modified. The DP has been developed over the past 30 years and according to this technique, the mixture design phase is very important considering the effect of CR on the grading distribution of aggregates. In addition, in order to obtain the optimum asphalt content, the absorption properties of the rubber must be considered. Today, research and practical applications show that CR has a high potential for the production of environmentally friendly asphalt mixtures that have high performance in terms of durability, road noise attenuation and crack resistance (Hanson et al. 2005; Trevino et al. 2009).

2.5 Methods and software for pavement and material analysis

2.5.1 Methods and software for pavement structure analysis

The methodologies and associated computer programs for simulating multilayer pavement responses include multi-layer elastic theory (e.g., BISAR and ELSYM5), finite element methods (e.g., ILLIPAVE, MICHPAVE), and semi-analytical techniques. General-purpose commercial finite element codes (e.g., ABAQUS and ANSYS) can also be employed. Most existing programs are based on the assumption of static loading and linear elastic material properties (see Table 2.1), although some programs have considered the dynamic response (see Table 2.2). The VEROAD program developed at the Delft University of Technology (Hopman 1996) treats the AC as a linear viscoelastic material.

Table 2.1 Examples of static forward analysis software for flexible pavements

Method or software	Author(s)	Features	Analysis Method
ELSYM 5	UC Berkeley	Linear elastic	Analytical multilayer analysis
BISAR	Shell Global, Inc	Linear elastic	Analytical multilayer analysis
Everstress	Washington DOT	Linear elastic	Analytical multilayer analysis
ILLIPAVE	University of Illinois	Elastic+stress-dependent soil	Finite element
TTI PAVE	Texas Transportation Institute	Elastic+Mohr-Columbia model	Finite element
MichPAVE	Michigan State University	Elastic+stress-dependent soil	Finite element
VEROAD	Hopman	Static viscoelastic	Analytical multilayer analysis
CAPA-3D	Scarpas	Material damages	Finite element

Table 2.2 Examples of dynamic forward analysis for flexible pavements

Method or software	Author(s)	Features	Analysis Method
AXIDIN	Antunes (1991)	Dynamic elastic	Two-dimensional finite element method
PUNCH	Kausel (1989)	Dynamic elastic	An explicit, closed-form solution for the Green functions
UTFWIBM	Roesset (1987)	Dynamic elastic	Fourier superposition
SAPSI	Chen (1987)	Damped-elastic	Multilayer analysis based on Kausel's formulation
SAPSI-M	Chatti and Yun (1996)	Damped-elastic, moving transient loads	Multilayer analysis based on Kausel's formulation
SCALPOT	Magnuson (1998)	Dynamic elastic	Haskell-Thompson transfer matrix approach
ViscoWave	Lee (2013)	Dynamic viscoelastic (no damping)	Analytical multilayer analysis
3D-Move Analysis	UNR	Dynamic, damping	Continuum-based finite-layer

2.5.2 Image analysis software and method for infrastructure material

The commonly used methods for infrastructure material, include several image processing and analysis software, e.g., Image processing & analysis system (IPAS) developed by UW-Madison, ImageTool developed by UT Health San Antonio (Wilcox et al. 2002), and ImageJ developed by the National Institutes of Health. Based on the algorithm in MATLAB, the Volumetricsbased Global Minima (VGM) developed by Zelelew et al. (2017A) can use the volumetric properties as the main criterion for establishing grey-level thresholds. The UIAIA developed by the University of Illinois can achieve 3D reconstruction technology by automating the determination of all the

aforementioned properties. The conventional examples of image analysis and software are shown in Table 2.1.

With the assistance of the above software and methods, a series of research results were obtained. Through the software iPas, Sefidmazgi et al. (2012) introduced and elaborated a method to characterize the internal structure of asphalt mixes using imaging analysis. Bessa et al. (2012) used ImageTool to characterize the different aggregates and HMA internal structure composed of those aggregates with different gradations. Zelelew et al. (2008) used VGM for processing computed tomography (CT) images of asphalt concrete. Cannone Falchetto et al. (2012) used ImageJ software to estimate the grain size distribution of BBR asphalt mixture beam specimens.

Table 2.3 Examples of pavement material image analysis software

Method or software	Author(s)	Features	Analysis Method
IPAS	UW-Madison	Image Processing & Analysis System	Image analysis of the internal aggregate structure of HMA
VGM	Zelelew (2007A)	volumetric properties as the main criterion for establishing grey-level thresholds	An algorithm based on MATLAB
UTHSCSA ImageTool	UT Health San Antonio: Wilcox (2002)	Conventional image processing software	Standard image processing functions
ImageJ	National Institutes of Health	Conventional image processing software	Standard image processing functions
UIAIA	University of Illinois	Reconstructing the 3D shape	Automating the determination of all the aforementioned properties

Chapter 3: Noise reduction mechanism of rubberized LNPs

It has been proved in a number of studies that the rubberized asphalt is superior to non-rubberized asphalt in noise reduction. A previous study conducted by County (1999) showed that rubberized asphalt reduces traffic noise levels by 4 dB over conventional non-rubberized asphalt. In a 10-year study, Bucka (2002) concluded that rubber overlays could reduce noise by 3 to 7 dB, while conventional asphalt can only reduce noise by 1 to 2 dB. A study by Ongel et al. (2008) obtained field measurements of 23 test sections at various locations in California, confirming that the rubber mixture has a lower level of noise intensity.

Even though the rubberized LNPs have been widely used in the urban traffic system for the purpose of noise-reducing, the mechanism of noise-reducing properties for the rubberized LNPs is not clear yet. Sandberg (2009) elaborated his view and attributed the low noise properties of ARFC to the following possible factors, such as the thick binder with its rubber made the chippings somewhat flexible as they sit in the mix, much lower stiffness than normal mixtures, and higher hysteretic losses. In addition, the embedment of chippings in the relatively thick binder film may also give a kind of "cushion" effect. The study of County (1999) showed that rubberized mixture can reduce noise energy by 60%, caused by the higher damping ratio. Biligiri (2013) also confirmed that the rubberized mixture will result in a higher damping ratio, which will attenuate the tire-road noise. Although many researchers have explored and inferred the mechanism of noise reduction in rubberized mixtures, there is currently no effective and specialized research to explore the mechanism of noise reduction.

In the period of 2008 to 2012, the road engineering lab of the University of Pisa and Regional Agency for Environmental Protection of Tuscany conducted the "LEOPOLDO" project, in which two gap-graded rubberized asphalts were designed to be LNPs, by DP and WP, respectively. During the project, laboratory and field tests were carried out to evaluate the mixtures' properties and in-situ performance, respectively, and two traditional LNPs, by open-graded mixtures and gap-graded mixtures with traditional SBS modifiers binder, were used as a comparison group.

In this study, the raw data from the "LEOPOLDO" project is used to be extracted and the noise-related parameters are analyzed in order to reverse the mechanism by which CR is added to the asphalt mixture by DP and WP to reduce noise. By better understand the mechanism of the rubberized asphalt mixture, the evidence for the selection of asphalt mixtures according to the specific traffic environment can be provided.

3.1 Research methods

3.1.1 Parameters related to tire/pavement noise

Typically, tire-pavement noise generation is divided into two main mechanisms involving different acoustic fields: vibration and aerodynamic mechanisms (Losa et al. 2010). The vibration mechanism is responsible for low-frequency noise emissions. They are produced by radial and tangential vibrations of the tread elements produced in the interaction between the tire and the road surface. The aerodynamic mechanism leads to high-frequency noise emissions. They are related to the compression and expansion of the enclosed air volume between the tire and the road surface. In particular, different frequency ranges are associated with these generation mechanisms: vibration is characterized by frequencies lower than 1000 Hz and air-pumping is characterized by frequencies higher than 1000 Hz (Sandberg et al. 2002).

As far as the surface layer, the main factors related to noise and vibration of tire/pavement are including porosity, elasticity, texture, friction and so on. According to these parameters, the conventional LNPs are identified and classified into three main categories: texture optimized types (gap-graded asphalt mixtures), high porosity types (open-graded asphalt mixtures) and hysteresis losses (AR mixtures; PERS) types (Sotil et al. 2006; Losa et al. 2010; Biligiri, 2013).

For the effect of asphalt mixtures' porosity on traffic-induced noise, the results of the noise test have shown that as the air voids increase, the noise level decrease (Hanson et al. 2004). In fact, the air voids are highly related to the sound absorption, and thus the tire/pavement noise. By increasing the air voids or the sound absorption, more noise energy is absorbed in the pavement and then the tire/pavement noise reduces.

In the case of stiffness modulus, it could play an important role in the tire/pavement sound generation, especially for surfaces with the same texture profile but different

aggregate and bitumen content, or the surfaces aged by compaction (Sandberg 1987; Vázquez et al. 2013). Lowering the pavement stiffness would tend to reduce tire vibration and hence tire/pavement noise generation (Vázquez et al. 2016). The study of Hemet et al. (2004) has shown that the reduction of the pavement stiffness could reduce substantially the rolling noise.

For the effect of pavement texture level on tire/pavement noise, according to the literature (Sandberg & Descornet 1980; Sandberg 1987; Losa et al. 2010),

(1) The pavement surface texture is in a low-frequency range with a wavelength of 10 mm~ 250 mm, which mainly affects the tire generated by the vibration of the tire. Increasing the surface texture level in this wavelength range can increase the vibration noise generated by the impact between the tire and the road surface.

(2) The pavement surface texture is in a high-frequency range with a wavelength of below 10 mm, which mainly affects the tire/pavement noise generated by aerodynamic. Increasing the surface texture level in this wavelength range can increase the gap between the tire and the road surface, thus reducing the noise generated by the air-pumping.

For the effect of adding crumb rubber to asphalt mixtures, the conclusion that it can reduce the tire/pavement has been confirmed, but the effects of different adding methods (DP and WP) to high-frequency noise or low-frequency noise are uncertain.

3.1.2 Research method based on control variables

Based on the pre-mentioned analysis, the factors influencing the low-noise ability of pavements are summarized in Table 3.1. With a boundary of 1000 Hz, tire/pavement noise can be divided into high-frequency range and low-frequency range (Sandberg 1987). For the low-frequency areas, reducing the texture and stiffness will contribute to improving the low-noise ability of the pavement; for high-frequency areas, improving the texture level and sound absorption, as well as air voids, will contribute to improving the low-noise ability. It should be noted that the effects of stiffness on high-frequency noise, as well as the effects of sound absorption and air voids on low-frequency noise actually exist. However, since these effects are extremely weak, they are not considered in the present study and they will be regarded as "Neutral". For the effect of the parameter "adding crumb rubber", it will be determined in this study.

Table 3.1 Relationship between the parameters and tire/pavement noise

Noise-related parameters	Air Voids	Stiffness modulus	Sound absorption	Texture level	Adding crumb rubber (wet process)	Adding crumb rubber (dry process)
Low-frequency noise <1000Hz)	Neutral	Negative (Nilsson et al. 1980; Hamet et al. 2004; Vázquez et al. 2016)	Neutral	Negative (Sandberg 2002)	To be determined	To be determined
High-frequency noise(>1000Hz)	Positive (Biligiri et al. 2014)	Neutral	Positive (Ahammed et al. 2011)	Positive (Sandberg 2002)	To be determined	To be determined

Notes: *Positive means that it is conducive to reducing the noise; Negative means that it is not conducive to reducing the noise; Neutral means that this factor has no effect on the noise or the effect is small that it can be ignored.

In order to understand the mechanism of adding rubber to the asphalt mixture to reduce noise, the control variable method is used in this study by setting up four experimental groups to control that the air voids, stiffness, and texture level are similar or the same. Gap-graded asphalt mixtures are used in this study because they have superior acoustic performance and have been widely used as LNPs. The four experimental groups are "gap-graded mixture + no crumb rubber added", "open-graded mixture + no crumb rubber added", "gap-graded mixture + adding crumb rubber (wet process)" and "gap-graded mixture + adding crumb rubber (dry process)", respectively. They are named as "GGS (Gap-Grade mixtures with SBS binder)", "OGS (Open-Graded mixtures with SBS binder)", "GGW (Gap-Grade mixtures with crumb rubber by Wet process)" and "GGD (Gap-Grade mixtures with crumb rubber by Dry process)", respectively. It should be noted that the properties of the asphalt mixture could not be very precisely defined, so the control variables (air voids, stiffness, texture level) are difficult to guarantee exactly the same; in this case, this study controls the variables similar and infers the effects of unknown parameters by comparing the known parameters.

3.2 Test results of noise-related parameters

The test results used for analysis in this study are from the raw data of "Leopoldo" project. These data are analyzed and extracted, especially the test results of the noise-related parameters, which are included in this chapter.

3.2.1 Air Voids

Table 3.2 shows the air voids results of the four asphalt mixtures as well as other volumetric parameters. All the asphalt mixtures meet the requirement of volumetric properties in the specification for gap-graded or open-graded asphalt mixtures. OGS shows high porosity with the air voids (VA) equal to 26.5%, by which it can obtain a good performance of noise absorbing. GGS has a greater continuity compared with GGW, and it shows a lower void in the mineral aggregate (VMA) value, but because of GGS's lower binder content, GGS and GGW are showing similar VA. It should be noted that with the similar volumetric properties, it is more evidenced to identify the effect of adding crumb rubber particles compared to typical SBS modified asphalt on noise reduction because it can eliminate the interference of porosity on noise reduction.

Table 3.2 Air voids results of the four asphalt mixtures as well as other volumetric parameters

Asphalt mixtures	Optimum binder content	Number of gyrations	V_A[a] (%)	VMA[b] (%)	VFA[c] (%)	G_{mb}[d] (kg/m^3)	G_{mm}[e] (kg/m^3)	V_G[f] (%)	V_B[g] (%)
OGS	AC=4.2 %	$N_{initial}$=10	37.7	37.9	16.3	1701	2492	62.1	6.2
		N_{design}=50	26.7	33.4	19.9	1825	2492	66.6	6.7
		N_{max}=130	24.5	31.3	21.9	1882	2492	68.7	6.9
GGS	AC=6.8 %	$N_{initial}$=10	15.3	27.3	44.1	2035	2402	72.7	12
		N_{design}=50	9.1	22	58.8	2184	2402	78	12.9
		N_{max}=130	6.5	19.8	67.2	2246	2402	80.2	13.3
GGW	AC=8.5 %	$N_{initial}$=10	12.19	26.44	53.90	2197	2502	73.56	14.25
		N_{design}=50	5.01	20.43	75.47	2377	2502	79.57	15.42
		N_{max}=130	2.17	18.05	87.96	2448	2502	81.95	15.88
GGD	AC=9.0 %	$N_{initial}$=10	14.75	29.99	50.79	1965	2305	70.01	15.23
		N_{design}=50	8.39	24.76	66.10	2112	2305	75.24	16.37
		N_{max}=130	5.51	22.39	75.38	2178	2305	77.61	16.88

Notes:

[a]air voids; [b]voids in the mineral aggregate; [c]voids filled with asphalt; [d]bulk density of the compacted mixture; [e]maximum density of the mix; [f]volume of aggregate, the bulk volume including the aggregate pores; [g]volume of effective asphalt binder;

3.2.2 Stiffness modulus

Figure 3.1 shows the indirect tensile stiffness modulus of the four asphalt mixtures as the temperature is equal to 20℃ and the rise time is equal to 125 ms. It can be observed that GGW shows the highest stiffness modulus among all the mixtures. In particular, GGW has a 35.6% higher stiffness modulus compared with GGS, demonstrating that rubberized mixtures (wet process) may generally have a higher stiffness than that of the mixture with SBS polymer-modified asphalt. It is proof that GGW is less susceptible to traffic loads and experiences less deformation compared with GGS. This finding is in agreement with the experimental tests developed in other studies (Lee et al. 2008; Navarro & Gamez 2010; Vazquez et al. 2016), where the inclusion of crumb rubber in the mixture by the wet process results in higher stiffness modulus than those without crumb rubber.

It can also be observed that the stiffness modulus of GGW is higher than that of GGD. This can be due to the better mixture compaction in the field of high temperatures (low frequencies), whereas in the field of low temperatures (high frequencies), this increase is due to the greater stiffness of AR as compared to polymer modified asphalt blended with CRM.
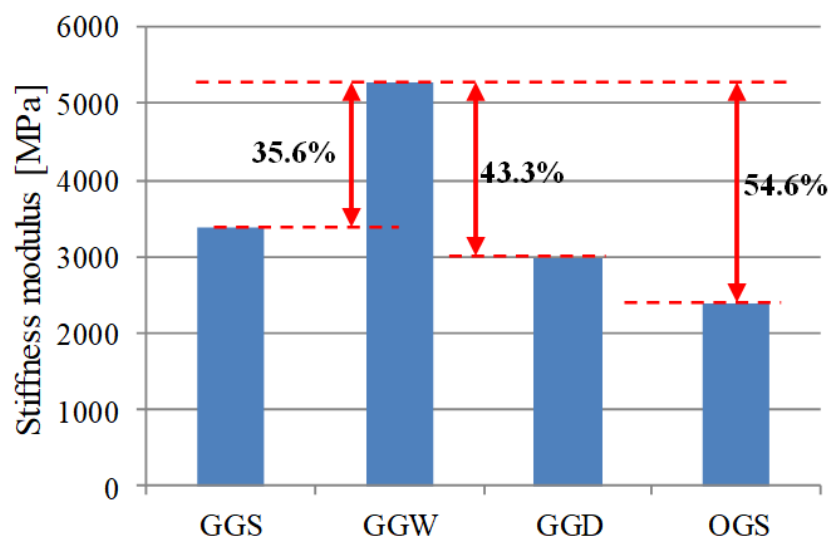
Figure 3.1 Indirect stiffness modulus of the four asphalt mixtures as the temperature is equal 20℃ and the rise time is equal 125 ms

3.2.3 Sound absorption

Figure 3.2 shows the box plots of the sound absorption of the four asphalt mixtures, including the first and third quartile and the maximum and minimum absorption values as well as the mean and median value found in the 250 to 4000 Hz frequency range. In this type of plot, the whiskers indicate the total range of the texture level for the whole section in a given category, and the boxes represent the range between the 25th and 75th percentiles. The median is represented by the line inside the box, and the dot is the average value (Ongel et al. 2007).

It can be found that OGS shows much higher sound absorption than GGS, GGW, and GGD, demonstrating the greater advantage of OGS over other mixtures as LNP by sound absorption. GGD shows much better sound-absorbing performance compared to the other gap-graded asphalt mixtures.
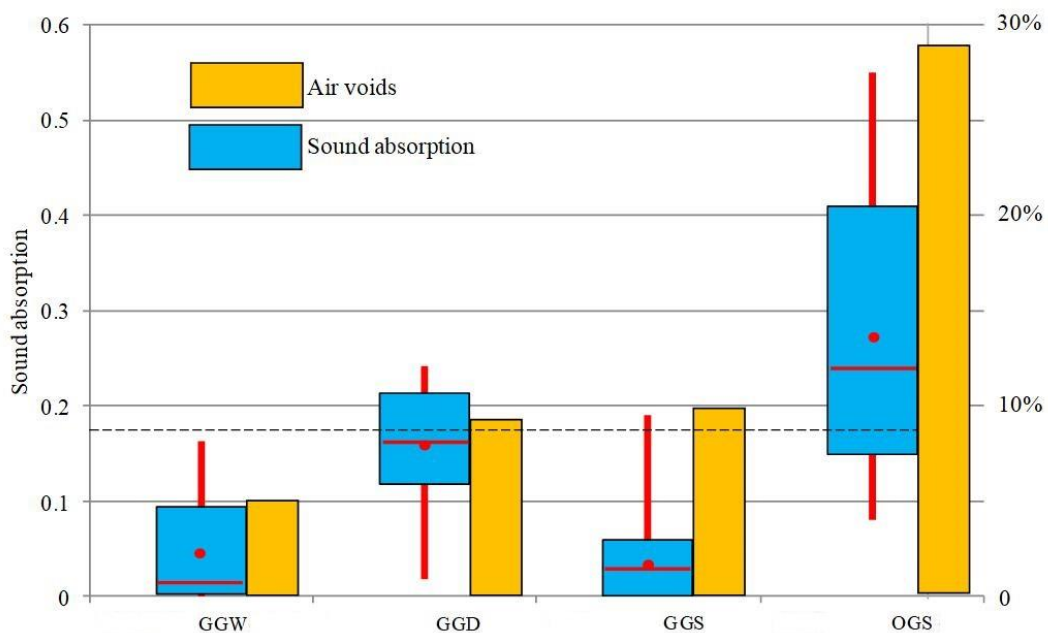
Figure 3.2 Sound absorption and air voids of the four asphalt mixtures

3.2.4 Texture level

Figure 3.3 shows the texture spectrum of the four surfaces with different asphalt mixtures at a similar time after the construction. Tire/pavement noise can be influenced by different factors and the pavement texture is one of the most important factors. If only pavement texture is considered for tire/pavement noise, OGS shows the best performance at a high-frequency range (low texture wavelength) but the poor

performance at low-frequency range (high texture wavelength), indicating a lower noise generated by air pumping but higher noise generated by tire/pavement vibration. Hence, OGS is more suitable for a highway or regional road with higher traffic speed, but not suitable for the urban road with lower traffic speed. GGS may be the optimized one for a relatively low speed since it has a lower texture level at the wavelength range [10 mm, 250 mm] and GGW may be more suitable for a relatively high speed since it has a higher texture level at the wavelength range [2 mm, 10 mm].
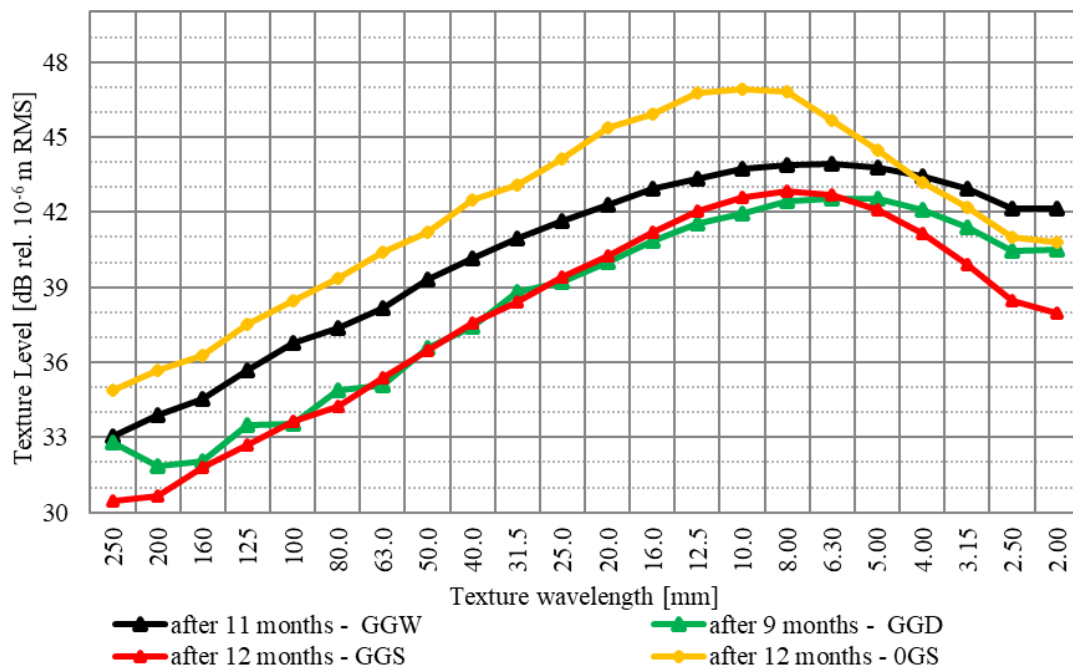
Figure 3.3 Texture levels of the pavements by the four asphalt mixtures

3.2.5 Tire/pavement rolling noise

Figure 3.4 shows the close proximity (CPX) noise at a speed of 50 km/h and all the values have been adjusted according to surface temperature, as described by the ISO standard (ISO/DIS-11819-2). All factors (from sub-chapter 3.21 to sub-chapter 3.24) related to tire/pavement noise are comprehensively reviewed, and the impacts of adding crumb rubber on noise are inferred.
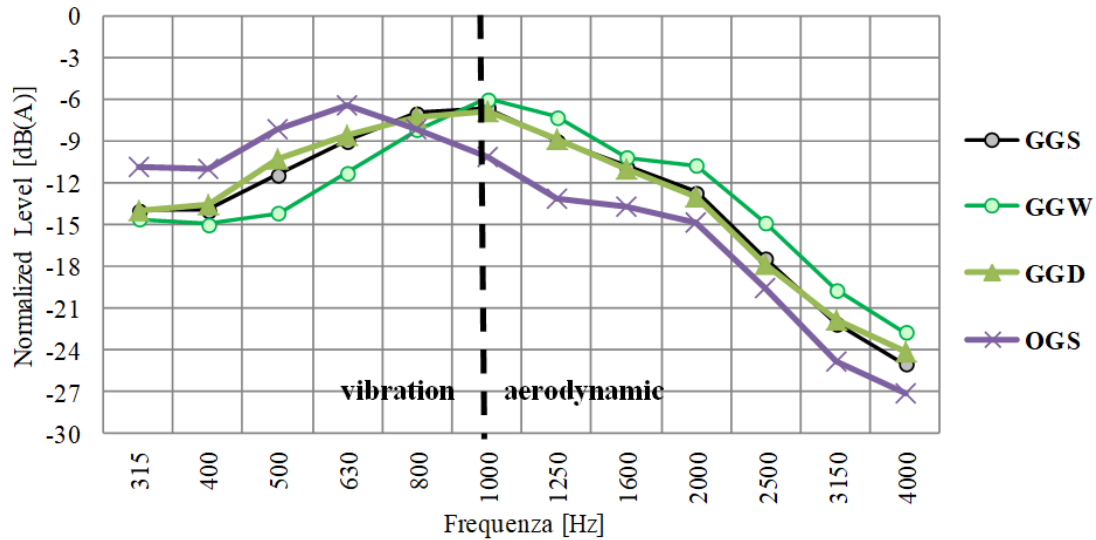
Figure 3.4 CPX noise levels of the pavements by the four asphalt mixtures

3.3 Noise reduction mechanism adding crumb rubber by DP and WP

3.3.1 Tires-pavement noise generation and research methods

According to the analysis in the sub-chapter 3.1.1, the parameters that may influence the low-noise ability of pavements can be summarized in Figure 3.5. With a boundary of 1000 Hz, tire/pavement noise can be divided into high-frequency range and low-frequency range. For low-frequency areas, reducing the texture and stiffness will contribute to improving the low-noise ability of the pavement; for high-frequency areas, improving the texture level, sound absorption, and air voids will contribute to improving the low-noise ability.
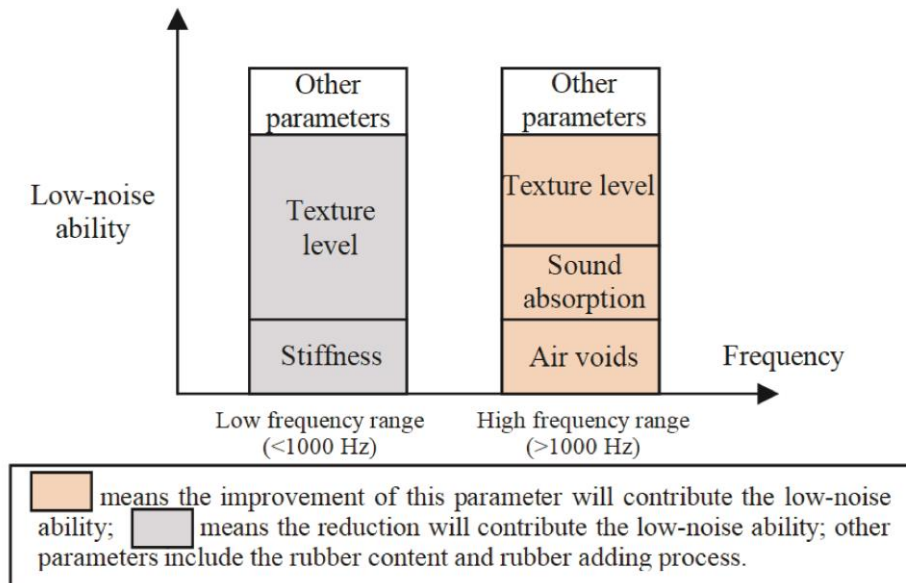
Figure 3.5 Effect of varying parameters on the low-noise ability

In order to better understand the effects of adding crumb rubber particles by the DP and WP, the noise-related testing results of asphalt mixtures, GGW, GGS, and GGD are used in this subchapter. Figure 3.6 and Figure 3.7 show two assuming examples of low-noise abilities of ACs in the low-frequency range and high-frequency range, respectively. Through these two examples, it will show how to refer the conclusion by using the "control variable methods".

As it can be observed from the Figure 3.6, in order to highlight the effect of the unknown factor (adding crumb rubber), the other known factors (texture level, air voids, and sound absorption) in the asphalt mixtures should be kept equal. However, it should be noted that it is very difficult to keep these factors equal in the actual designing process. An alternative approach is that although these known factors contribute unequally to low-noise abilities, the effects of adding crumb rubber particles by DP and WP can be inferred inversely by the comparison of the contribution values of known factors. For example, as we can see from the comparison of "AC with SBS" and "AC with CRM (DP)" in Figure 3.6, AC with CRM (DP) has higher texture level and stiffness, which are not conducive to low-noise ability (see its color), but it shows higher low-noise ability. Hence it can be inferred the effects of "rubber content" and "DP" on low-noise ability. Similarly, as it can be seen from the comparison of "AC with SBS" and "AC with CRM (DP)" in Figure 3.7, AC with CRM (DP) has lower texture level, sound absorption, and air voids, which are conducive to low-noise ability (see its

color), but it shows lower low-noise ability. Hence it can be inferred the negative effects of "rubber content" and "DP" on low-noise ability.
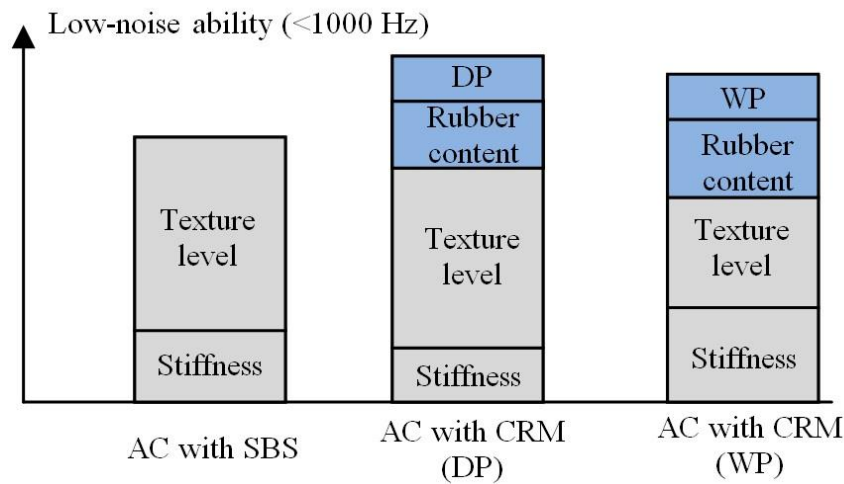
Figure 3.6 An example of low-noise abilities of varying AC in the low-frequency range
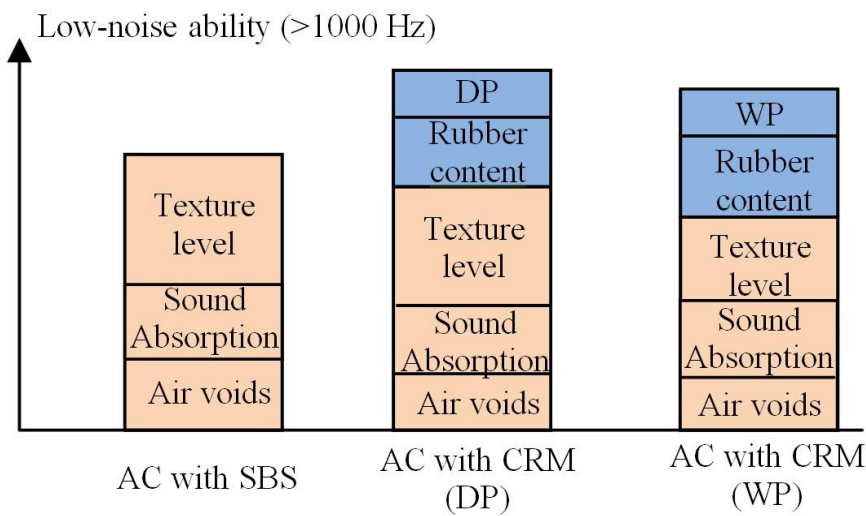
Figure 3.7 An example of low-noise abilities of varying AC in the high-frequency range

3.3.2 Sound absorption mechanism

The absorption coefficient is a function of the air void content and the proportion of acoustic energy not reflected by the surface of the material for a normal incidence plane wave (Lu & Harvey, 2011). When sound waves hit material with high air voids, the waves travel through the air paths in the material, and sound energy is dissipated by the frictional and viscous losses in the pores and the vibration of the small particles of the

material (Ongel et al. 2007). Therefore, in principle, for two materials having the same energy dissipation capacity, a higher air voids mean a larger sound absorption coefficient (Lu & Harvey 2011; Praticò et al. 2017).

Figure 3.8 shows the box plots of the sound absorption of the four asphalt mixtures, including the first and third quartile and the maximum and minimum absorption values as well as the mean and median value found in the 250 to 4000 Hz frequency range. The air voids of the four asphalt mixtures are also listed in order to evaluate its effect on sound absorption.

By comparing GGW and GGS, it can be found that although GGW has lower air voids (5.01%) compared to the GGS (9.1%), GGW shows similar or even higher (in certain frequency ranges) sound absorption coefficient. Similarly, by comparing GGD and GGS, it can be found that although GGD has similar air voids (8.39%) compared to GGS (9.1%), GGD shows obviously higher sound absorption coefficient. These are proof that the effect of adding crumb rubber particles by DP or WP can improve the acoustic absorption performance of asphalt mixtures since the rubber particles can use their viscous energy consumption, that is, the damping mechanism, to convert the acoustic energy or mechanical energy into heat dissipation. However, it should be noted that since GGD has a higher value of air voids and sound absorption coefficient compared to GGW, it is difficult to compare such effect between WP and DP. On the other hand, it should be noted that GGW and GGD have higher asphalt content compared to GGS. Therefore, the higher CR content allows more bitumen to be added to the mixture, thereby increasing the energy dissipation capacity of the material.
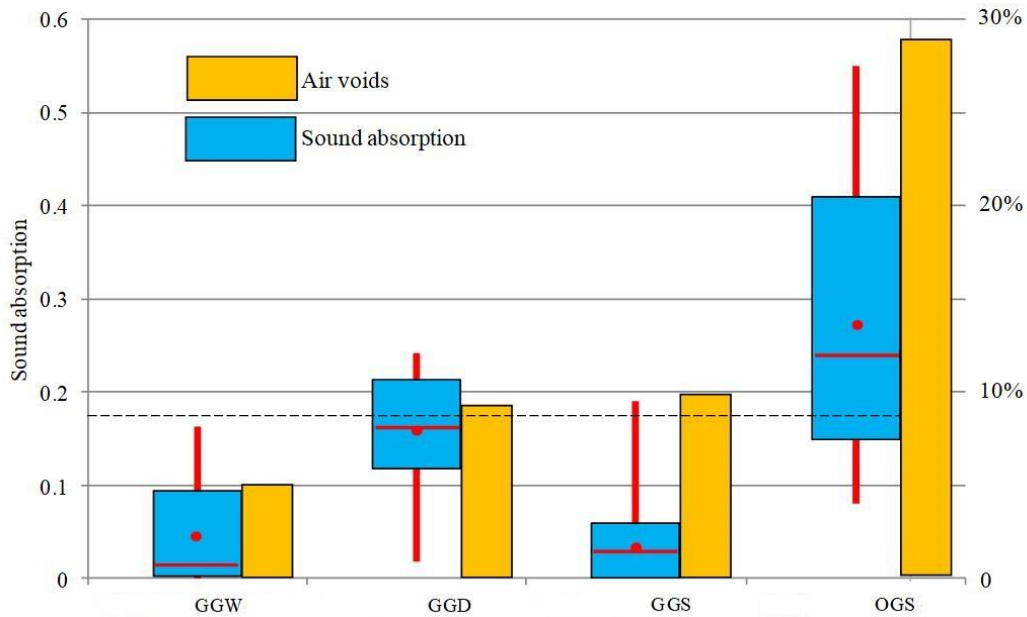
Figure 3.8 Sound absorption and air voids of the four asphalt mixtures

3.3.3 Tire/pavement noise reduction mechanism

As it is known to all that the pavement texture can have a significant effect on noise reduction, which has been discussed in sub-chapter 3.1.1. In this part, the texture level and CPX noise level are evaluated and compared, in order to infer the effect of factors other than texture levels on low noise ability.

Figure 3.9 shows the comparison of normalized CPX noise levels between GGS and GGW as well as other parameters that can influence the noise generation. It can be found that at the low-frequency range: the texture level is GGS<GGW and the stiffness modulus is GGS<GGW; both of the two parameters should contribute GGS to having a better performance of noise reduction, but actually GGW is showing lower noise level. Since all the other noise-related parameters (likes, VA and sound absorption) are equal or will not have much influence on low-frequency noise, it can be inferred that by adding crumb rubber by WP, the vibration generated by tire/road may be effectively reduced because of the higher damping of asphalt rubber, thereby reducing low-frequency noise.

On the other hand, at the high-frequency range, tire/pavement noise is usually generated by aerodynamic mechanism, a complex process that combines multiple factors, likes air pumping, stick-slip, stick-snap et al. The influencing factors, observed from the experiments, include pavement texture and sound absorption coefficient. It can be found from Figure 3.8 that GGS and GGW show similar values of air voids and sound

absorption coefficients, but GGW has a higher texture level, which should contribute GGW to having a better performance of noise reduction, but the actual result is that GGW is showing lower low-noise ability. Hence, it can be predicted that adding crumb rubber by means of WP may not improve the noise reduction in high-frequency range and it even has a negative effect. Such a negative effect in the high-frequency range agrees with the results reported by Paje et al. (2013) and Vazquez et al. (2016), who explained that the mechanism of high-frequency noise is much more complex, the negative effect cannot be predicted very accurately. It may due to the lower dispersion of the sound or higher reflections (Vazquez et al. 2016) as well as the increase of stick-slip and stick-snap mechanisms which may be caused by adding crumb rubber particles in WP. However, it should be noted that adding crumb rubber by WP can affect high-frequency noise, but it may not necessarily be a decisive factor, or it can be regarded as a "Neutral" factor.

In summary, through adding crumb rubber particles in the asphalt mixture by WP, the noise generated by the vibration mechanism can be effectively reduced; for noise generated by the aerodynamic mechanism, such effect is weak or it may have a negative effect, which can be regarded as "Neutral".
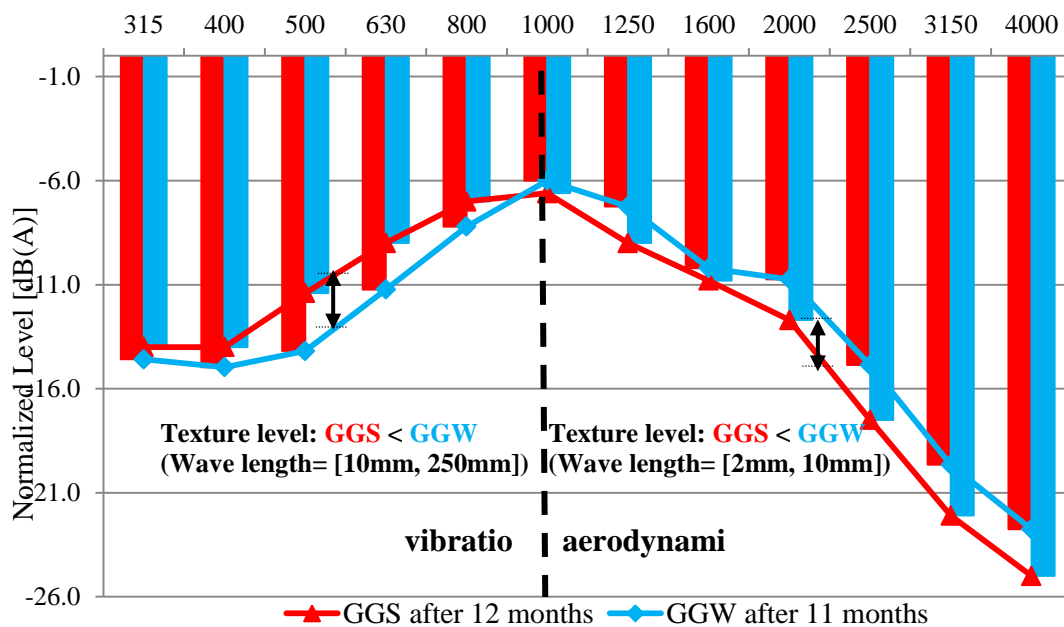
V_A: **GGS (9.1%)** ≈ **GGW (8.92%)**

Sound absorption: GGS (0.039) ≈ GGW (0.037)

Stiffness modulus: GGS (3392MPa) <GGW (5270MPa)
(T=20℃; rise time=125ms)

Rubber content: GGS (0) <GGW (1.8%)

Figure 3.9 Comparisons between GGS and GGW

Figure 3.10 Contributions of different parameters at a low-frequency range
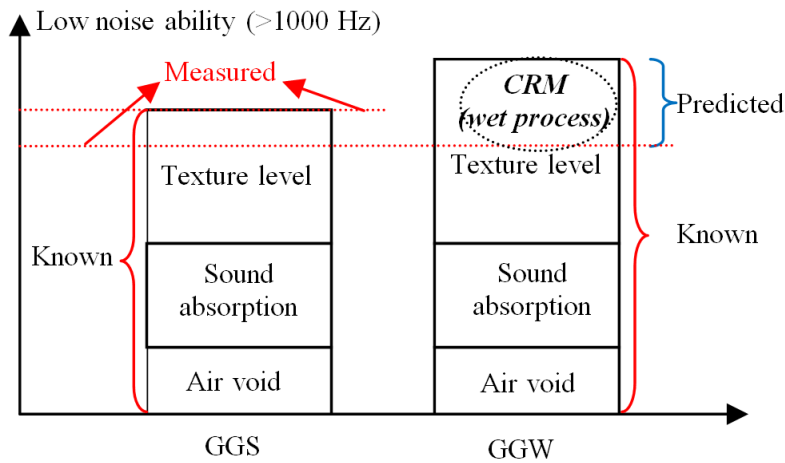
Figure 3.11 Contributions of different parameters at a high-frequency range

Figure 3.12 shows the comparison of normalized CPX noise levels between GGD and GGW as well as other parameters that can influence the noise generation. At the low - frequency range: the texture level is GGD<GGW and the stiffness modulus is GGD<GGW; the two asphalt mixtures are added by similar crumb rubber contents, which are 1.82% and 1.7%, respectively. These parameters should contribute to GGD to having a better performance of noise reduction, but actually, GGW shows a lower noise level. The only difference is that one is used by the DP and the other one is used by WP. Hence, it can be inferred that the addition of the crumb rubber particles by the WP may be more effective than the one by the DP to reduce noise generated by vibration mechanism. This may be explained that rubber particles, which are playing the role of aggregates during DP, are outside of the real aggregates and such internal structure is similar to the conventional asphalt mixtures without crumb rubber, and the damping

improvement is very limited. In contrast, when the crumb rubber particles are added by the WP, they will form asphalt rubber, which is distributed throughout the structure and can greatly increase the damping of the asphalt mixture.

As far as the high-frequency range, as shown in Figure 3.12, the texture level is GGD<GGW, which should contribute GGW to having a better performance of noise reduction, but actually, GGD shows a lower noise level. It may be inferred that the higher sound absorption coefficient of GGD results in a lower noise level. Because sound absorption is playing an important role in high-frequency noise-reduction, which is related to the aerodynamic mechanism.

In summary, the mechanism of reducing the noise level by adding the rubber particles to the asphalt mixture by WP is that it may effectively reduce the noise generated by the vibration, compared to non-rubberized asphalt mixtures. It should be noted that such vibration reduction can also reduce the generation of vibration waves from the vibration source and realize the design concept of the anti-vibration pavement.

The mechanism of reducing the noise by adding the rubber particles to the asphalt mixture by DP is that it can more effectively improve the sound absorption coefficient of the asphalt mixture compared with non-rubberized gap-graded asphalt mixtures, thereby reducing the noise generated by the aerodynamic mechanism.

Based on the above analysis of the noise reduction mechanism of rubberized LNPs, GGW may be the optimized surface layer of the developed vibration and noise absorption system. Because it not only has an excellent performance in reducing tire/pavement noise but also reduces the vibration wave generated at the tire/pavement interface and realizes the design concept of anti-vibration pavement.
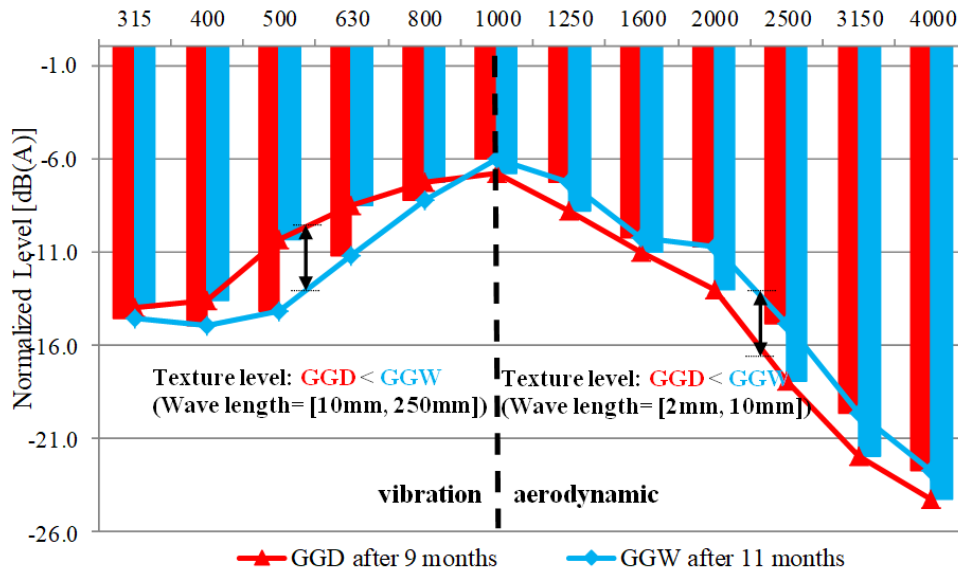
V$_A$: GGD (8.39%) ≈ GGW (8.92%)

Sound absorption: GGD (0.15) > GGW (0.039)

Stiffness modulus: GGD (2987MPa) < GGW (5270MPa)
(T=20℃; rise time=125ms)

Rubber content: GGD (1.82%) ≈ GGW (1.7%)

Adding rubber process: GGD (DP) GGW (WP)

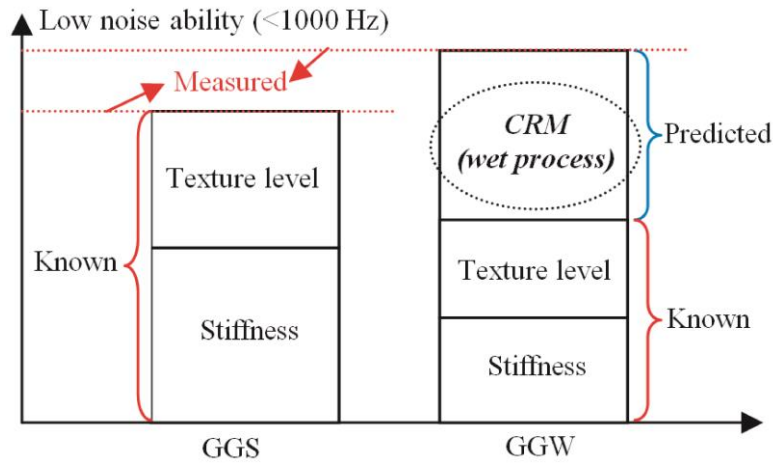Figure 3.12 Comparisons between GGD and GGW
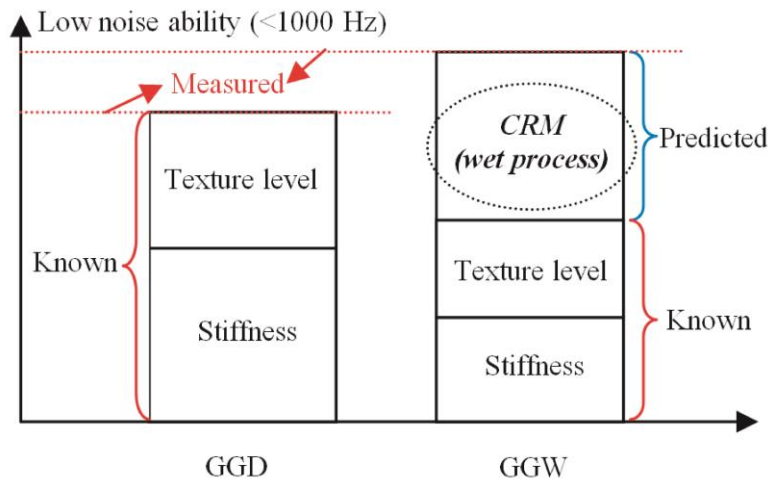
Figure 3.13 Contributions of different parameters at a low-frequency range
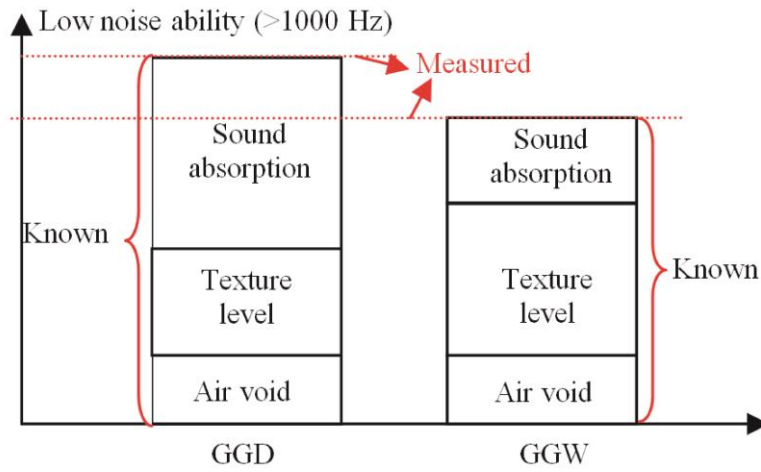
Figure 3.14 Contributions of different parameters at a high-frequency range

Chapter 4: Development of a novel calculation model for characterizing the damping effect in the pavement system

Damping has been widely used in the design of heavy machinery and large structural members (Biligiri 2013). Research has used damping effects in embankments and bridges to distinguish vibration damping capabilities of two different materials (Schubert et al. 2010; Wang & Höeg 2010). Furthermore, damping ratios of the asphalt mixtures (including asphalt overlays for rehabilitation) were estimated in various other studies to understand damping and vibratory mechanisms along with the estimation of moduli (or stiffness) of these mixtures (Hochuli et al. 2001; Chatti et al. 2004; Broutin & Theillout 2010).

In pavement engineering, in order to account for damping and mass inertia effects, damping properties must be defined for all pavement layers. The sources of damping could be an arbitrary damping factor, friction factor, or viscoelastic material behavior. It is worth noting that although many studies have utilized the "damping ratio" in pavement engineering, which is a basic vibrational parameter used to determine the damping capacity, no similar work has been undertaken in characterizing the damping effect in pavement engineering.

4.1 Construction of damping matrix

In the vibration field, in order to characterize the damping effect, the most commonly used method is through constructing a damping matrix. The damping matrix of the structure should not be calculated based on the structural dimensions and the damping property of the materials. One might think that the damping matrix of a structure should be determined from the damping properties of a single element, just as the way to determine the stiffness matrix of the structure. However, determining the damping matrix in this way is impractical because the damping properties of the material are not well established, unlike the elastic modulus calculated for the stiffness. Even if these

characteristics are known, the resulting damping matrix does not account for most of the energy consumed by, e.g., the friction at the steel joints, the opening, and closing of cracks in the concrete, the non-structural components, the pressure of the partition walls and the friction between the structures itself, some of which are even difficult to identify. Therefore, the damping matrix of the structure should be determined according to its modal damping ratio, which takes into account all the energy dissipation mechanisms (Chopra 2007). Damping is generally specified by numerical values for the modal damping ratios, and these are sufficient for analysis of linear systems with classical damping. Two procedures for constructing the damping matrix for a structure from the modal damping ratios are presented.

4.1.1 Classical damping matrix

Classical damping is an appropriate idealization if similar damping mechanisms are distributed throughout the structure (e.g., a multistory building with a similar structural system and structural materials over its height). Rayleigh damping is developed for constructing a classical damping matrix for a structure by modal damping ratios. As a first step toward constructing a classical damping matrix somewhat consistent with experimental data, Rayleigh damping is considered as:

$$c = \alpha m + \beta k \tag{4.1}$$

where c, m, and k are damping matrix, mass matrix, and stiffness matrix, respectively; α is the mass proportional Rayleigh damping coefficient, in s^{-1}; β is the stiffness proportional Rayleigh damping coefficient, in s. The modal damping ratio of the n_{th} mode is

$$\zeta_n = \frac{\alpha}{2}\frac{1}{\omega_n} + \frac{\beta}{2}\omega_n \tag{4.2}$$

where ζ_n and ω_n are the damping ratio (%) and natural frequency (Hz), respectively. The coefficients α and β can be determined from specified modal damping ratios ζ_i and ζ_j for the i_{th} and j_{th} modes, respectively. Expressing Eq. (4.2) for these two modes in matrix form leads to

$$\frac{1}{2}\begin{bmatrix} 1/\omega_i & \omega_i \\ 1/\omega_j & \omega_j \end{bmatrix}\begin{Bmatrix} \alpha \\ \beta \end{Bmatrix} = \begin{Bmatrix} \xi_i \\ \xi_j \end{Bmatrix} \tag{4.3}$$

where ω_i and ω_j are the natural frequencies of the i_{th} and j_{th} mode, respectively; ζ_i and ζ_j are the modal damping ratios of the i_{th} and j_{th} mode, respectively. These two algebraic equations can be used to determine the coefficients α and β. If both modes are assumed to have the same damping ratio ζ, which is reasonable based on experimental data, then

$$\alpha = 2\xi\frac{\omega_i\omega_j}{\omega_i + \omega_j} \tag{4.4}$$

$$\beta = 2\xi\frac{1}{\omega_i + \omega_j} \tag{4.5}$$

4.1.2 Non-Classical damping matrix

The assumption of classical damping is not appropriate if the system to be analyzed consists of two or more parts with significantly different levels of damping (Chopra 2007). One such example is a soil–pavement system. While the underlying soil can be assumed as elastic in the analysis of many structures, soil–pavement interaction should be considered in the analysis of structures with very short natural periods. The modal damping ratio for the soil system would typically be much different from the one of structure, say 0.02 for the soil region compared to 0.05-0.1 for the pavement layers. (Zeng et al. 2001) Therefore, the assumption of classical damping would not be appropriate for the combined soil-pavement system, although it may be reasonable for the structure and soil regions separately.

In addition, the assumption of classical damping may not be appropriate either for structures with special energy-dissipating devices or on a base isolation system (Chopra 2007). For example, pavements with a special energy-dissipating layer (a damping layer or vibration-absorbing layer) can not be characterized by constructing the classical matrix.

The nonclassical damping system has complex modal properties and it may be solved by the method proposed by Foss through the complex-modal analysis method (Foss

1956). However, this method has not been widely used in practical structural analysis. The reasons are mainly two aspects: first, the characteristic complex modal involved is 2N x 2N order, which is doubled compared to normal modal analysis. The complex mathematical operations must be performed and it can greatly increase the computational complexity; second, the characteristics of complex mode cause difficulties in explaining the physical meaning of the system. Therefore, most scholars generally avoid using complex damping methods in research.

4.1.3 Reviewing of existing methods in pavement engineering

So far several researchers have tried to get meaningful values of Rayleigh damping coefficients α and β (or damping matrix); in the specific case of AC pavements, some researchers have defined damping coefficients for the pavement layers instead of considering viscoelasticity. In general, these existing methods can be divided into two types:

(1) In the first type, the damping matrix for each individual subcomponent (each layer) was assembled, where the frequency range was considered that of the entire undamped system. Typically, in this method, the natural frequency of the road system was calculated firstly. Then the classical damping matrix to represent each layer or each material was calculated by Rayleigh damping and the nonclassical damping matrix was assembled via standard finite element techniques (e.g., define/input alpha and beta in FEM software) (Ling & Newcomb 1991; Zeng et al. 2005; Al-Qadi et al. 2008; Tang et al. 2013; Xu 2014). The weakness of this method has been pointed out by Wang et al. (2008): such method results in a non-orthogonal global matrix and cannot be decoupled, thus obscuring the meaning of the mode shape and natural frequency between the sub-components and the entire system, and ignoring the interaction of sub-components. It should be noted that, in the research field of vibration, non-orthogonal damping may be decoupled in line with the correct physical meaning by the so-called forced decoupling which is to ignore the non-diagonal coupling coefficient in the damping matrix but the errors caused can be large or small (Park et al. 1992; Clough et al. 1995).

(2) In the second type, the natural frequency of each individual subcomponent (each layer) was calculated firstly in order to form a classical damping matrix by the Rayleigh damping. Either empirically estimating (Uddin & Garza 2010), or

separating each sub-component as a free-free boundary condition (Wang et al. 2009), was used to calculate the natural frequency of each individual subcomponent (each layer). This method suffers from the drawback that it is lacking in an effective method to calculate the natural frequency of each subcomponent (layer), which may result in large errors compared to the actual condition. In addition, the method to separate each sub-component to obtain natural frequency also ignores the interactions between sub-components.

In order to overcome the weaknesses of the existing methods, a modified damping model is established. This modified model consists of two main steps:

(1) According to the method proposed by Liang et al. (2017), in order to characterize the damping difference between different layers, the multi-layered structure is divided into sub-layers, each of which consists of materials of similar physical properties. (E.g. asphaltic materials can be regarded as one sub-layer; granular materials and soils can be regarded as one sub-layer); then each sub-layer is treated as a system to select the corresponding Rayleigh damping parameter (Liang et al. 2017).

(2) The Rayleigh damping parameters are determined to make sure the target damping ratio (the small-strain material damping) and modal damping ratios calculated from natural frequencies match best by linear time-domain solutions (Kwok et al. 2007).

The detailed introduction of the proposed model to characterize the damping effect is described in the following sub-chapters.

4.2 A novel model for characterizing the damping effect in road structures

4.2.1 Development of the damping matrix for road structures

In this part, a novel calculation model will be proposed by combining the principal method for nonclassical system introduced by Chopra et al. (2007) and the improved model proposed by Liang et al. (2017), who has modified the method to characterize the damping difference between layered soils.

As a multilayer system, the pavement consists of finite layers over a semi-infinite subgrade. The different paving materials of the layered structure have significantly different damping. To characterize the difference between the different layers, the road structure can be divided into several sub-layers, depending on the materials, and each subsystem chooses the corresponding Rayleigh damping parameters to form the damping matrix (Liang et al. 2017). Generally speaking, the road structure can be divided into the asphaltic layer and granular material layer (including the soil) according to similar physical property and the damping ratio, as shown in Figure 4.1. Based on this road structure division, the schematic to assemble the damping matrix in road engineering can be obtained, where the conventional road structure is divided into two subcomponents according to the different physical and damping properties. One subcomponent is the finite asphaltic layer, and the other one is the sum of subbase and infinite subgrade, both of which have similar physical and damping properties (Zeng et al. 2001). The stiffness and mass matrix of the combined AC (Asphaltic materials) – S+S (Subbase+Soil) system is assembled from the corresponding matrix for the two subsystems. The portion of these matrixes associated with the common degree of freedoms (DOFs) at the interface {I} between the two subsystems include contributions from both subsystems (Chopra et al. 2007).

As far as the two subsystems, since both of them have similar physical and damping property, the classical damping matrix can be applied directly, which can be described as,

$$\frac{1}{2}\begin{bmatrix} 1/\omega_{i(AC)} & \omega_{i(AC)} \\ 1/\omega_{j(AC)} & \omega_{j(AC)} \end{bmatrix}\begin{Bmatrix} \alpha_{(AC)} \\ \beta_{(AC)} \end{Bmatrix} = \begin{Bmatrix} \xi_{i(AC)} \\ \xi_{j(AC)} \end{Bmatrix} \tag{4.6}$$

$$\frac{1}{2}\begin{bmatrix} 1/\omega_{i(S+S)} & \omega_{i(S+S)} \\ 1/\omega_{j(S+S)} & \omega_{j(S+S)} \end{bmatrix}\begin{Bmatrix} \alpha_{(S+S)} \\ \beta_{(S+S)} \end{Bmatrix} = \begin{Bmatrix} \xi_{i(S+S)} \\ \xi_{j(S+S)} \end{Bmatrix} \tag{4.7}$$

where ω, α, β, and ζ are the corresponding natural frequency, Rayleigh damping parameters, and damping ratio, respectively. Finally, the nonclassical damping matrix can be assembled via standard finite element techniques. E.g., define/input Rayleigh damping parameter $\alpha_{i(AC)}, \beta_{j(AC)}, \alpha_{i(S+S)}, \beta_{j(S+S)}$ in FEM software directly.

However, it should be noted that here the $\omega_{i(AC)}, \omega_{j(AC)}, \omega_{i(S+S)}, \omega_{j(S+S)}$ are the natural frequencies without the consideration of interactions between two subsystems, as shown in Figure 4.2. These values should be modified by characterizing the interaction in order to construct a new classical damping matrix of each subsystem.
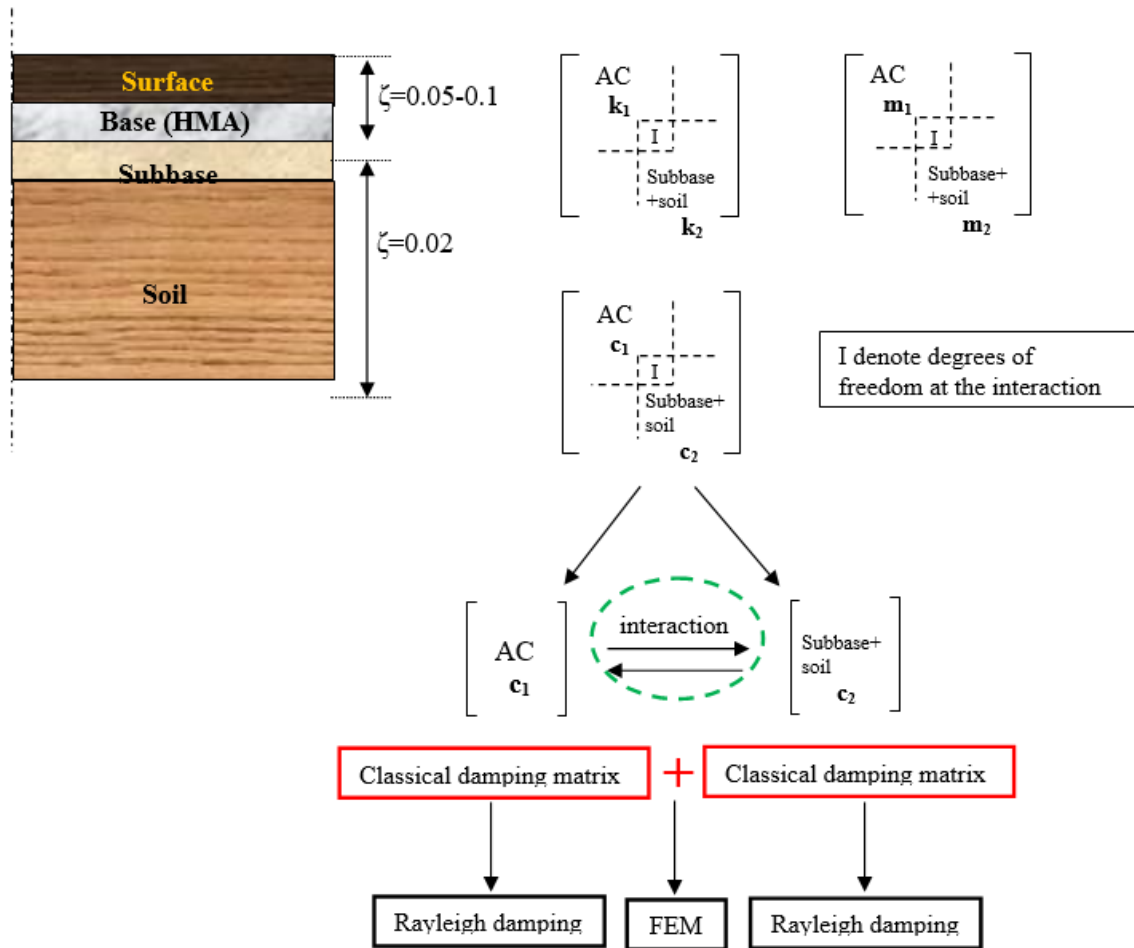
Figure 4.1 Schematic of solving nonclassical damping matrix problem in road engineering
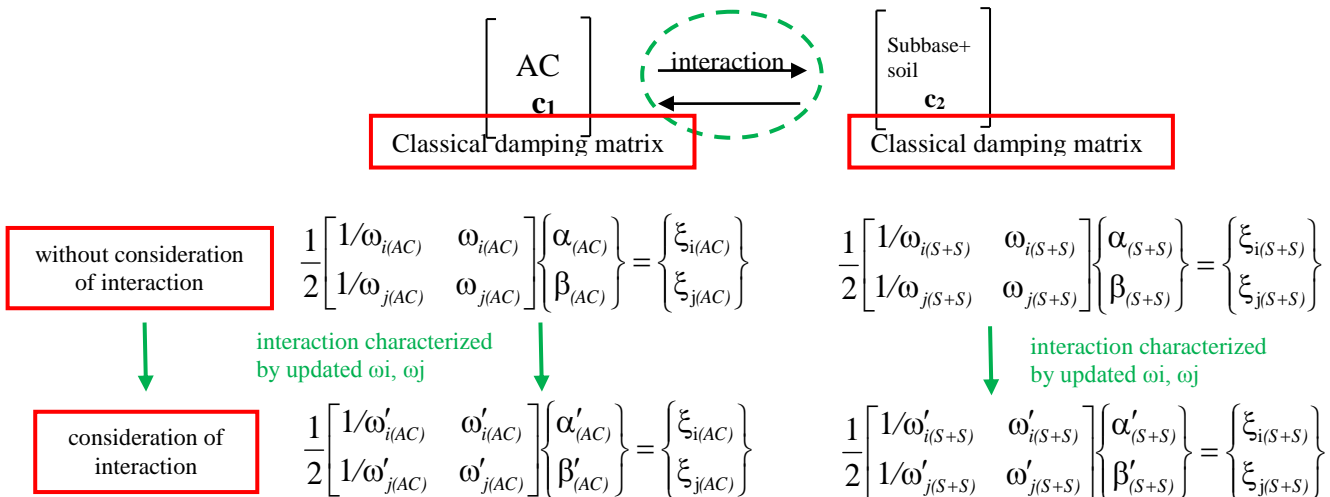
$$\mathbf{c}_{(AC)} = \alpha'_{(AC)}\mathbf{m}_{(AC)} + \beta'_{(AC)}\mathbf{k}_{(AC)} \qquad \mathbf{c}_{(S+B+S)} = \alpha'_{(S+B+S)}\mathbf{m}_{(S+B+S)} + \beta'_{(S+B+S)}\mathbf{k}_{(S+B+S)}$$

Figure 4.2 Schematic of characterizing the interaction between subcomponents

As far as the "subbase+soil" layer is concerned, its thickness is so large that the effect of the asphaltic layer on its natural frequency can be disregarded. As a result of uncomplicated boundary conditions, $\omega_{i(S+S)}$, $\omega_{j(S+S)}$ can be extracted directly from the FE model by ABAQUS. However, for the finite layers (AC layer), the support effect from the infinite layer is causing complicated boundary conditions so that the $\omega_{i(AC)}, \omega_{j(AC)}$ cannot be extracted directly. In order to solve this problem, an idealized shear beam model proposed by Dobry et al. (1976) to estimate the fundamental period is used.
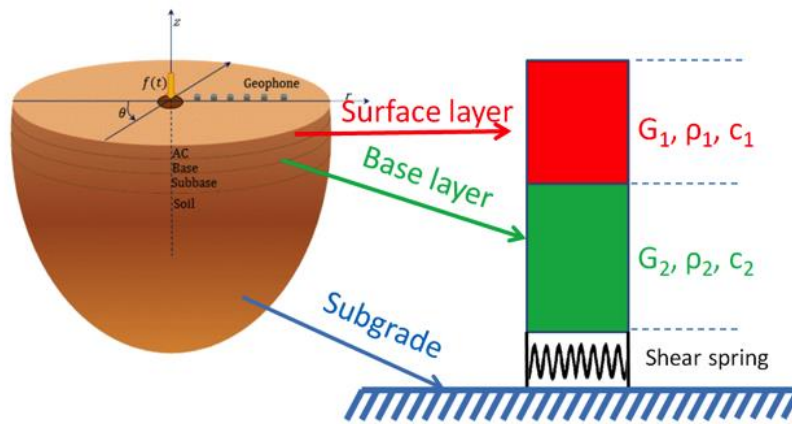
Figure 4.3 Shear beam model for pavement

In this model, the multilayer system is transformed into a layered system composed of linear elastic shear beams, without considering the horizontal length, as shown in Figure 4.3. Each shear beam is considered to be homogeneous for the same cross-sectional area and extends indefinitely in the horizontal direction. The support effect of the subgrade on the pavement system is modeled by a shear spring, which takes into account the shear stiffness of soil.

The parameters of each layer needed for the computation of the fundamental period are including the mass density ρ, the shear-wave velocity c, and the thickness of the pavement, H. Alternatively to c, the shear modulus can be specified by $G = \rho c^2$.

Considering an infinitesimal segment of one layer, the transverse free shear vibration is analyzed (see Figure 4.4). The shear displacements at the bottom and top of the micro-

segment, and the shear force at the top of the micro-segment are assumed as u,

$u + \dfrac{\partial u}{\partial y} dy$ and $Q + \dfrac{\partial Q}{\partial y} dy$, respectively. The differential equation for free vibration of the

shear beam can be obtained,

$$\frac{\partial^2 u}{\partial t^2} = c^2 \cdot \frac{\partial^2 u}{\partial y^2} \tag{4.8}$$

where y is the vertical coordinate of the micro-segment and t is the vibration time. The general solution of u(y, t) satisfying Eq. (4.8) is an infinite series. If the shear beam vibrates in the first mode at the fundamental frequency, then,

$$u(y,t) = U(y) exp(i\omega t) \tag{4.9}$$

where U(y) is the first modal shape and i is $\sqrt{-1}$. Substituting Eq. (4.9) into Eq. (4.8), one can obtain the vibration mode shape equation as follows,

$$\frac{d^2 U(y)}{dy^2} + \frac{\omega^2}{c^2} U(y) = 0$$

$$\Rightarrow U(y) = A cos(\frac{\omega}{c} y) + B sin(\frac{\omega}{c} y) \tag{4.10}$$

Correspondingly, the mode shape equations for surface and base layer in the pavement model can be given as follows,

the surface layer,

$$U_1(x) = A_1 cos\frac{\omega x}{c_1} + B_1 sin\frac{\omega x}{c_1} \tag{4.11}$$

and the base layer,

$$U_2(x) = A_2 cos\frac{\omega x}{c_1} + B_2 sin\frac{\omega x}{c_1} \tag{4.12}$$

where $U_1(x)$ and $U_2(x)$ are the first mode shapes of the surface layer and base layer, respectively. Taking into account the boundary conditions, the natural frequency can be determined as the solution of the system composed of those vibration shapes.
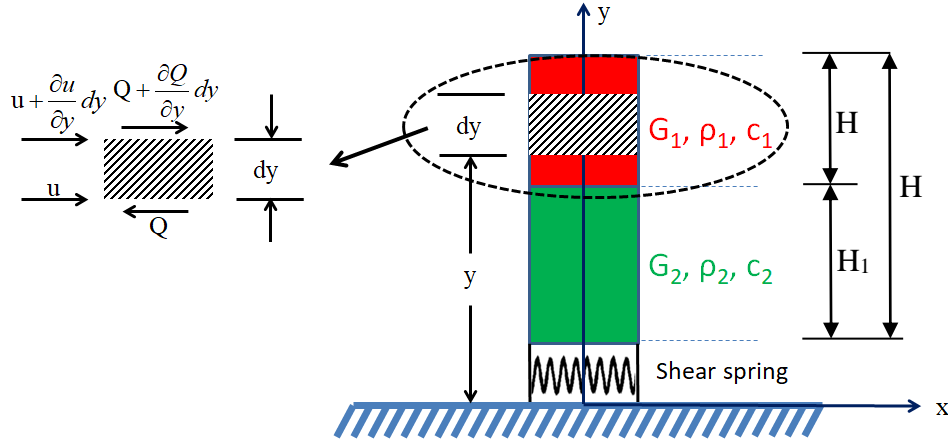
Figure 4.4 Infinitesimal segment section of one layer
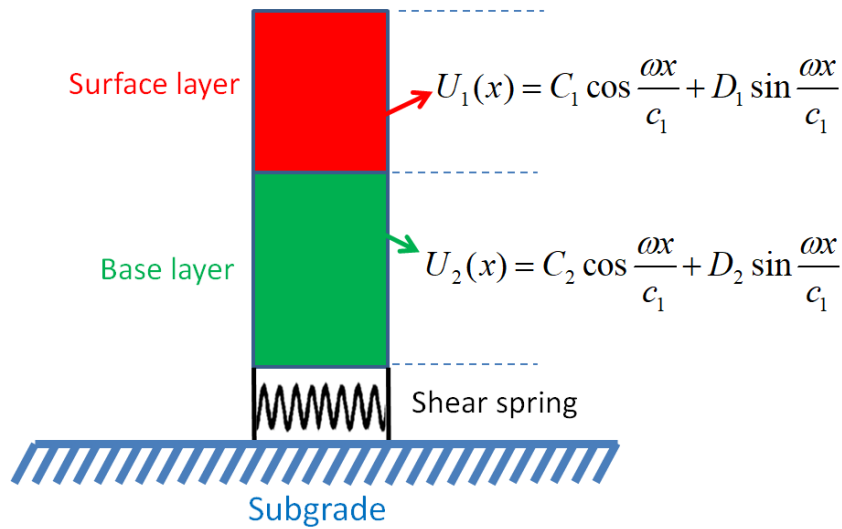
Figure 4.5 Pavement shear beam model

Boundary conditions at the top and bottom of the beam, and the displacement and stress continuity conditions at the interfaces are as follows:

The free boundary condition at the top of the beam is,

$$\frac{dU_1(x)}{dx}\Big|_{x=H} = 0 \tag{4.13}$$

The stress continuity condition at the bottom of the beam is,

$$G_2 \cdot \frac{dU_2(x)}{dx}\bigg|_{x=0} = -k \cdot U_2((x)\big|_{x=0}$$ (4.14)

The displacement and stress continuity conditions at the interface of the two layers are,

$$G_1 \frac{dU_1(x)}{dx}\bigg|_{x=H_2} = G_2 \frac{dU_2(x)}{dx}\bigg|_{x=H_2}$$ (4.15)

$$U_2(H_2) = U_1(H_2)$$ (4.16)

Substituting Eq. (4.11) into Eq. (4.13):

$$tan(\frac{\omega}{c_1}H) = \frac{B_1}{A_1}$$ (4.17)

Substituting Eq. (4.11) and Eq. (4.12) into Eq. (4.14):

$$\frac{Kc_2}{G_2\omega} = \frac{B_2}{A_2}$$ (4.18)

Considering Eq. (11) and Eq. (12) as well as Eq. (4.15), (4.16), (4.17) and (4.18), the implicit solution of the natural frequency ω (the natural frequency of AC layer) can be given by,

$$tan(\frac{\omega}{c_1}H) = \frac{c_2G_1G_2\omega sin(\frac{\omega}{c_1}H_2) - c_1G_2^2\omega tan(\frac{\omega}{c_2}H_2)cos(\frac{\omega}{c_1}H_2) + c_2^2G_1K tan(\frac{\omega}{c_2}H_2)sin(\frac{\omega}{c_1}H_2) + c_1G_2Kc_2 cos(\frac{\omega}{c_1}H_2)}{c_2G_1G_2\omega cos(\frac{\omega}{c_1}H_2) + c_1G_2^2\omega tan(\frac{\omega}{c_2}H_2)sin(\frac{\omega}{c_1}H_2) + c_2^2G_1K tan(\frac{\omega}{c_2}H_2)cos(\frac{\omega}{c_1}H_2) - c_1G_2Kc_2 sin(\frac{\omega}{c_1}H_2)}$$ (4.19)

where ω is the natural frequency (Hz); c_1, c_2 are the shear-wave velocities (m/s) of the surface layer and base layer, respectively; H_1 and H_2 are the thicknesses (m) of the surface layer and base layer, respectively; G_1 and G_2 are the shear modulus (Pa) of the surface layer and base layer, respectively. K is the shear stiffness (N/m) of the subgrade. Considering that Eq. (4.19) is a periodic function, in order to make the solving process easier, it can be transformed into,

$$y(\omega) = tan(\frac{\omega}{c_1}H) - \frac{c_2 G_1 G_2 \omega \sin(\frac{\omega}{c_1}H_2) - c_1 G_2{}^2 \omega tan(\frac{\omega}{c_2}H_2) \cos(\frac{\omega}{c_1}H_2) + c_2{}^2 G_1 K tan(\frac{\omega}{c_2}H_2) \sin(\frac{\omega}{c_1}H_2) + c_1 G_2 K c_2 \cos(\frac{\omega}{c_1}H_2)}{c_2 G_1 G_2 \omega \cos(\frac{\omega}{c_1}H_2) + c_1 G_2{}^2 \omega tan(\frac{\omega}{c_2}H_2) \sin(\frac{\omega}{c_1}H_2) + c_2{}^2 G_1 K tan(\frac{\omega}{c_2}H_2) \cos(\frac{\omega}{c_1}H_2) - c_1 G_2 K c_2 \sin(\frac{\omega}{c_1}H_2)}$$

(4.20)

Values of ω are set from 0, 1, 2…to 50000 rad/s in order to obtain the function curve of y(ω). In this way, the solutions of the periodic function, ω_1 ω_2 $\omega_{3\ldots}\omega_n$, can be obtained by using the 'solver' function of excel.

As one example shown in Figure 4.6, according to the relationship between ω and y(ω), the first modal frequency, second modal frequency … nth modal frequency can be obtained.
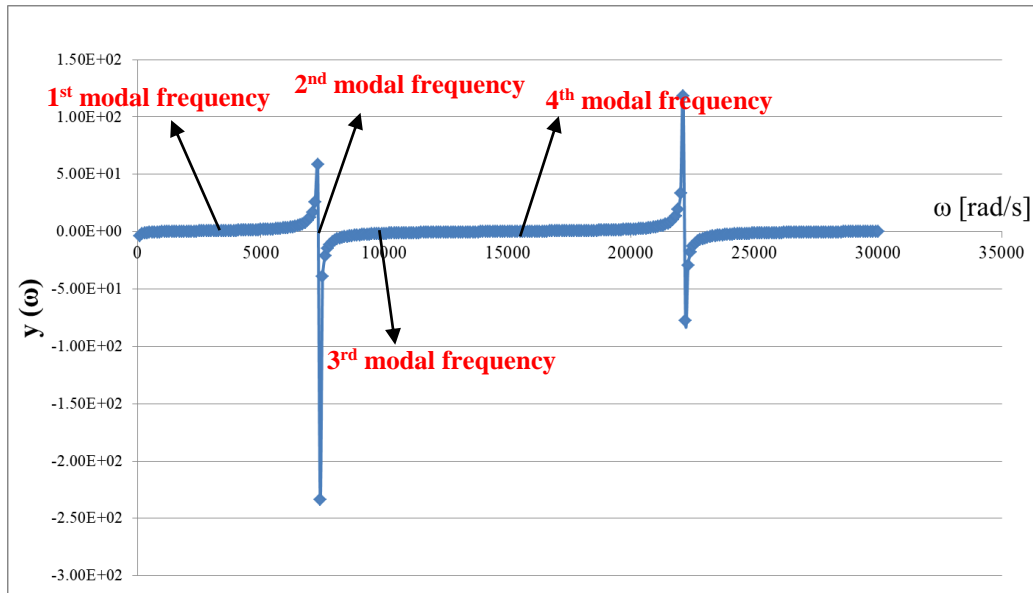
Figure 4.6 Relationship between ω and y(ω)

4.2.2 An improved method to determine Rayleigh damping parameters

The road structure is divided into different layers according to similar physical properties as well as damping properties, and the damping properties of each layer are characterized. The next step is to determine the Rayleigh damping parameters to make sure the target damping ratio (the small-strain material damping) and modal damping calculated from natural frequencies match best by linear time-domain solutions (Kwok et al. 2007).

As far as modal damping calculated from natural frequencies, a popular scheme that is often consistent with experimental data is Rayleigh damping. This method considers the damping matrix [C] as the combination of the mass proportional damping and the stiffness proportional damping, which can be described as,

$$c = \alpha m + \beta k \tag{4.21}$$

where α is the Rayleigh coefficient for the mass proportional damping whilst β is the Rayleigh coefficient for stiffness proportional damping. The relationship between α, β and the fraction of damping ξ at circular frequency ω for one-degree-of freedom system is given by,

$$\zeta_n = \frac{\alpha}{2}\frac{1}{\omega_n} + \frac{\beta}{2}\omega_n \tag{4.22}$$

From Eq. (4.22), it can be conjectured that there is a relationship between damping and frequency whilst damping is mostly regarded as frequency independent in a limited frequency range by most researchers, who use the small strain material damping to be taken as the constant target damping to the form of the Rayleigh damping formulation (Kwok et al. 2007). Consequently, the Rayleigh damping coefficients, α and β should be appropriately formulated in order to fit the experimental results.

Typically, there are two principal methods for determining the parameters α and β to be used in FEM analysis. The first one was proposed and applied by Idriss (1973) in the QUAD4 software for geotechnical seismic analysis, and then it was applied by some researchers of pavement engineering (Wang et al. 2009; Sun et al. 2013), who assumed that the contributions of mass and stiffness proportional coefficients are the same. In this way, α and β can be given as,

$$\alpha = \xi_1 \omega_1 \tag{4.23}$$

$$\beta = \frac{\xi_1}{\omega_1} \tag{4.24}$$

where ξ_1 is the damping ratio and ω_1 is the natural frequency (rad/s) of the system. The relationship between frequency and damping ratio is described in Figure 4.7, and it is obvious that it results in an overestimation of damping in all frequency ranges, determining a lower dynamic response of the system.
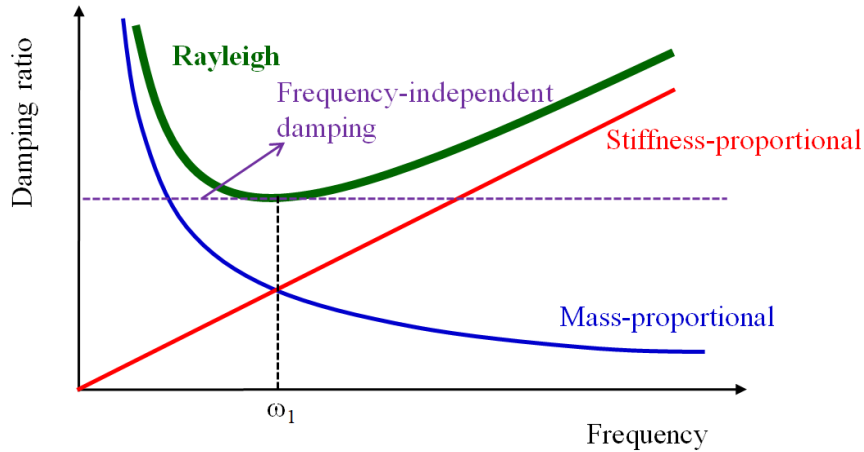
Figure 4.7 Relationship between damping & freq. by QUAD4

Hudson et al. (1994) developed appropriate improvements to the shortcomings of using only the fundamental frequency to determine the damping coefficient and modified the QUAD4 as QUAD4M, which was also applied in the other pavement engineering research (Ju et al. 2007; Al-Qadi et al. 2008).

This method uses the first two natural frequencies ω_1 and ω_2 to determine the reference frequency for α and β; particularly, ω_1 is the first fundamental frequency, and $\omega_2 = n\omega_1$, where n is an odd number greater than ω_e/ω_1; ω_e is the dominant frequency. The coefficients α and β can be determined by these relationships:

$$\alpha = 2\xi \frac{\omega_1 \omega_2}{\omega_1 + \omega_2} \tag{4.25}$$

$$\beta = 2\xi \frac{1}{\omega_1 + \omega_2} \tag{4.26}$$

As shown in Figure 4.8, this method can take into account both the natural frequencies and spectral characteristics of the structure but underestimate the damping between ω_1 and ω_2 as well as overestimate the damping outside the considered frequency range.
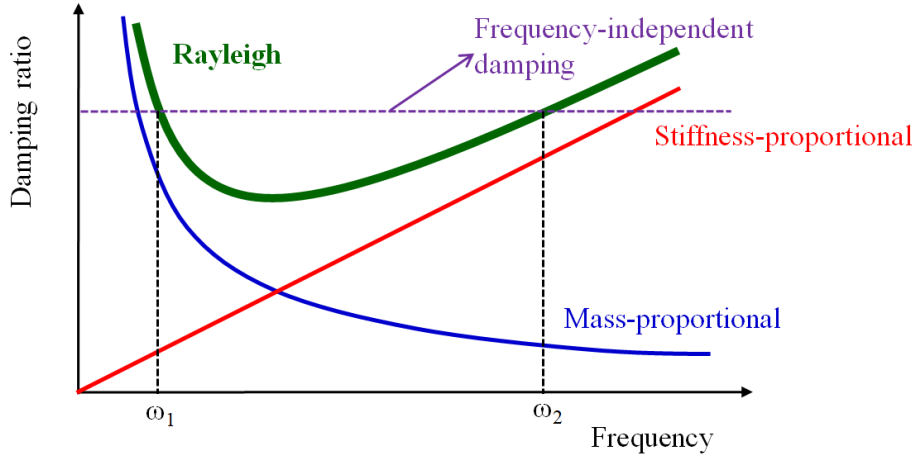
Figure 4.8 Relationship between damping & freq. by QUAD4M

Most dynamic analyses consider frequency ranges between ω_1 and ω_2, and hence it is very essential to improve the decoupling accuracy in such frequency range in order to make the damping ratio close to the so-called frequency-independent one. In this study, an improved method developed by Song et al. (2017) is simplified and applied. In the method, the damping coefficients are calculated by applying the least square method to determine the least square sum of the difference between the calculated damping ratio of each modal and the actual damping ratio within the cutoff frequency. The formula is given as follows:

$$\min_{\alpha,\beta} \sum_{i=1}^{n} \left(\frac{\alpha}{2\omega_i} + \frac{\beta\omega_i}{2} - \xi \right) \tag{4.27}$$

However, it should be noted that in order to apply the method, each natural frequency of entire models in the cut off range should be calculated, and this may lead to an excessive computational burden; in addition, unlike some large structures, road structure tends to consider more about lower-order modes. Based on the above considerations, the method is simplified as follows,

The differential of the Eq. (4.22) is given by,

$$\frac{d\xi}{d\omega} = -\frac{\alpha}{2\omega^2} + \frac{\beta}{2} = 0 \tag{4.28}$$

$$\Rightarrow \omega = \sqrt{\frac{\alpha}{\beta}} \tag{4.29}$$

Substituting Eq. (4.29) into Eq. (4.22), the minimum value of the damping ratio is given by,

$$\xi_{min} = \sqrt{\alpha\beta} \tag{4.30}$$

The damping ratio at the selected frequency range boundary can be given by,

$$\xi_{max} = \frac{\alpha}{2\omega_a} + \frac{\beta\omega_a}{2} \tag{4.31}$$

$$\xi_{max} = \frac{\alpha}{2\omega_b} + \frac{\beta\omega_b}{2} \tag{4.32}$$

Note that ω_a and ω_b can be determined by the method described in QUAD4M. The frequency-independent damping ratio is regarded as the average value of ξ_{min} and ξ_{max},

$$\xi_0 = \frac{1}{2}(\xi_{min} + \xi_{max}) \tag{4.33}$$

In this way, the Rayleigh damping coefficients can be determined by making all the damping ratios (in the considered range frequency) close to the frequency-independent one, as shown in Figure 4.9. In the process of the practical application of this method, just combine Eq. (4.30), Eq. (4.31), Eq. (4.32) and Eq. (4.33) by considering 4 equations and 4 unknown parameters.
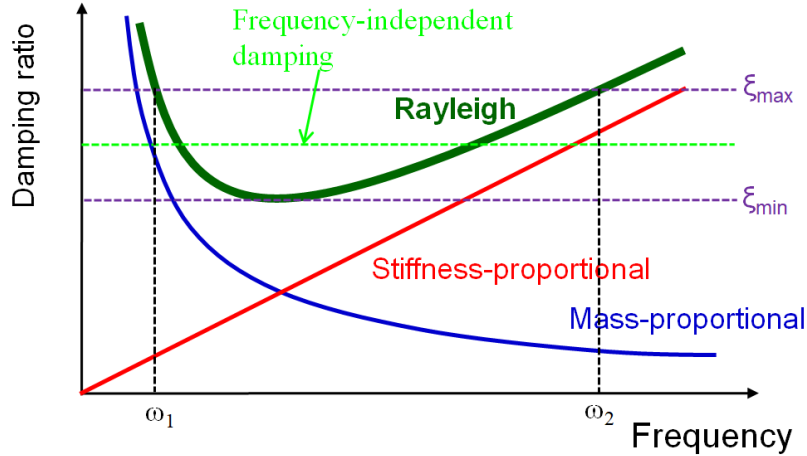
Figure 4.9 Relationship between damping & freq. by the proposed method

4.3 Model Calibration

In order to evaluate the accuracy of the developed method, a calibration process is conducted in this part. A FEM simulation based on the developed method in Chapter 4.2 is established in order to compare to in-situ experimental tests of FWD loads. In order to examine the applicability of the proposed method, measurements are carried out at two in-situ fields, which are non-rubberized asphalt pavement and rubberized asphalt pavement, named as Pavement 1 and Pavement 2, respectively.

4.3.1 Description of the FEM simulation

For the pavement structure, the dynamic analysis can be performed by the following equation in which the damping and inertia effects are presented.

$$[M]\{\ddot{U}\} + [C]\{\dot{U}\} + [K]\{U\} = \{P\} \tag{4.34}$$

where [M] = mass matrix, [C] = damping matrix, [K] = stiffness matrix, {P} = external force vector, $\{\ddot{U}\}$ = acceleration vector, $\{\dot{U}\}$ = velocity vector, and {U} = displacement vector. Eq. (4. 34) can be solved using explicit or implicit integration methods in ABAQUS. In this study, the implicit analysis is selected because of its stability and efficiency. The same loads conducted in the FWD tests of Pavement 1 and Pavement 2 are applied in the simulation, as shown in Figure 4.10. CAX4R, the 4-node

axis-symmetric reduced integral element is selected in order to improve the calculation accuracy and to reduce calculation time.

In the FEM model, the pavement structure is assumed to have constant properties in horizontal planes and the traffic loads are modeled by considering a circular footprint, as shown in Figure 4.11. The layer moduli, density and Poisson's ratio of Pavement 1 and Pavement 2 are back-calculated from FWD load tests and are shown in Table 4.1 and Table 4.2, respectively. The damping ratios are obtained by optimizing the values from the studies by Zhong et al. (2002) and Chatti et al. (2004). The damping ratios of various layers as well as the corresponding Rayleigh damping coefficients α and β are shown in Table 4.3. The FE model is meshed by refining the load area as well as the upper structure and generating coarse mesh away from the load as well as the underlying structure. The models of different meshes are tried until the results convergent and the optimized mesh is shown in Figure 4.11.
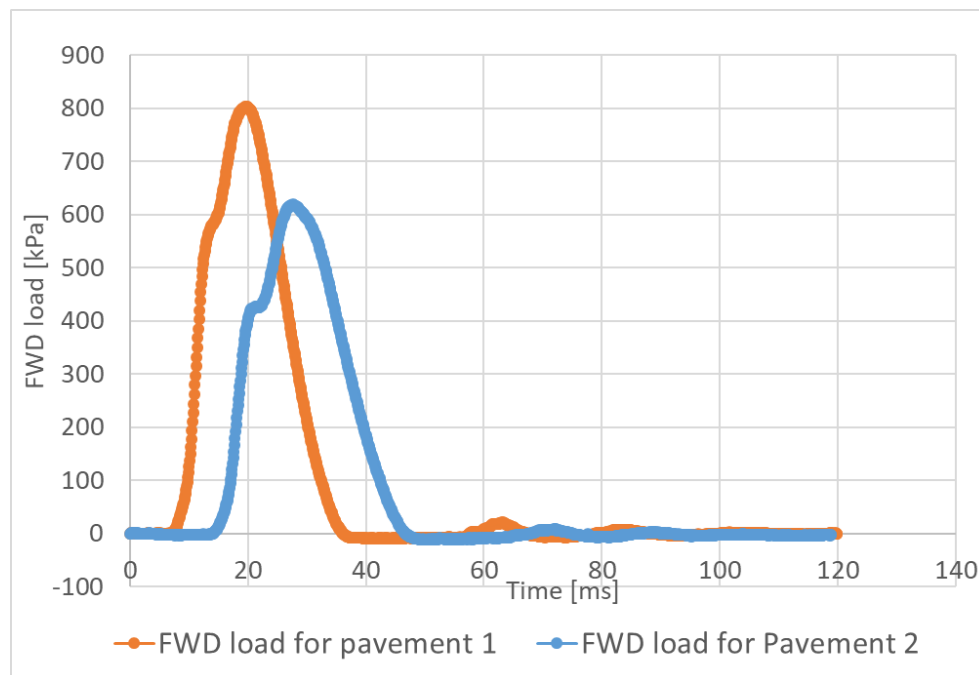
Figure 4.10 FWD loads for pavement 1 and pavement 2
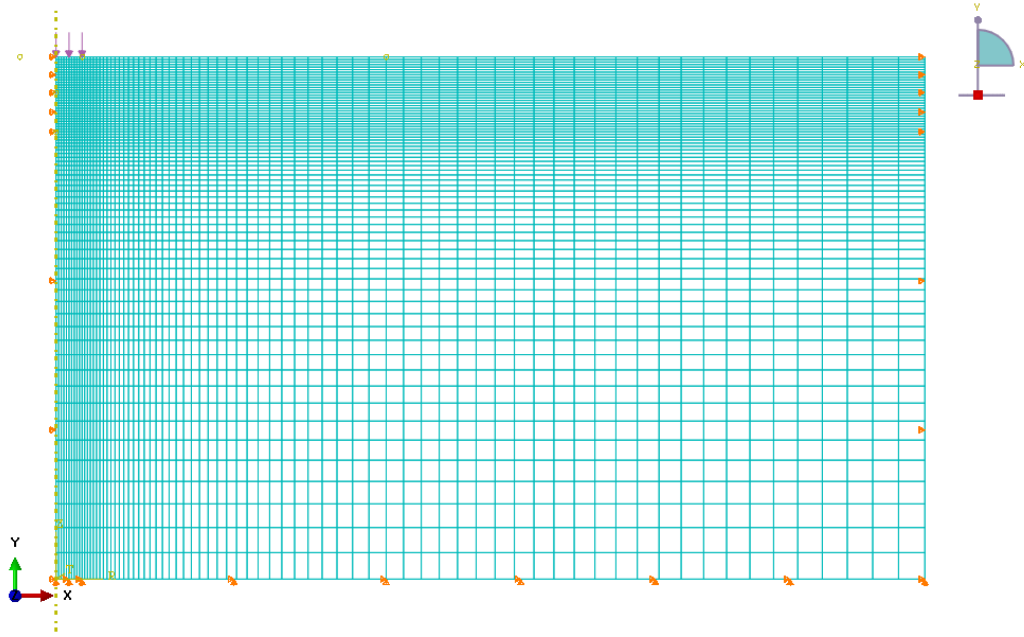
Figure 4.11 Schematic of FEM model in Abaqus

Table 4.1 Properties of the pavement structure 1

Layers	Thickness (cm)	Young's Modulus (MPa)	Poisson ratio	Density (Kg/m³)
Surface layer	20.5	5680	0.3	2400
Base layer	22.5	660	0.3	2000
Subgrade	-	110	0.35	1500

Table 4.2 Properties of the pavement structure 2

Layers	Thickness (cm)	Young's Modulus (MPa)	Poisson ratio	Density (Kg/m³)
Surface layer	20.4	2657	0.3	2400
Base layer	29.2	73	0.3	2000
Subgrade	-	66	0.35	1500

Table 4.3 Damping parameters for pavement 1 and pavement 2

Pavements	Layers	Damping ratio	Alpha	Beta
	Surface layer	0.05	89	2.5E-5
Pavement 1	Base layer	0.03	3.2	0.0043
	Subgrade	0.03	3.2	0.0043

	Surface layer	0.1	198	5E-5
Pavement 2	Base layer	0.03	3.2	0.0043
	Subgrade	0.03	3.2	0.0043

4.3.2 Comparison between numerical results and in situ FWD measurements

The results of the FE model are compared to those of FWD tests. As far as Pavement 1, the recorded peak deflection basin, the dynamic response of sensors G1 (at the center of the loading plate), G5 (500 mm away from the loading center) and G9 (1900 mm away from the loading center) are used in this study as benchmarks to validate the FEM. For Pavement 2, the recorded peak deflection basin, the dynamic response of sensors G1 (at the center of the loading plate), G5 (500 mm away from the loading center) and G8 (1500 mm away from the loading center) are used.

The numerical results of the peak deflection basin of Pavement 1 and Pavement 2 are completely overlapping of the field measurement data, as shown in Figure 4.12. For Pavement 1, Figure 4.13a, 4.13b, and 4.13c compare the deflection time histories for measurement and simulation at G1, G5, and G9, respectively. With the exception of a small magnitude difference at G1 and dephasing at G9, good agreements are achieved. As far as the magnitude difference at G1, it can be explained that considering the FWD masses are interfering with pavement vibration, theoretically speaking, the deflection time history should be a vibration curve along with the pavement-air interface similar to the FEM result. For dephasing at G9, it can be influenced by the heterogeneity of pavement layers or subgrade. As far as Pavement 2, Figure 4.14a, 4.14b, and 4.14c compare the measured and simulation results at G1, G5, and G8, respectively. Similarly, good agreements are achieved except for the small difference in amplitude at G8. These differences can be explained by the heterogeneity of soil or pavement, which leads to small-amplitude differences during vibration wave propagation. In any case, as shown above, these errors are considered acceptable for the developed method.
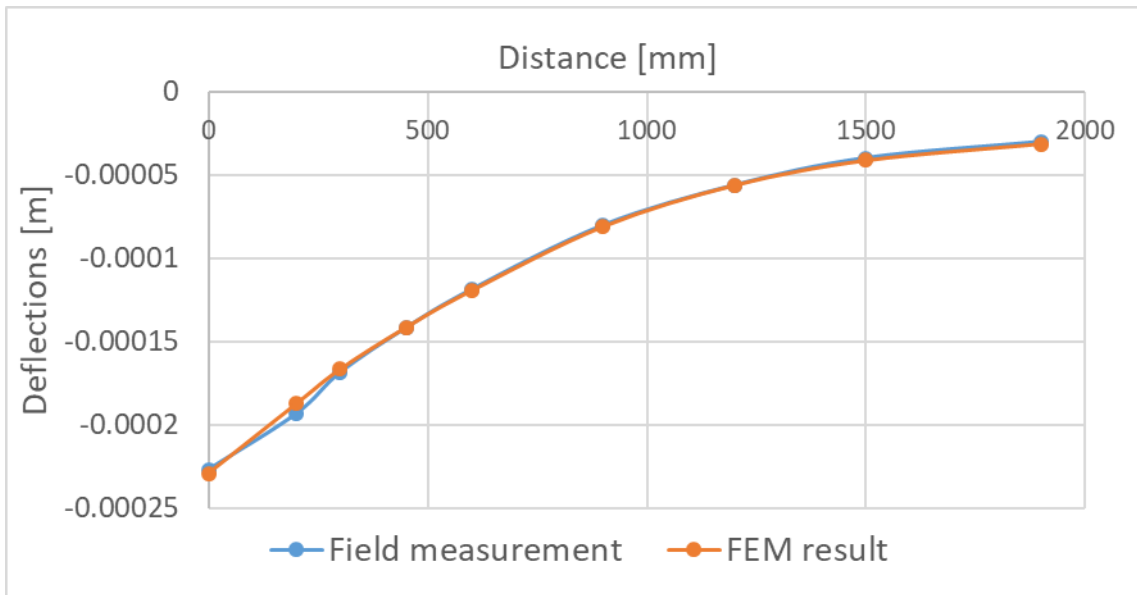
(a) Pavement 1
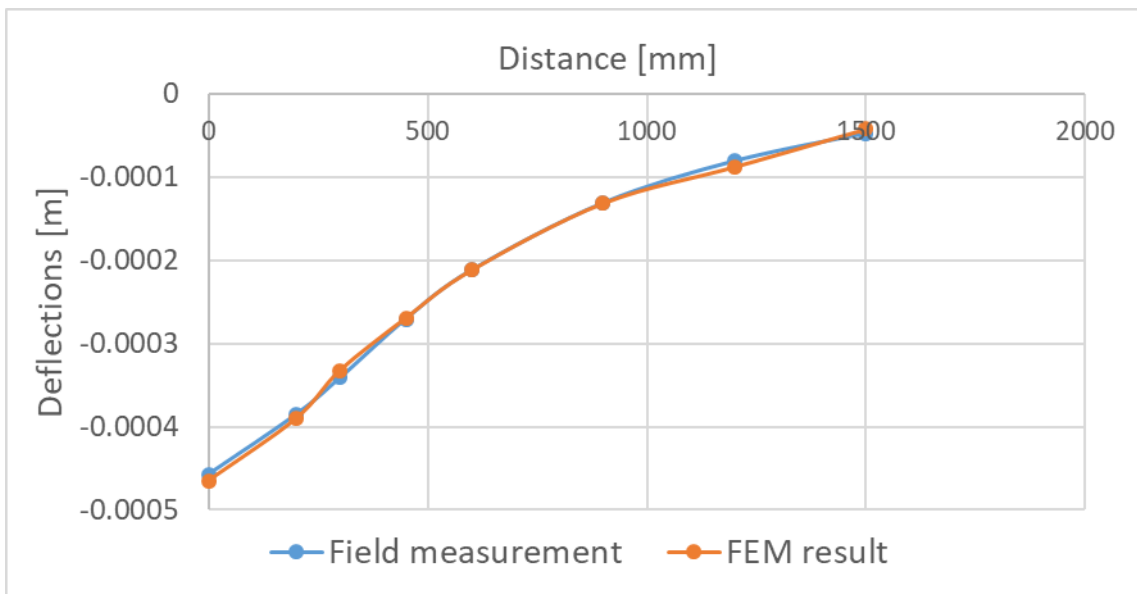
(b) Pavement 2

Figure 4.12 Deflection basin for field measurement and FEM results
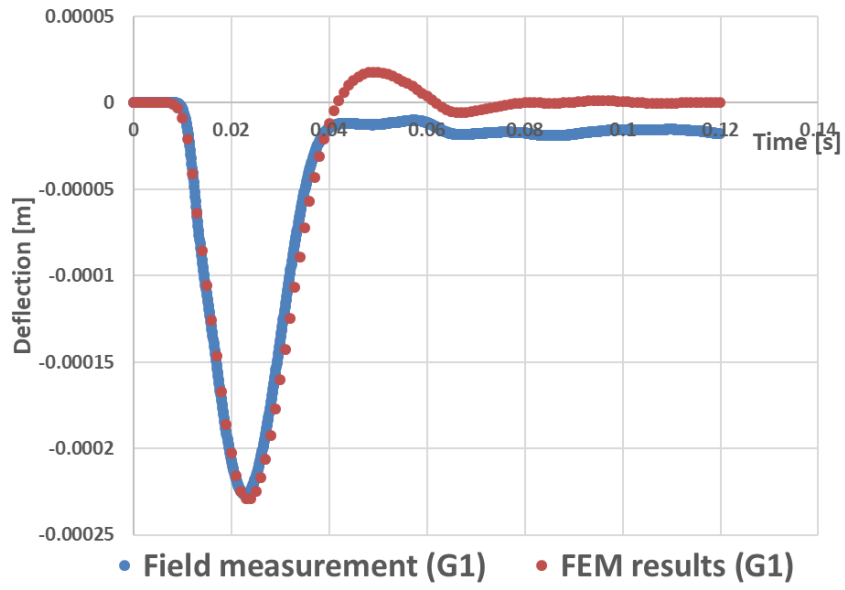
(a)
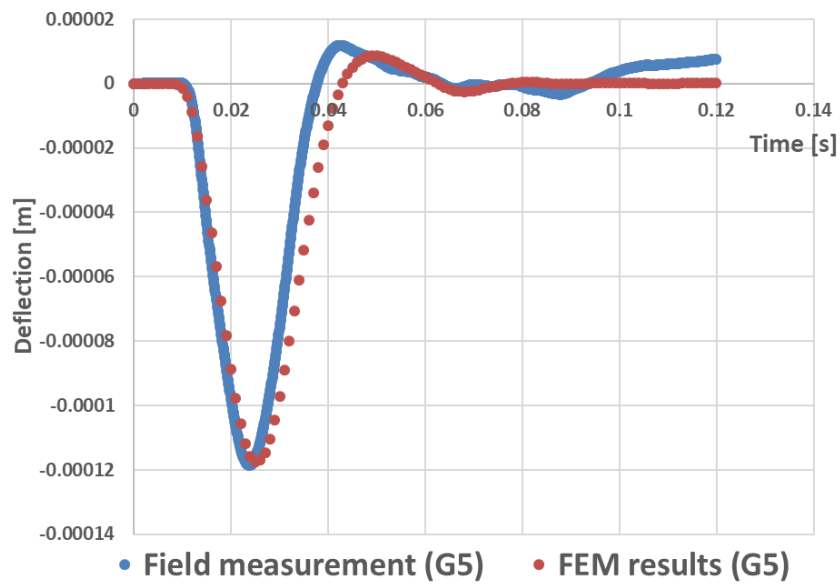
(b)
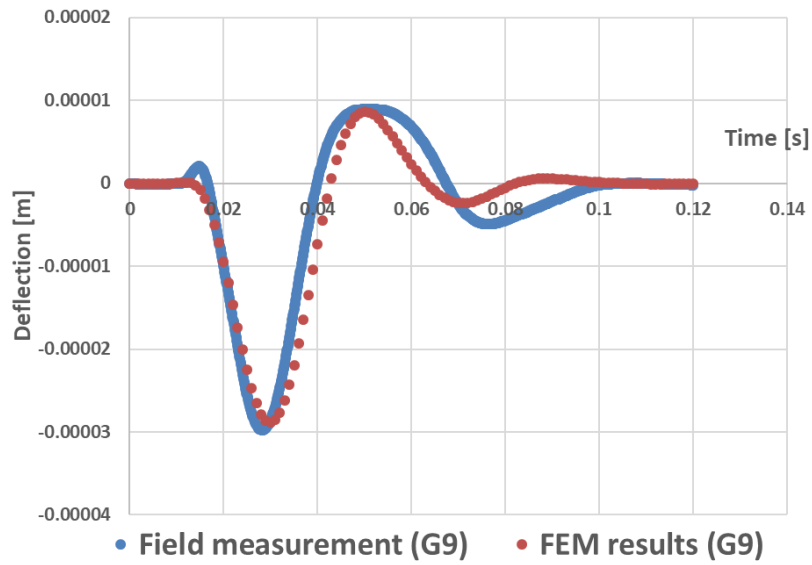
(c)

Figure 4.13 Deflection time histories of FEM results and field measurement at different points: (a) G1, (b) G5 and (c) G9 (Pavement structure 1)
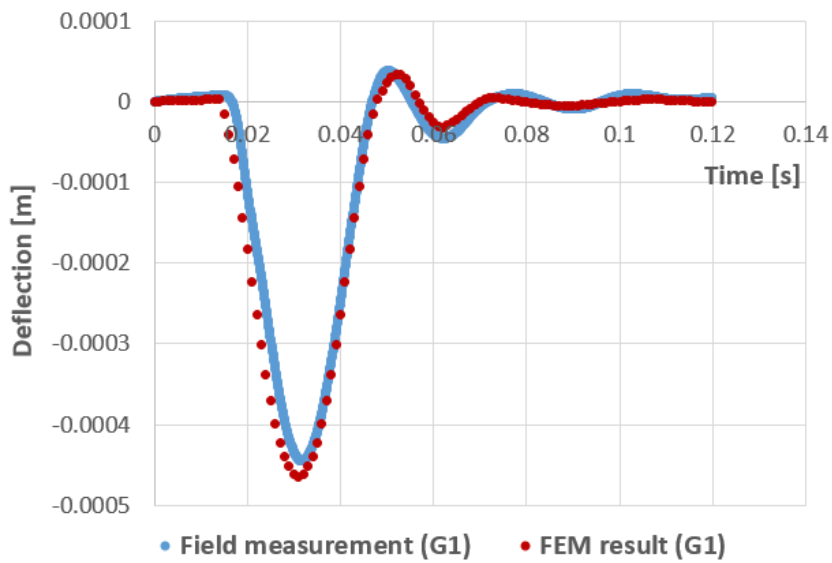
(a)
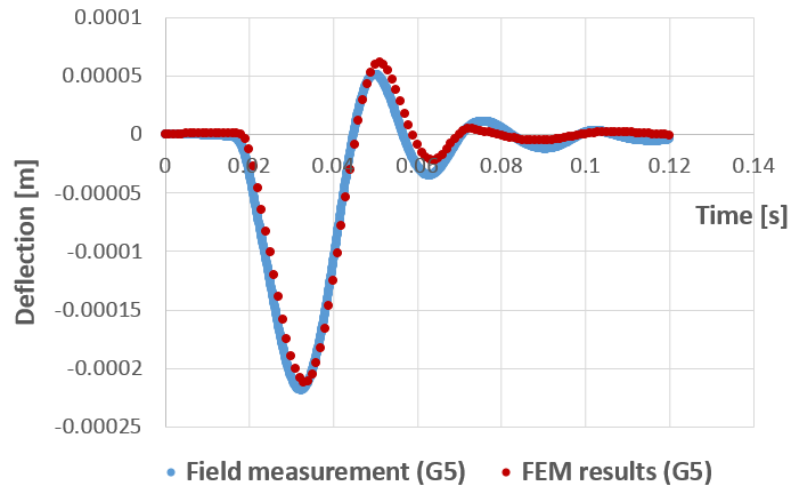
(b)
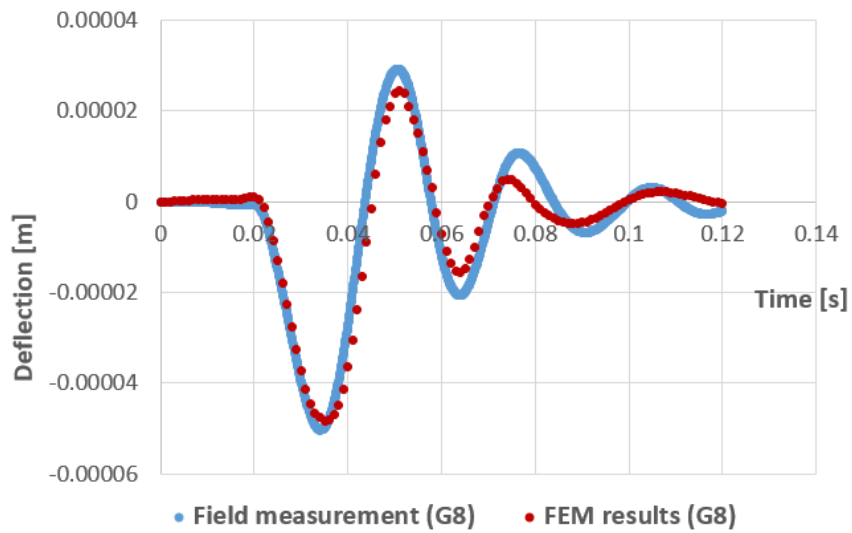
(c)

Figure 4.14 Deflection time histories of FEM results and field measurement at different points: (a) G1, (b) G5 and (c) G8 (Pavement structure 2)

Chapter 5: Parametric study of the effect of damping layer on pavement response

5.1 Effect of damping layer on the low-vibration ability of the pavement system

The vibration response analysis of the road structure is an extremely important step before the development of the new road system since it is essential to verify whether it makes sense to lay a damping (vibration-absorbing) layer in the pavement structure. In this part, the effects of three important design parameters, the damping ratio of the damping layer material, the damping layer position and thickness, on vibration reduction of the pavement structure are analyzed.

5.1.1 Description of the FE model

The pavement structure established in this study is shown in Figure 5.1, with a 4 m width of pavement structure and 30 m width of the surrounding environment composed of compacted soil. The road system is composed of an AC layer with a thickness of 0.205 m, a subbase layer with a thickness of 0.2 m, and subgrade. Five points are monitored for the time histories of acceleration during the simulations: Point A, directly underneath the load; Point B, 2 m away from the loading point, is still on the pavement though; Point C, 4 m away from the loading point, is at the boundary between the pavement and the surrounding soil; Point D, 10 m away from the loading point; Point E, 30 m away from the loading point, as shown in Figure 5.1. The vibrations at points A, B and C are closely related to the tire/pavement noise at low-frequency range and the ones at point E and F are related to the impact (vibration) on the surrounding environment.

The root-mean-square accelerations recorded at the five selected points are monitored in order to evaluate the vibration attenuation. The root-mean-square acceleration, A_{RMS}, is given by,

$$A_{RMS} = \sqrt{\frac{1}{T} \int_0^T a^2(t)dt}$$

(5.1)

where a(t)= acceleration at time t, and T= duration of vibration. The root-mean-square refers to a common mathematical method of defining the effective magnitude. For a uniform sine wave, the root-mean-square value is 0.707 times the peak value or 0.354 times the peak-to-peak value. For repeated loading situations such as loading generated by a vehicle on the road, the root-mean-square acceleration represents the average repeated loading amplitude (Zeng 2005). The root-mean-square acceleration is important in determining both the pavement and the ground vibration intensity. By comparing the root-mean-square of the monitoring points, the capacity of the damping layer in vibration attenuation can be determined.
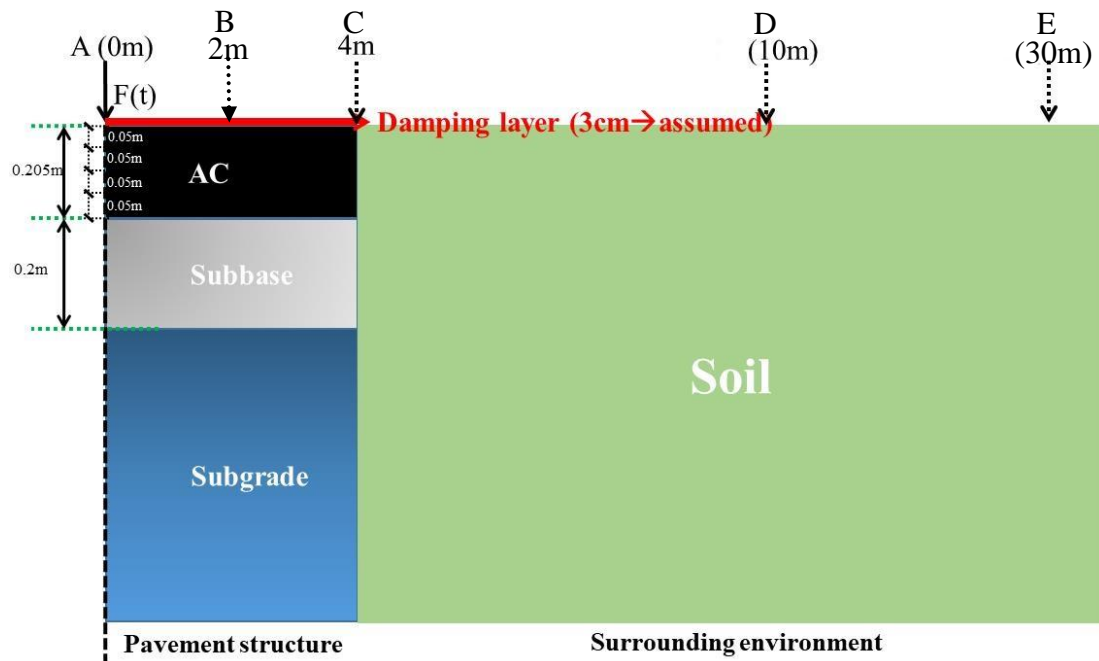
Figure 5.1 Pavement structure and surrounding environment

The simulation process is conducted by considering three aspects: varying damping ratios of the damping layer material, varying damping layer positions, and varying damping layer thicknesses. As far as the damping ratios, five configurations are carried out to determine the effects on vibrations reduction, changing from 0.02, 0.05, 0.1, 0.15, to 0.2. The input of damping characterization is conducted according to the method developed in Chapter 4.

The properties of the AC, damping layer, subbase, subgrade and soil of the surrounding environment are shown in Table 5.1. These properties are obtained by the back-calculation from FWD in-situ tests conducted in "Faentina" località Borgo S. Lorenzo, Firenze, which represents a conventional road structure in Italy.

Based on the master curves of Mix 1 and Mix 2 described in Chapter 6, the elastic modulus of the damping layer is estimated and obtained by selecting reasonable loading frequency and temperature in the master curve (See Figure 6.13 in Chapter 6). In this study, the loading frequency is consistent with the actual FWD load applied to the pavement structure and the temperature is consistent with the one when the FWD test is conducted. The determined values are shown in Table 5.1.

Table 5.1 The properties of materials in the pavement system

Layers	Elastic modulus (MPa)	Poisson's ratio	Damping ratio	Density (Kg/m^3)
AC	5680	0.3	0.04	2400
Damping layer	1310	0.3	Varying[*]	2400
Subbase	660	0.3	0.02	2000
Subgrade	110	0.35	0.02	1500
Soil of surrounding environment	110	0.35	0.02	1500

Note: *damping ratios are varying from 0.02, 0.05, 0.1, 0.15 to 0.2

As far as the position of the damping layer, five configurations are carried out to determine the effect of the parameter 'DISTANCE TO TOP', which is changing from 0 cm, 5 cm, 10 cm, 15 cm to 20 cm. As far as the thickness of the damping layer, three configurations are carried out with thickness varying from 10 mm, 20 mm, to 30 mm. A special condition when the thickness is equal to 0 cm, is used as a reference. The summary of the different configurations can be found in Table 5.2.

Table 5.2 The configurations of different layers in the pavement system

Layers	Thickness [mm]	Distance to top [cm]
AC	205	-
Damping layer	0, 10, 20, 30	0, 5, 10, 15, 20
Subbase	200	-
Subgrade	-	-
The soil of the surrounding environment	-	-

Point A

(Load point)

Point C

(10m away from Point A)

Point E

(30m away from Point A)
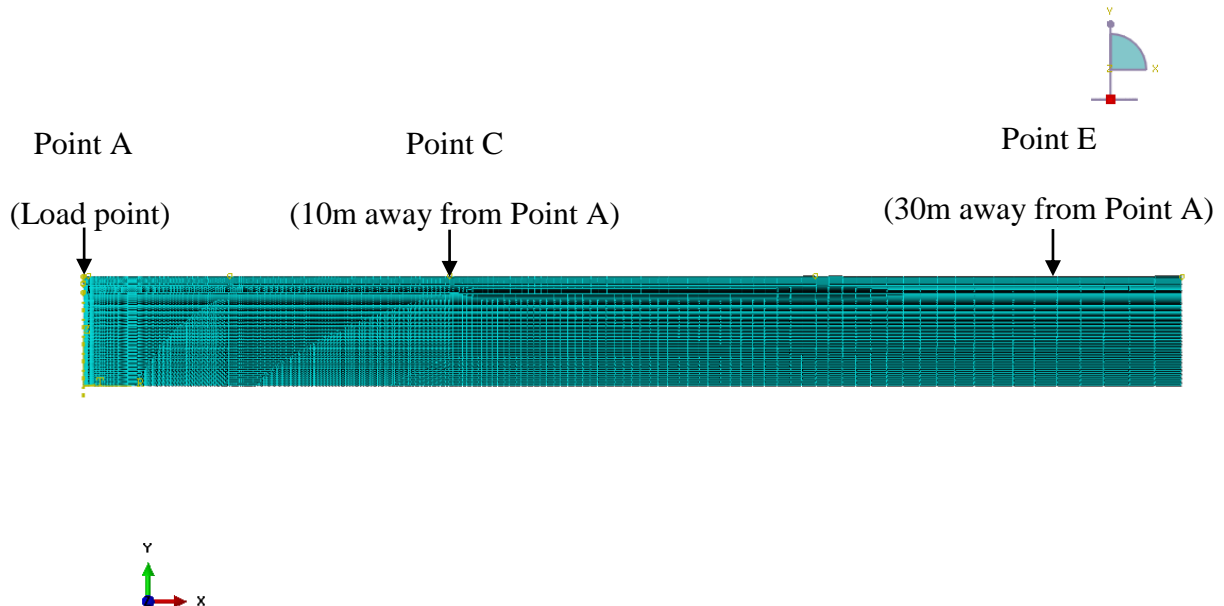
Figure 5.2 FE model shown in Abaqus

The FE model is followed by the one established in Chapter 4, which has been calibrated by comparing it to the in-situ test results. The implicit analysis is also selected in this study because of its stability and efficiency. CAX4R is selected as the mesh element type in order to improve the calculation accuracy and to reduce calculation time. The FE model is meshed by refining the load area as well as the upper structure and by generating coarse mesh at the area away from the load as well as the underlying structure. The models of different meshes are tried until the results are convergent and the optimized mesh is shown in Figure 5.2. The same load (the FWD

load for pavement 1) conducted in the FWD test is also applied in the simulation, as shown in Figure 4.10.

5.1.2 Results and analysis

5.1.2.1 Sensitivity analysis of monitoring points on vibration reduction

Vibration reduction at different monitoring points can be different. In this section, when the damping layer is at the bottom & top of the asphalt layer and its thickness is equal to 30 mm will be set as an example to show the influences of varying monitoring points on vibration reduction. When the damping ratio of the damping layer is changing from 0.02 to 0.2, the vibration reductions at A, B, C, D, and E are monitored. The results of vibration reductions when the damping layer is at the bottom of the asphalt layer and at the top of the asphalt layer are shown in Table 5.3 and Table 5.4, respectively.

Table 5.3 Vibration reduction when the damping layer was at the bottom of the asphalt layer

Monitoring points	Distance to loading point[a] [m]	$A_{RMS}(\xi=0.02)$ [dm/s^2]	$A_{RMS}(\xi=0.2)$ [dm/s^2]	Vibration reduction[b]
A	0	22.74	21.97	3.41%
B	2	4.96	4.209	15.16%
C	4	2.65	2.15	18.65%
D	10	1.14	0.92	18.97%
E	30	0.11	0.091	15.59%

Notes: [a] "Distance to loading point" means the distance from the monitoring point to the loading point. [b] "Vibration reduction" means the reduction of vibration at the monitoring points (Similarly hereinafter)

Table 5.4 Vibration reduction when the damping layer is at the top of the asphalt layer

Monitoring points	Distance to loading point [m]	$A_{RMS}(\xi=0.02)$ [dm/s^2]	$A_{RMS}(\xi=0.2)$ [dm/s^2]	Vibration reduction
A	0	22.82	21.68	5.01%
B	2	5.03	4.24	15.62%
C	4	2.72	2.19	19.53%
D	10	1.15	0.92	19.66%
E	30	0.10	0.09	15.93%

In order to better understand the influences of varying monitoring points, the relationship between the distance of monitoring points and vibration reductions are shown in Figure 5.3. The maximum vibration reduction is observed when the monitoring point is approximately 3 m to 30 m away from the loading point and the vibration reduction is about 15%. With the increase of distance to the loading point, the vibration reduction increases firstly and then decreases. The maximum value of vibration reduction appears at a distance of 5-6 meters. In addition, it can also be observed that regardless of whether the damping layer is at the top or at the bottom of the asphalt layer, similar results are obtained.

When loading point is monitored, the minimum vibration reduction appears and it can be explained that the displacement and phase difference in the pavement response depend on pavement stiffness characteristic (elastic modulus, Poisson's ratio, thickness) as well as the mass characteristic (density) instead of damping characteristics. Although the damping ratio is changing from 0.02 to 0.2, the other parameters (elastic modulus, Poisson's ratio, density as well as thickness) stay the same. Hence, minor displacement and phase difference can be estimated, resulting in a minor difference in A_{RMS}. When the distance from a monitoring point to loading point increases, the damping effect of the damping layer is playing a predominant role, where gradually increasing displacement and phase difference can be found. However, when the distance continues to increase, the damping effect of the surrounding soil is playing a predominant role, which is not affected by the damping layer and this is why the vibration reduction reduces in the end. It can be predicted when the distance is far enough, the effect of vibration reduction may decrease until it vanishes.
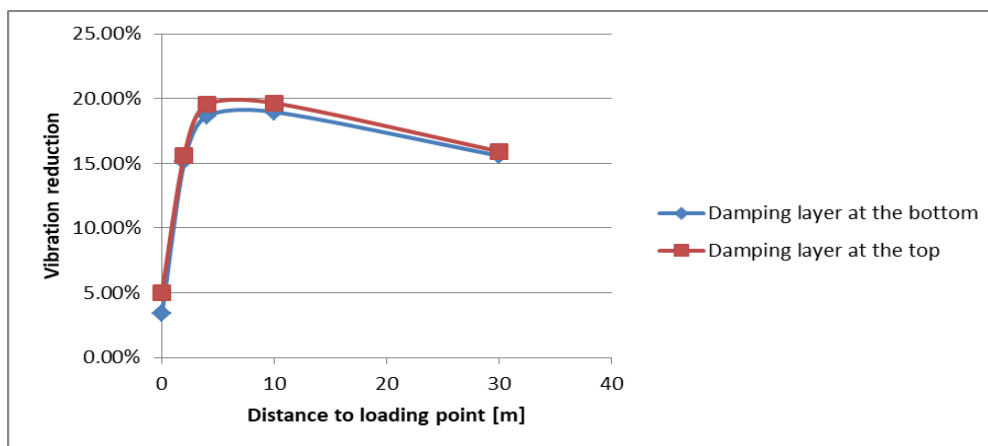
Figure 5.3 Relationship between the distance of monitoring point and vibration

reduction

5.1.2.2 Sensitivity analysis of varying loading on vibration reduction

As a special vibration structure, the pavement may vibrate differently with varying loads. In order to evaluate the sensitivity of varying loads, besides the FWD load applied in the FEM simulation, another two loads are also selected with the loading times of 90 ms and 24 ms, respectively. The three selected loads are shown in Figure 5.4. When the damping layer is at the bottom of the asphalt layer, the relationship between the positions of monitoring point and vibration reduction is shown in Table 5.5 and Figure 5.5. It can be observed that with different loading times (frequencies), the maximum vibration reduction appears at a different distance. However, the three loading times (frequencies) are showing a very similar trend.

Based on the analysis in the sub-chapter 5.1.2.1 and this sub-chapter, where the sensitivity of vibration reduction with varying monitoring points and loadings have been confirmed, in order to reduce computation in the subsequent simulation, only the three points of A, C and E are monitored and only the FWD load is selected.
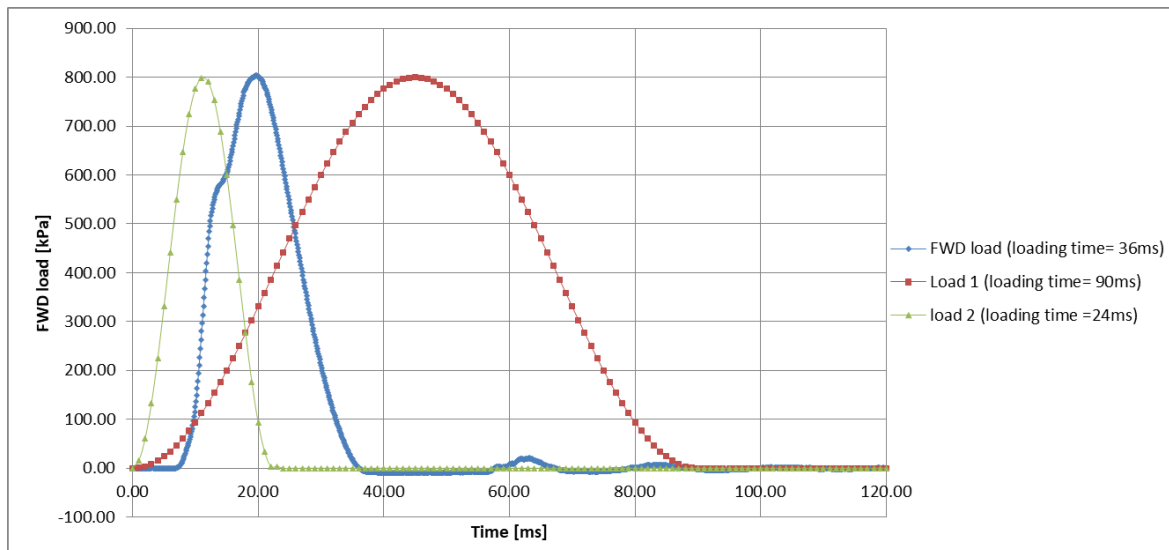
Figure 5.4 Three loads to compare

Table 5.5 Vibration reduction when the three loads were input

Monitoring points	Distance to loading points [m]	Vibration reduction [FWD load (loading time =36 ms)]	Vibration reduction [Load 1 (loading time =90 ms)]	Vibration reduction [Load 2 (loading time =24 ms)]
A	0	3.41%	1.93%	3.67%
B	2	15.16%	6.91%	12.16%
C	4	18.65%	14.42%	16.69%
D	10	18.97%	18.54%	18.35%
E	30	15.59%	14.13%	12.73%
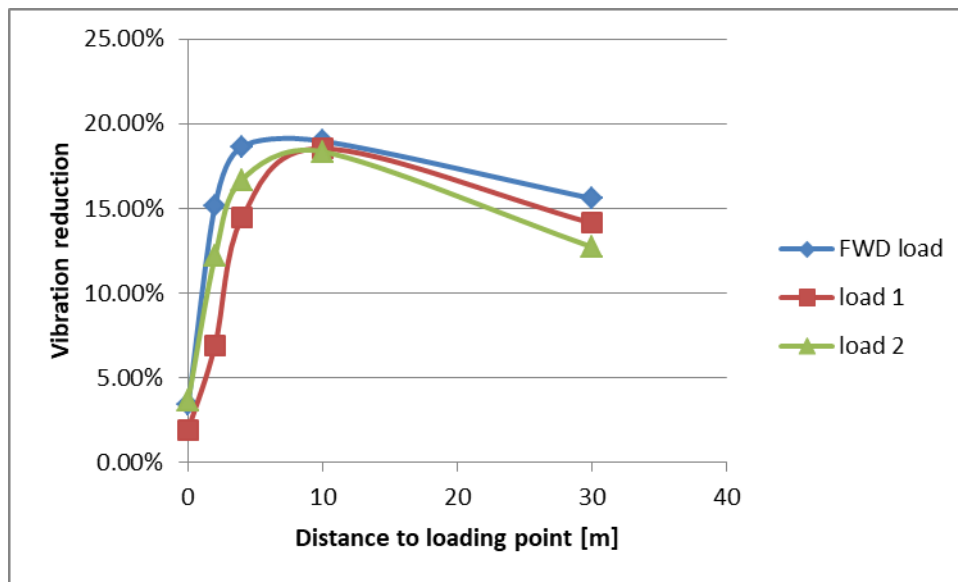
Figure 5.5 Relationship between the distance of monitoring point and vibration reduction

5.1.2.3 Effect of damping ratio on vibration response

The A_{RMS} of the three monitoring points A, C, and E (see Figure 5.2) with varying damping ratios, damping layer thickness and damping layer position are summarized in Appendix I.

Five damping ratios are selected to determine the effect of damping ratios on vibration response of the pavement structure. The simulation results of A_{RMS} at point A with varying damping ratios are shown in Figure 5.6. (The thickness of the damping layer is 10 mm.) It can be obviously found that with the increase of the damping ratio, the A_{RMS} decrease. In addition, this reduction has obvious linearity. This may be explained that,

compared to other layers (asphalt layer, base layer, and subgrade), the damping layer is playing a predominant role to characterize the damping property of the whole system, causing the vibration reaction of the whole system to have a strong linearity with the damping property of the damping layer, even close to ignoring the damping properties of other structural layers. It should be noted that the damping layer is playing a predominant role in characterizing the damping property of the whole system, instead of the dynamic response of the whole system, which mainly depends on the mass matrix and stiffness matrix.

Figure 5.7 and Figure 5.8 are simulation results of A_{RMS} at point A when the thicknesses are 20 mm and 30 mm, respectively. It can be found that very similar results are obtained compared to the results when the thickness is 10 mm, demonstrating that the rule "the linear attenuation of A_{RMS} with the increase of the damping ratio," is still applicable even if the thickness of the damping layer changes.

In such a linear relationship, the 'slope' of the A_{RMS} curve represents the effect of varying damping ratios, and the higher slope value, the more obvious the effect of vibration reduction. Therefore, a higher slope value is preferable during the process of optimizing the damping layer position. Unfortunately, it can be observed from Figure 5.6 to Figure 5.8, the slope values are very close; although there is a higher slope value for the condition of "distancetotop0cm", such a difference does not have practical significance.
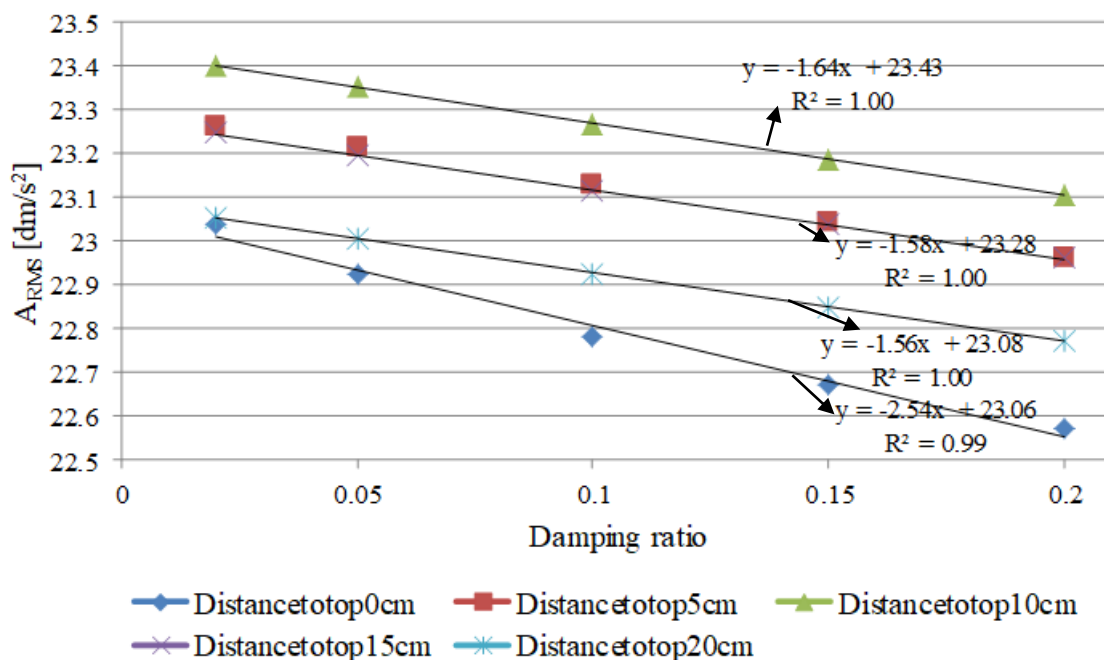
Figure 5.6 Effect of damping ratios (at Point A; the thickness = 10mm)
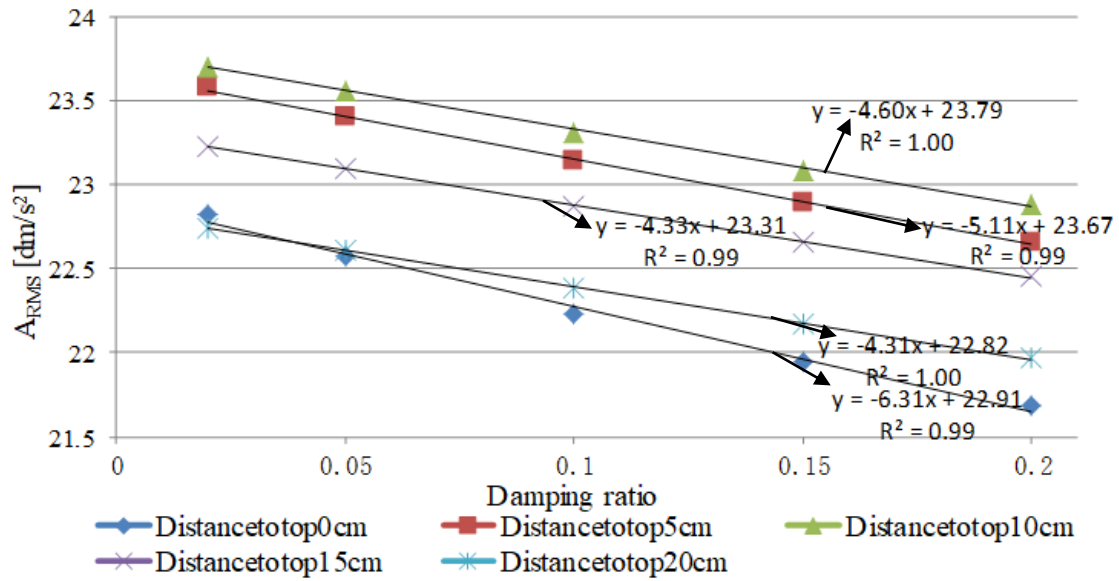
Figure 5.7 Effect of damping ratios (at Point A; the thickness = 20mm)
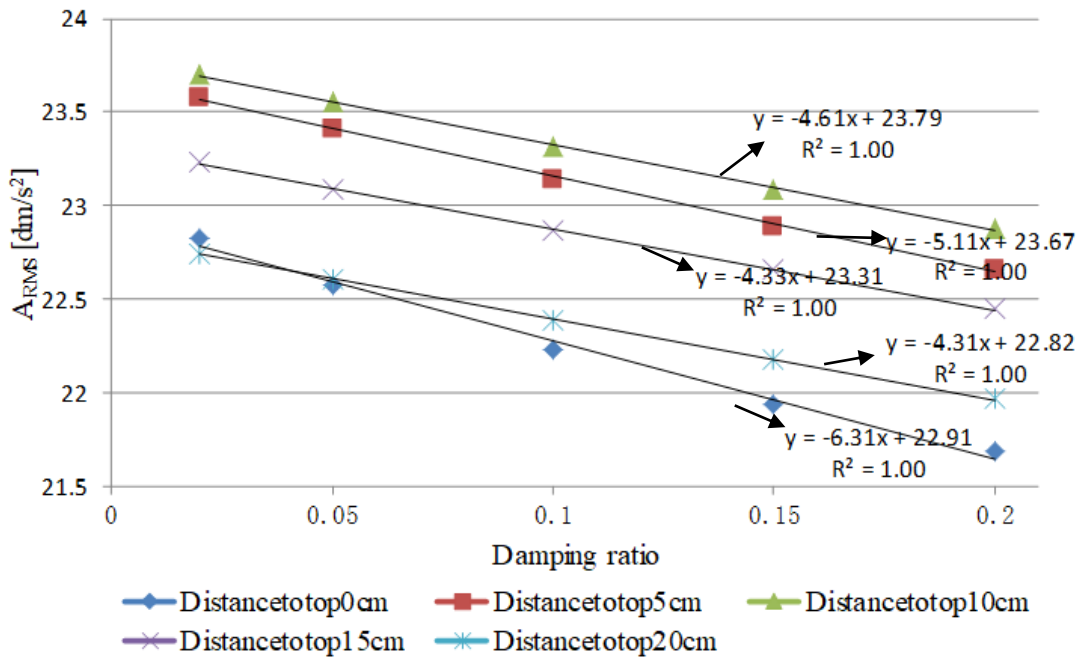
Figure 5.8 Effect of damping ratios (at Point A; the thickness = 30mm)
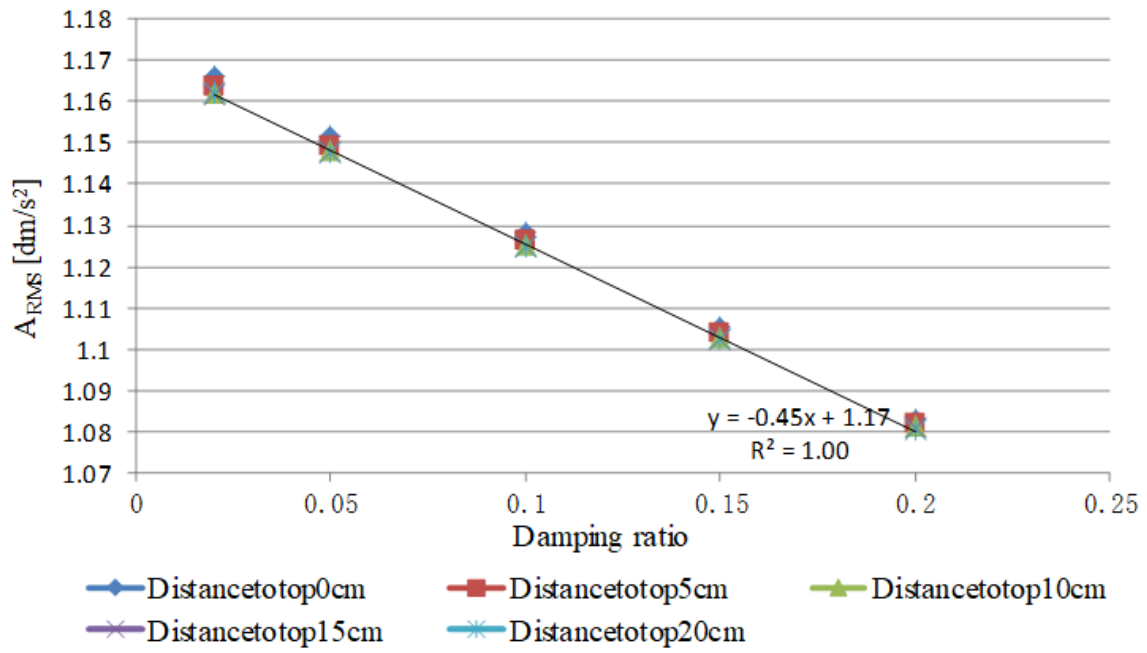
Figure 5.9 Effect of damping ratios (at Point C; the thickness = 10mm)
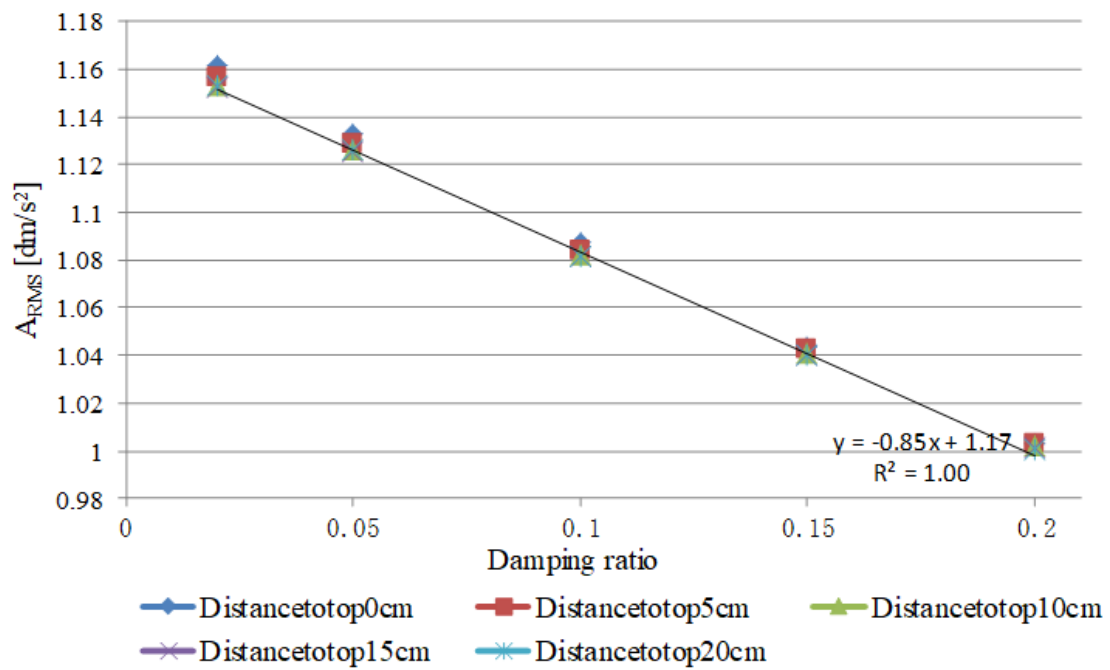
Figure 5.10 Effect of damping ratios (at Point C; the thickness = 20mm)
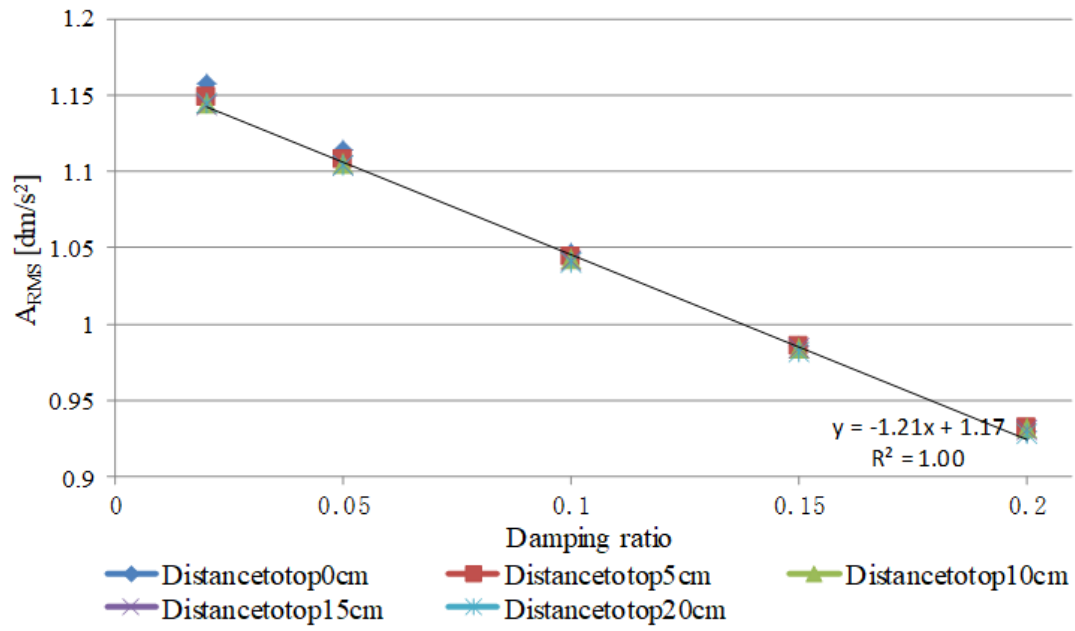
Figure 5.11 Effect of damping ratios (at Point C; the thickness = 30mm)
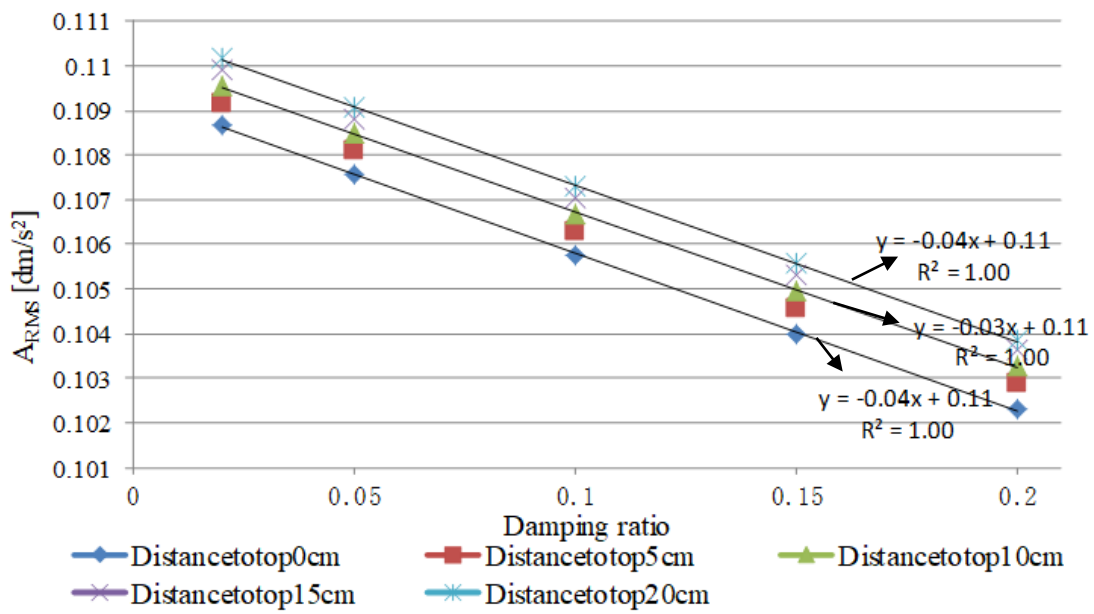
Figure 5.12 Effect of damping ratios (at Point E; the thickness = 10mm)
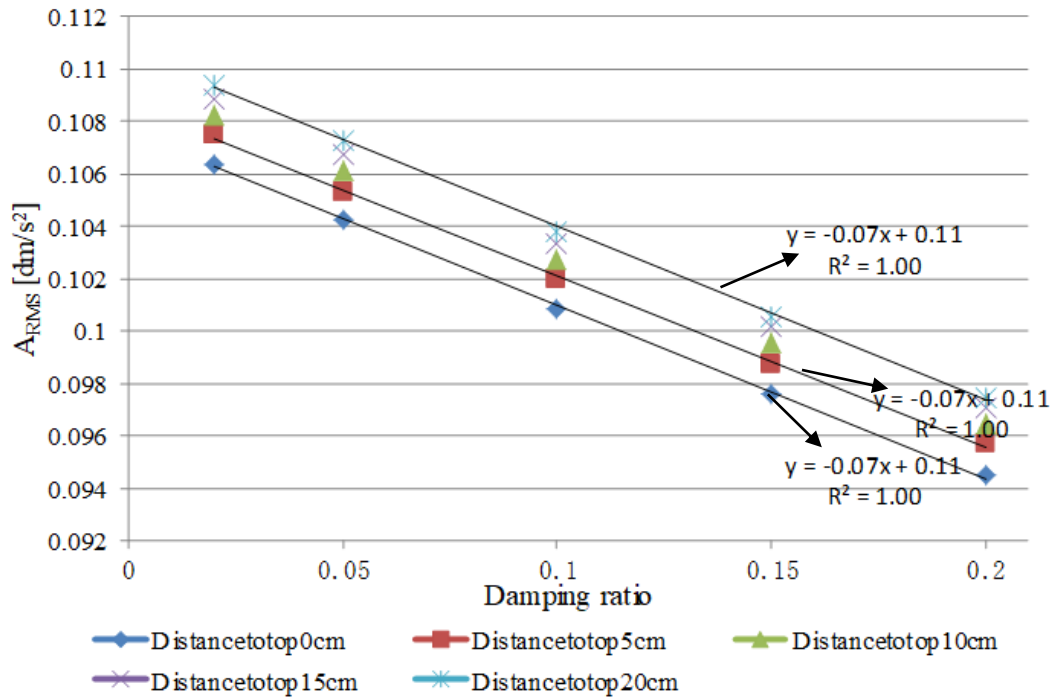
Figure 5.13 Effect of damping ratios (at Point E; the thickness = 20mm)
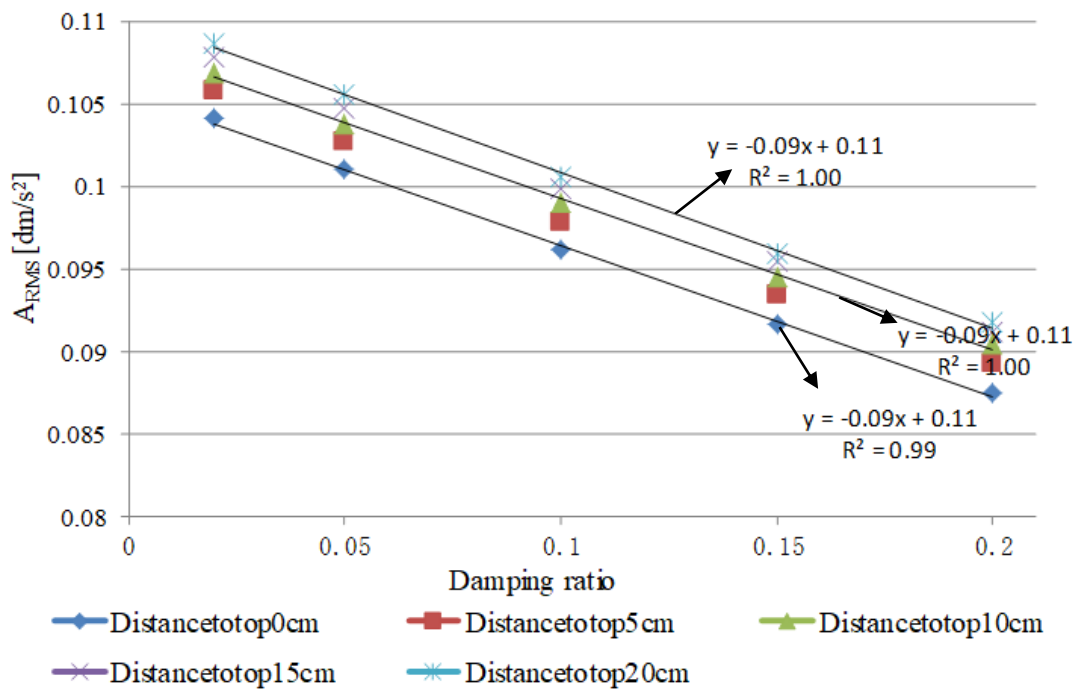
Figure 5.14 Effect of damping ratios (at Point E; the thickness = 30mm)

Figure 5.9 to Figure 5.14 are the results of the effects of damping ratios at point C and point E, with three different thicknesses (10 mm, 20 mm, and 30 mm). The similar linear relationship between damping ratio and A_{RMS} can also be found at point C and point E, demonstrating that the damping layer is playing a predominant role to characterize the damping property of the whole system.

Besides, it can obviously be found that the varying damping layer positions have a relatively obvious effect at point A as well as point E compared to point C. Hence, it can be concluded that optimizing the damping layer position is useful to improve the vibration-reducing performance at Point A (representing the place on the pavement) and Point E (representing the place far from the pavement), but almost useless at Point C (representing the place close to the pavement). When thickness is 30 mm and the damping ratio changes from 0.02 to 0.2, the vibration at 10 m away from the pavement can reduce about 20% and the one at 30 m away from the pavement can reduce about 15%, demonstrating that such an improvement can lead to significant benefits in reducing the impact of traffic-induced vibrations on the surrounding environment and building.

As it is known that the damping property of the asphalt material is highly dependent upon the environmental conditions to which they are exposed. As time and temperatures change, the damping ratio will vary even if the same loading situation. However, according to the loss factor of the viscoelastic materials, the damping ratio at the same condition (the same temperature, load, boundary condition) can be roughly compared. For example, as far as the pavement structure with normal temperature and load, the damping ratios of soil, conventional asphalt mixture, and rubber modified asphalt mixture can be regarded as 0.02, 0.05 and 0.1, respectively. Hence, in order to obtain the obvious vibration reduction effect, the damping ratio of the asphalt mixture specially for the damping layer should arrive at 0.15-0.2, which is almost 3-4 times higher compared to conventional asphalt mixtures and 2 times higher compared to rubberized asphalt mixtures. This conclusion will be used as the design target of asphalt mixtures for the damping layer.

5.1.2.4 Effect of damping layer position on vibration response

When the thickness of the damping layer is 30 mm, the effects of the damping layer position on A_{RMS} at Point A, Point C, and Point E are evaluated, as shown in Figure 5.15-5.17. The horizontal axis represents the distance from the damping layer to the top. It can be found that varying damping layer positions have a relatively obvious effect at point E (6% difference) compared to point C (almost 0% difference) and point A (2% difference); at point C, changing the position of the damping layer has almost no effect on the vibration response of the system. Hence, it can be concluded that the most meaningful point to select the optimized damping layer position is point E. From the

values of A_{RMS} at point E (see Figure 5.17), it can be found that the damping layer placed at the top is the optimal position. However, it is known that the damping layer cannot work as a surface layer and the second choice might be the optimized position. Hence, it is determined that the optimized position for the damping layer is 5 cm or 10 cm away from the top. It should be noted that even a 6% difference is still not a "convincing value". Therefore, the selection of the optimized position should take into account the mechanical response of the pavement structure, which will be introduced in the sub-chapter 5.2.
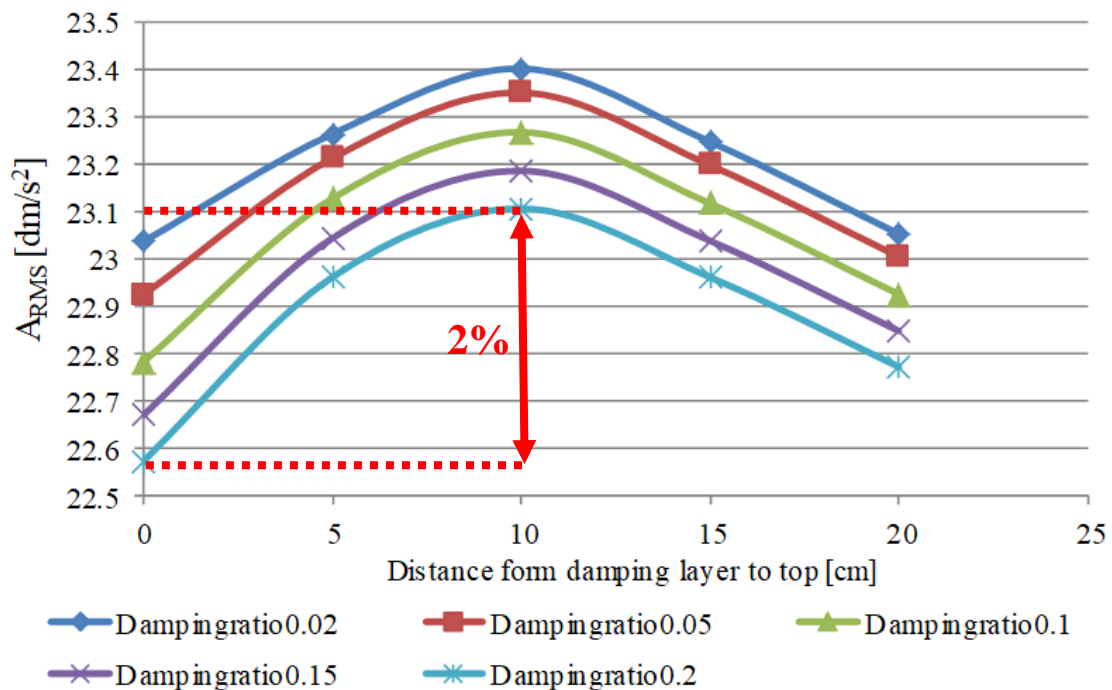
Figure 5.15 Effects of damping layer position (Point A)
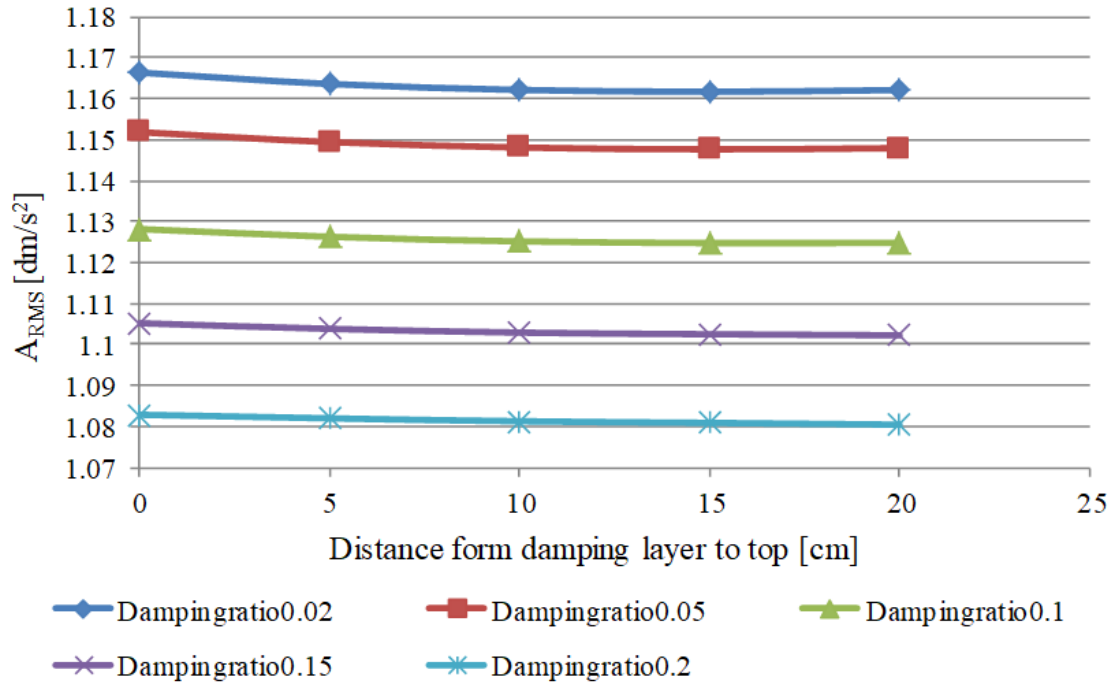
Figure 5.16 Effects of damping layer position (Point C)
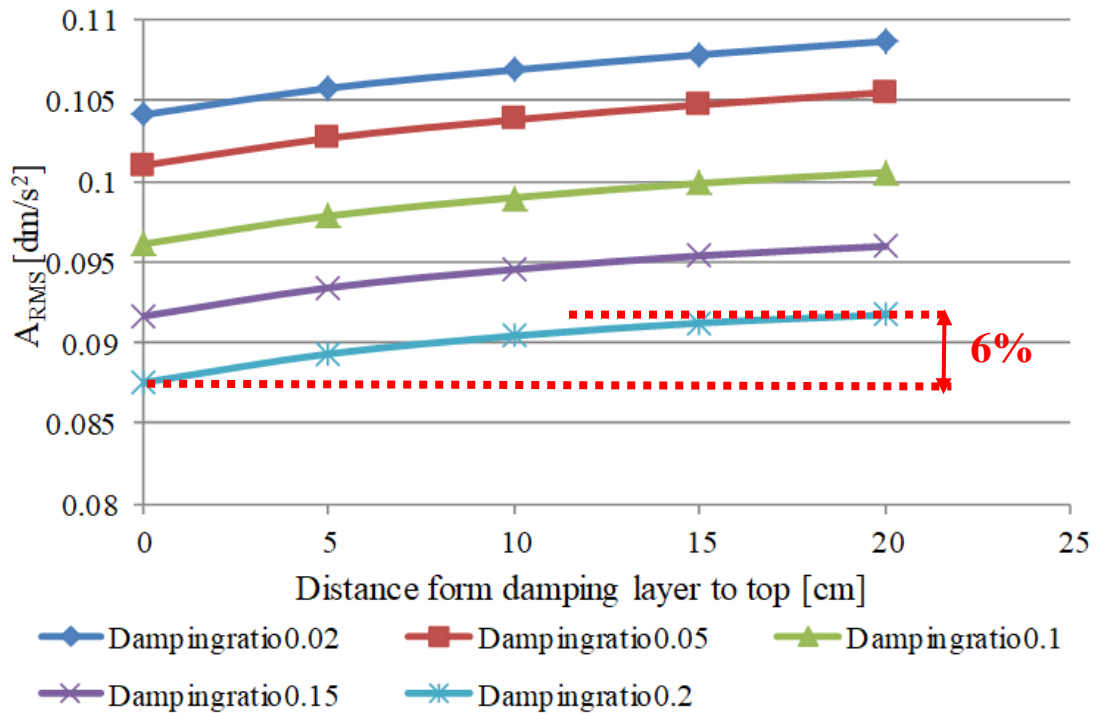
Figure 5.17 Effects of damping layer position (Point E)

5.1.2.5 Effect of damping layer thickness on vibration response

Another very essential design parameter for pavement is thickness. In this series of simulations, the thickness of the damping layer varies from 0 mm, 10 mm, 20 mm to 30

mm. The effect of damping layer thickness at point A is shown in Figure 5.18. It can be found that the increasing thickness of the damping layer does not necessarily reduce the vibration response at point A. For example, when the damping layer is 5 cm away from the top, with the increasing thickness of the damping layer (the damping ratio is 0.02 or 0.05), the vibration is increasing instead of decreasing, demonstrating that when the damping ratio is small, the increasing thickness of the damping layer may have a negative effect. This can be explained when the damping ratio is small, the main factor affecting the vibration response is the stiffness characterization (elastic modulus & Poisson's ratio). The elastic modulus of the damping layer is given as 1310 MPa which is a relatively small value compared with the one of the asphalt layer (5679MPa). Hence, it is possible that the increasing thickness has a negative effect.

However, such a negative effect can only occur when the monitoring point is point A. Considering the vibration reductions at point B and point C, it can be concluded that with the increase of the thickness the vibrations reduce. In addition, the reduction is almost linear and the rates of reduction are almost constant for all thicknesses, from which it can be concluded that 'the thicker the damping layer, the better performance of the vibration reduction' instead of being able to determine a threshold (optimized) value. Therefore, it is difficult to find the optimized thickness by only considering the vibration-reduction ability. However, based on the consideration of construction cost and pavement structure reliability as well as the reference values from literature (Dondi et al. 2005; Grandi, 2008), 30 mm seems to be the optimized thickness.
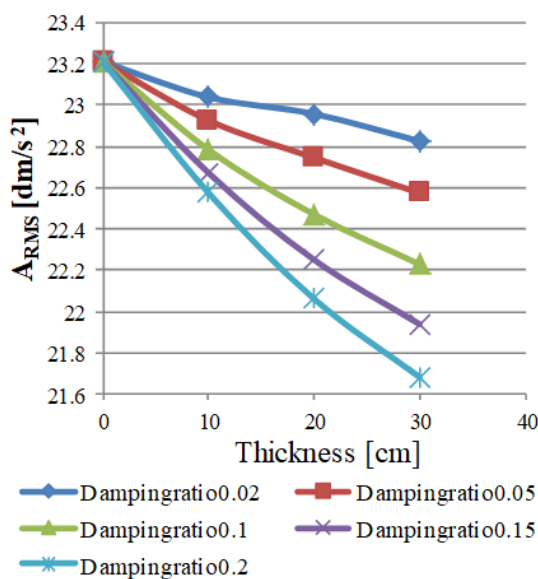
(1) Distance to the top is 0cm   (2) Distance to the top is 5cm
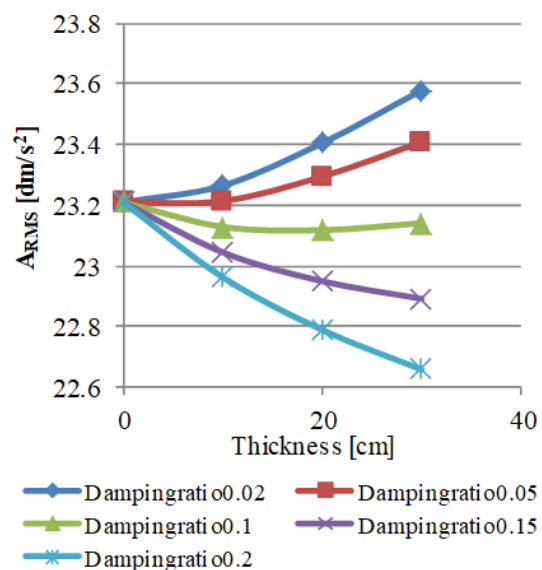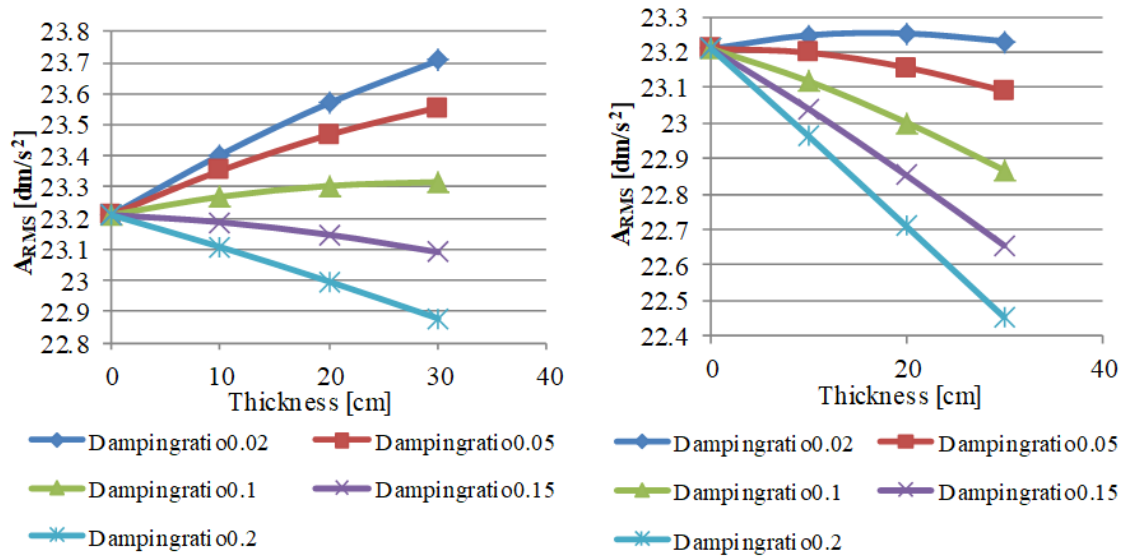
(3) Distance to the top is 10cm

(4) Distance to the top is 15cm
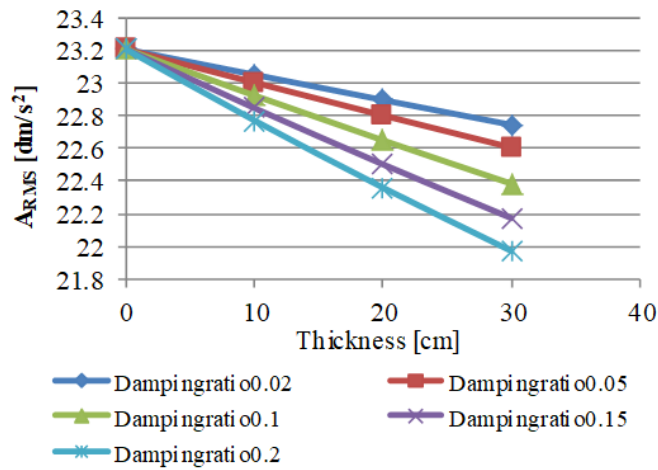
(5) Distance to the top is 20cm

Figure 5.18 The effects of damping layer thickness at point A
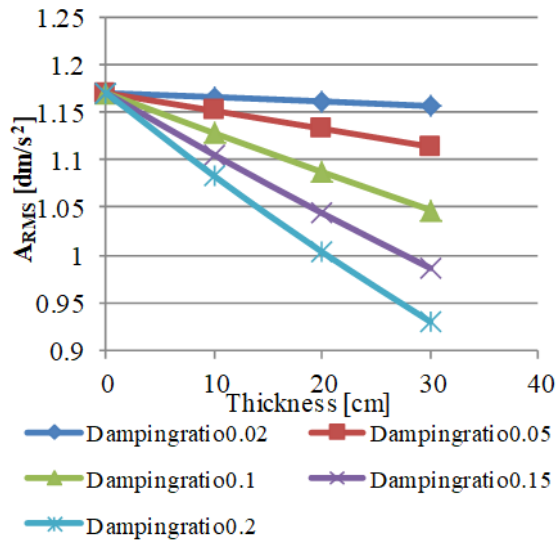
(1) Distance to the top is 0cm
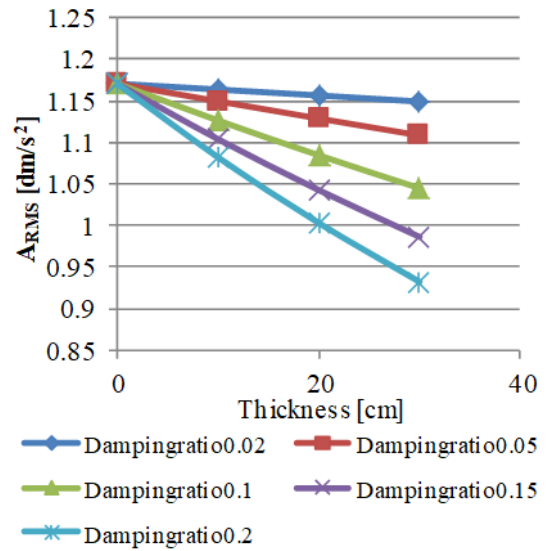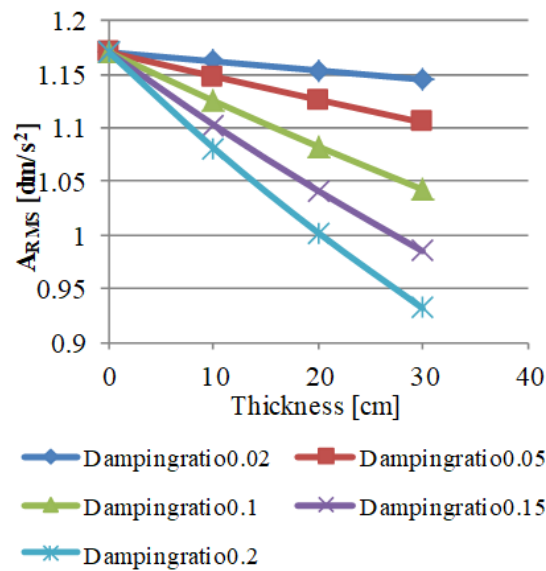
(2) Distance to the top is 5cm

(3) Distance to the top is 10cm
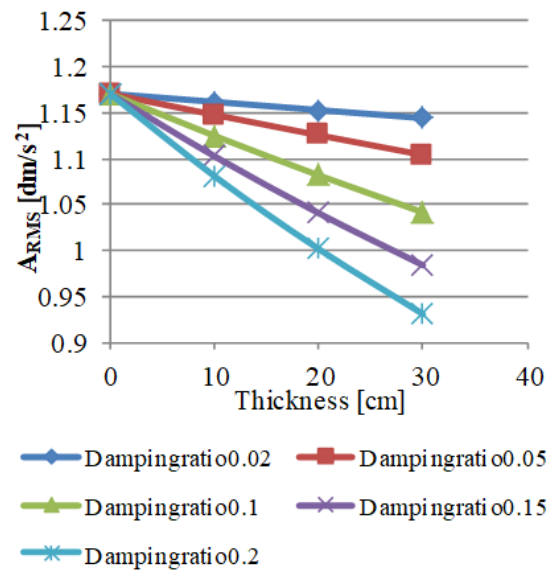
(4) Distance to the top is 15cm
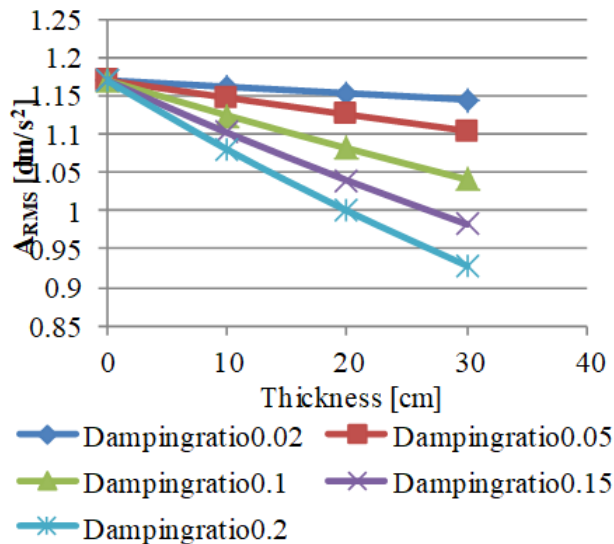
(5) Distance to the top is 20cm

Figure 5.19 The effects of damping layer thickness at point B
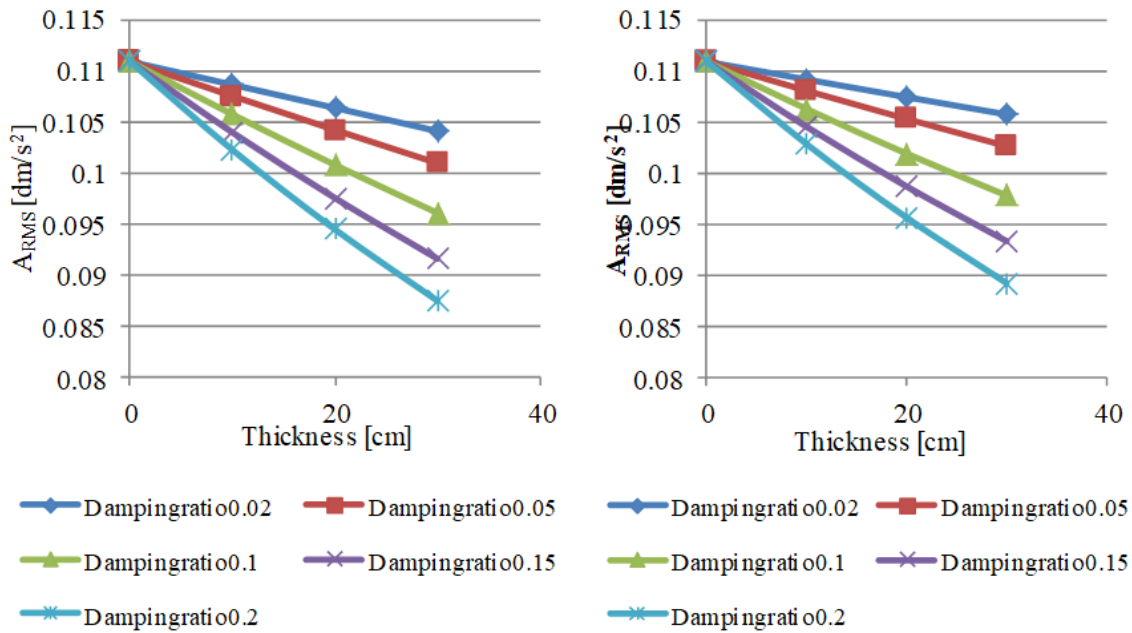
(1) Distance to the top is 0cm
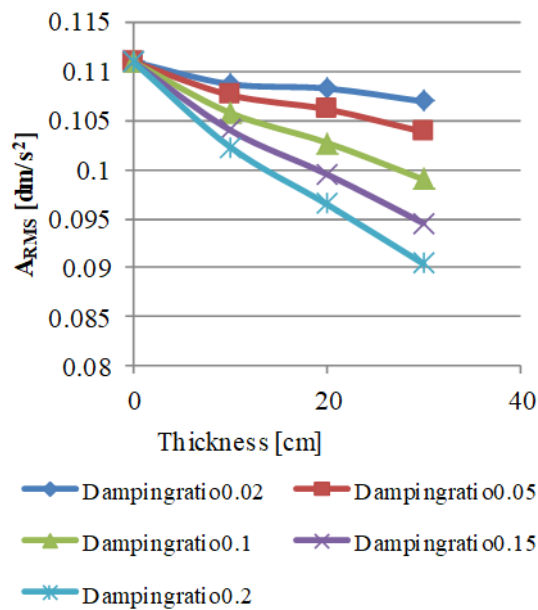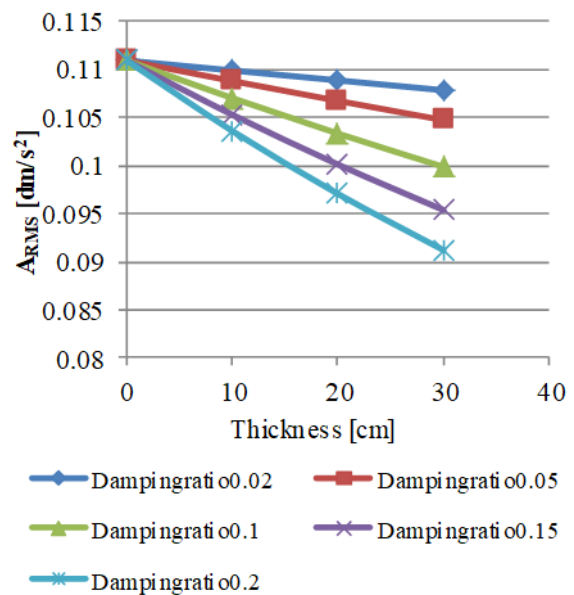
(2) Distance to the top is 5cm

(3) Distance to the top is 10cm

(4) Distance to the top is 15cm
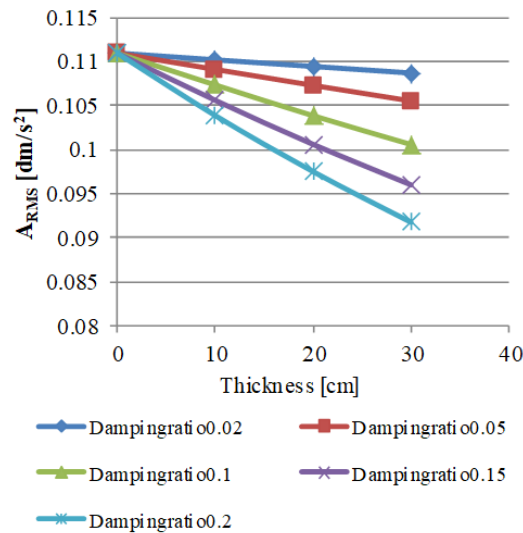
(5) Distance to the top is 20cm

Figure 5.20 The effects of damping layer thickness at point C

5.2 Effect of the damping layer on mechanical response and pavement performance

According to the analysis in Chapter 5.1, it is difficult to determine the optimized position of the damping layer by only considering the vibration response of the road system. In addition, it is known that the reliability of pavement structure during the working process is also a very important design consideration. In this part, based on the reliability of pavement structures, the mechanical response and pavement performance are compared when the damping layer is laid at varying positions.

5.2.1   Effect of the damping layer on the mechanical response

The static analysis software BISAR and dynamic analysis software 3D-Move are selected as the calculation tools for the mechanical response. The same pavement structures described in Table 5.2 are selected. The condition that the damping layer laid at the top of the asphalt layer is not in consideration.

As far as the static analysis is concerned, the horizontal strain, vertical strain and Mises strain along the vertical axis of the loading position are evaluated, as shown in Figure 5.21-5.23.

As far as the horizontal strain is concerned, the most important and sensitive location is at the bottom of the asphalt layer, where there is a 'large tensile strain' (See Figure 5.21). Another sensitive position required special attention is the one in the damping layer, where the tensile strain may occur.

It can be observed from Figure 5.21, as far as the 'large tensile strain' is concerned, all the positions show similar values, except when the damping layer to top=20 cm, which shows a little higher value compared to others. As far as the tensile strain occurs in the damping layer, when the damping layer to top=5 cm (compressive strain occurs) and the damping to top=10 cm (minimum tensile strain occurs) are more preferable. Figure 5.22 shows the vertical strain along with the depth with varying damping layer position. It can be observed that according to vertical strain occurring in the damping layer, the priority ranking is without damping layer > damping layer to top = 20 cm > damping layer to top = 15 cm > damping layer to top = 10 cm > damping layer to top = 5 cm, which is contradictory to the results when the horizontal tensile strain is concerned. Hence, in order to further explore the optimized position, Mises strain along the vertical axis of the loading position is analyzed, as shown in Figure 5.23. It can be observed that the minimum Mises strain occurs when the damping layer to top=5 cm, which is the position maximum vertical strain occurs. From a more conservative perspective, we believe that the second-best option may be chosen, that is, damping layer to top = 10 cm, as the optimized damping layer position.
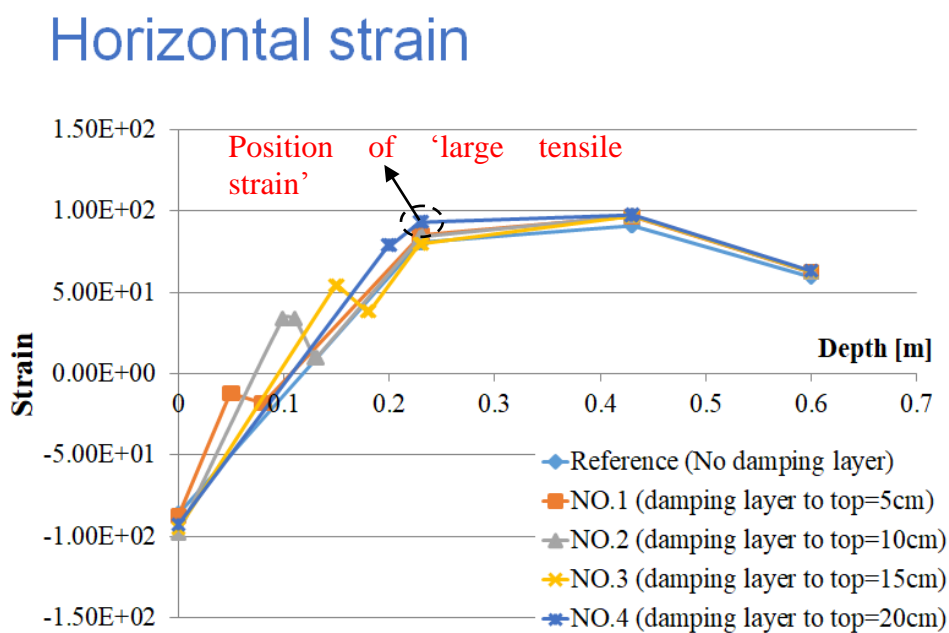
Figure 5.21 Horizontal strain along the vertical axis of the loading position
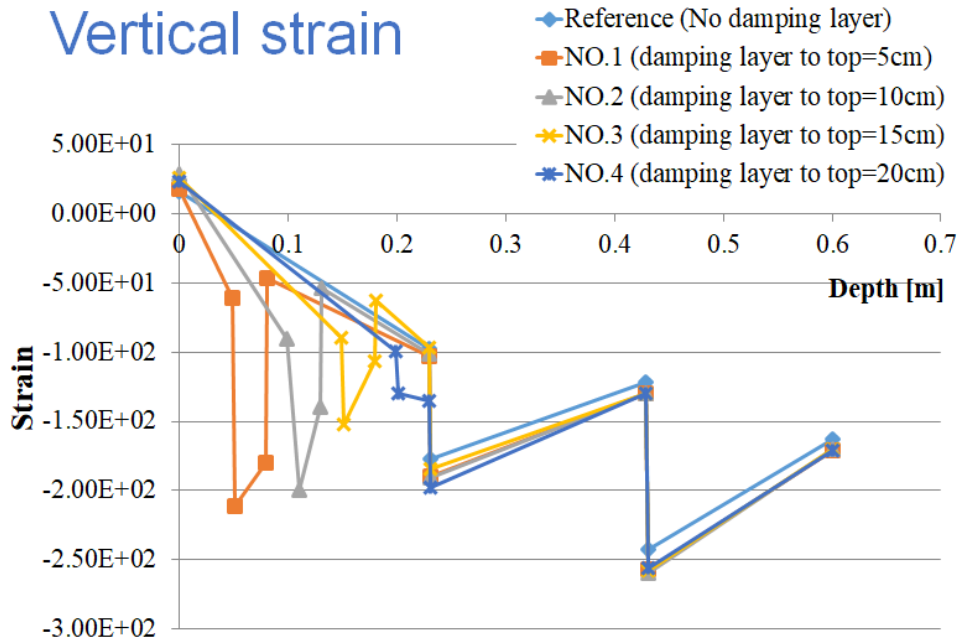
Figure 5.22 Vertical strain along the vertical axis of the loading position
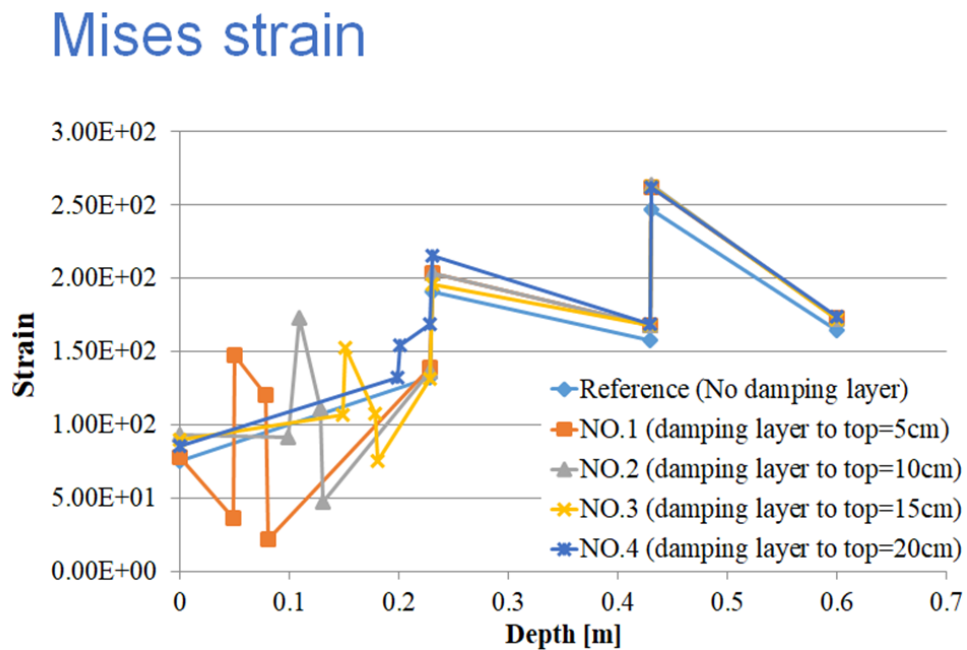
Figure 5.23 Mises strain along the vertical axis of the loading position

3D-Move software developed by the University of Nevada is used for the dynamic analysis. It is conducted at 20 °C representing, the intermediate temperature where fatigue cracking and permanent deformation may be expected to be a problem. For the purpose of this study, the contact stress distribution at the tire–pavement interface is modeled using a circular load area with a uniform contact pressure equal to the tire inflation pressure, which is defined in the 3D-Move software. As the major step

undertaken in the dynamic analysis, the normal strain response histories evaluated for the 5 pavement structures under 72 km/h vehicle speeds are selected, and the longitudinal strain, transverse strain and vertical strain histories at the bottom of asphalt layer are presented in Figure 5.24. It can be observed that, though the peak values of both strains occur at a similar time, their characteristic shapes are different. While longitudinal strain history (ε_{xx}) has both compressive and tensile components, the transverse strain history (ε_{yy}) has only tensile components.

From the perspective of minimizing the strain (longitudinal, transverse, vertical) at the bottom of the asphalt layer, it is the optimum choice when the distance from the damping layer to the top is 5 cm, 10 cm or 15 cm. However, it should be noted that the horizontal and vertical strain at the bottom of the asphalt layer is not the only parameter that needs to be monitored as previously mentioned. Based on this consideration, the maximum longitudinal, transverse, and vertical strains at the center of the tire are also computed within the entire pavement structures and the results are presented in Figure 5.25.

As far as the longitudinal strain is considered, the distance from the damping layer to the top equal 10 cm or 15 cm seems to be the optimal choice because they have minimal strain at the damping layer location, and the same conclusion is obtained considering the transverse strain. For the vertical strain, results very similar to static analysis are obtained, which is contrary to the results of horizontal strain. However, it should be noted that a thin damping layer thickness (3 cm) has been considered to address the possible large vertical strain, so the mechanical response of the horizontal strain should probably be considered more. Therefore, considering the horizontal tensile strain of the damping layer and the bottom of the asphalt, 10cm from the top can be the optimized position for the damping layer.

Combined with the above mechanical analysis and the vibration-reduction analysis in the previous chapters, the optimized damping layer position is considered to be 10 cm from the top. This conclusion will also be verified in sub-chapter 5.2.2 based on the pavement performance.
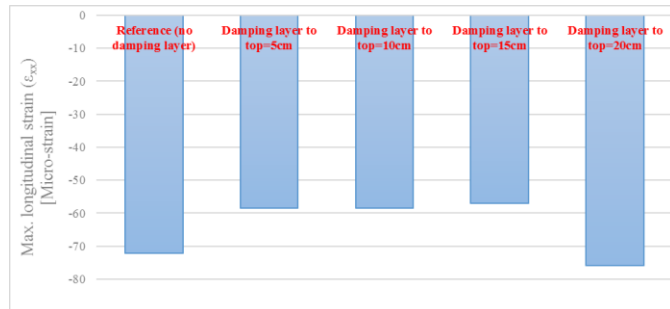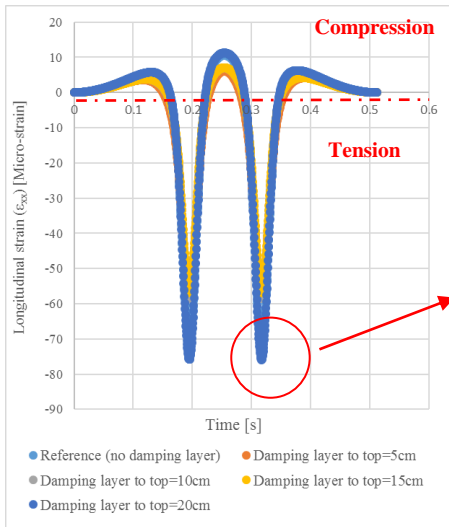
(1)
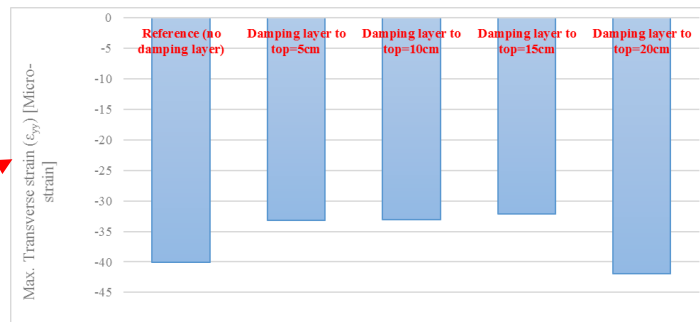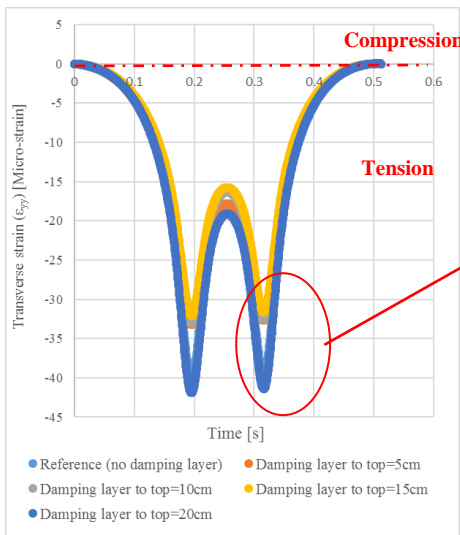
(2)
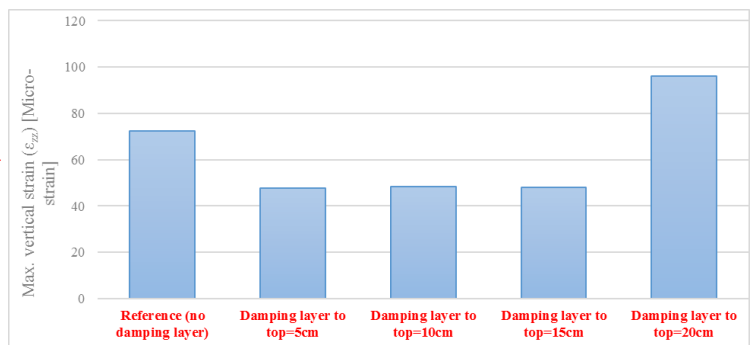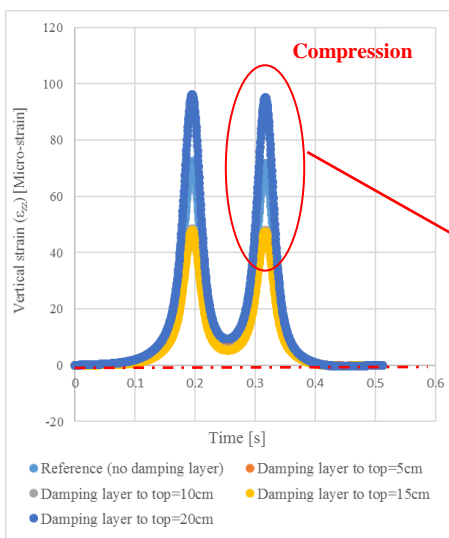
(3)

Figure 5.24 (1) Longitudinal strain (ε_{xx}); (2) transverse strain (ε_{yy}); (3) vertical strain (ε_{zz}) histories at the center of the tire at the top, middle, and bottom of asphalt layer at 72 km/h
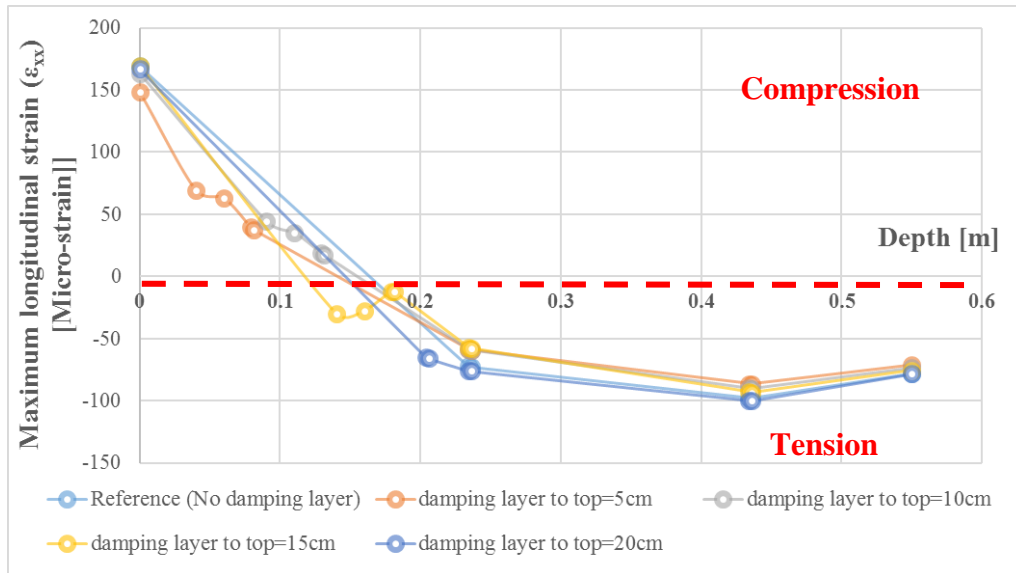
(1)
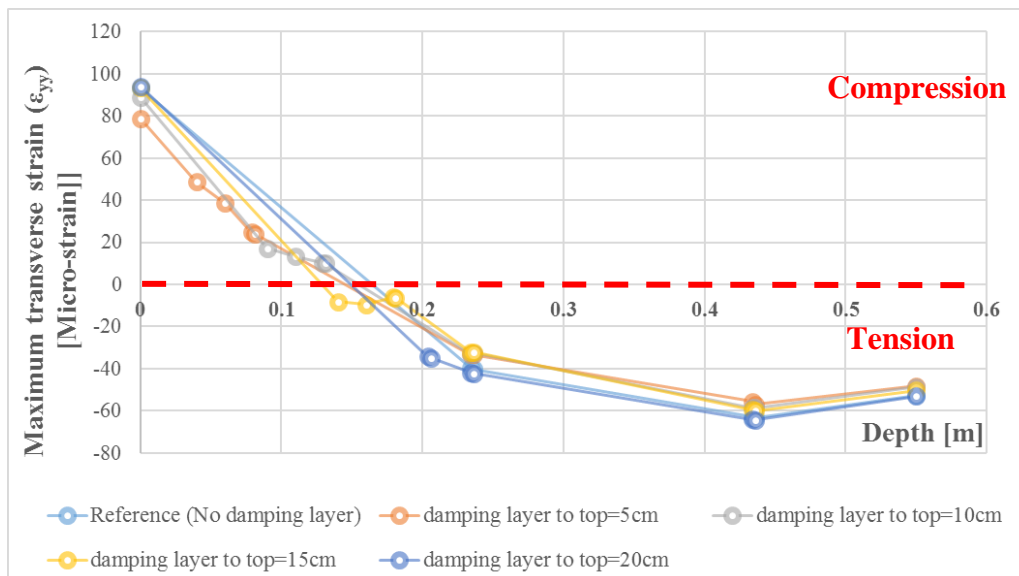
(2)
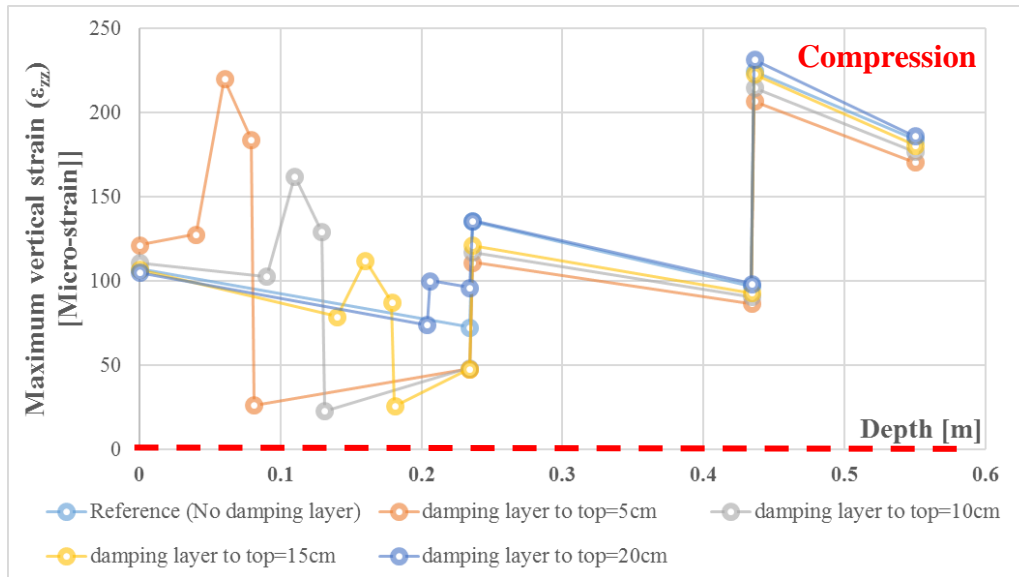
(3)

Figure 5.25 Maximum longitudinal, transverse, and vertical strains at the center of the tire in the pavement

5.2.2 Effect of the damping layer on pavement performance

5.2.2.1 Description of the method

In order to select the optimized position of the damping layer, the effects of the damping layer on pavement performance (rutting, cracking et al.) are evaluated in this part. 3D-Move Analysis software is used for calculating the pavement performance of AC, subbase, and subgrade (Eslaminia et al. 2012). It uses a continuum-based finite-layer approach to compute pavement response and can account for important pavement response factors such as moving loads, three-dimensional contact stress distributions (normal and shear) of any shape, and viscoelastic material characterization for the pavement layers (Siddharthan et al. 1998; Siddharthan et al. 2005).

1) Load

As shown in Figure 5.26, the dual tire tandem axle load configuration with four circular contact areas is selected. The contact pressure is assumed to be uniform over the contact area with a magnitude of 862 kPa and the half axle load is 90 kN (22.5 kN/tire).
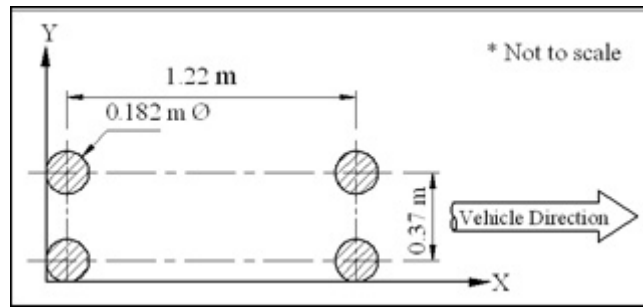
Figure 5.26 Load condition

2) Traffic information

The traffic information is shown in Figure 5.27. The one-way average daily repetition of the design axle is 200. The percentage of design axles in the design lane is 90%.

Figure 5.27 Traffic information
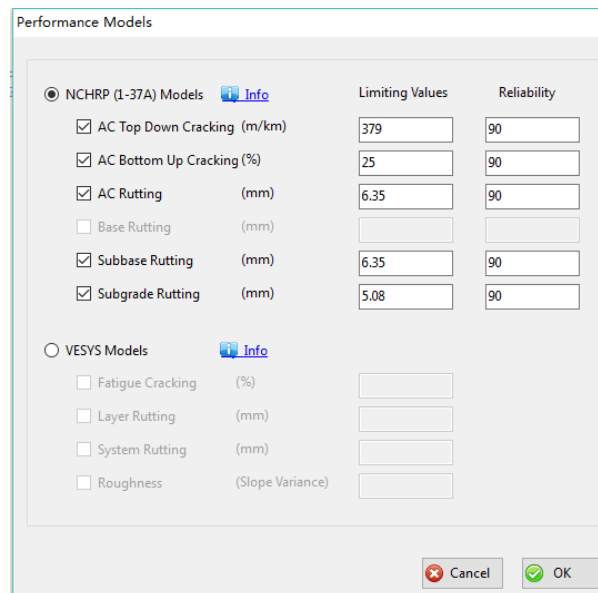
Table 5.6 Pavement structures

Configurations	Distance from AC top to damping layer top (cm)
Reference	Without the damping layer
Damping layer to top=0 cm	0
Damping layer to top=5 cm	5
Damping layer to top=10 cm	10
Damping layer to top=15 cm	15
Damping layer to top=20 cm	20

Six configurations of pavement structures are selected in order to see the effect of the damping layer position on pavement performance. The distance from the AC top to the damping layer top varies from 0 cm, 5 cm, 10 cm, 15 cm, to 20 cm, as shown in Table 5.6. The mechanical properties of different layers in Table 5.1 are used and the temperature of the AC layer is set at 20℃.

3) Performance model

NCHRP (1-37A) models are selected as the performance model to evaluate the AC rutting, subbase rutting, and subgrade rutting. The limiting values and reliability of the above factors are shown in Figure 5.28.

Figure 5.28 Performance models

5.2.2.2 Results and analysis

Table 5.7 shows the results of pavement performance after 972000 times design axle load repetitions. It can be found that as far as the subbase rutting and subgrade rutting, no meaningful difference is found for varying damping layer position.

As far as AC rutting is concerned, it can be found that only when the damping layer to top=10 cm and the damping layer to top=20 cm are within the limits of the specification (see Figure 5.26). However, according to analysis in Chapter 5.2.1 (or see Figure 5.21), when the damping layer to top=20 cm, the maximum horizontal tensile strain can occur and this position is not preferable. Therefore, the damping layer to top=10 cm can be

regarded as the optimized position according to the comprehensive considerations of damping characteristics (sub-chapter 5.1.2), mechanical responses (sub-chapter 5.2.1) and pavement performances (sub-chapter 5.2.2).

Table 5.7 Pavement performance for varying configurations (T=20℃)

Configurations	AC rutting (mm)	Subbase rutting (mm)	Subgrade rutting (mm)
Without the damping layer	3.86	0.44	1.87
Damping layer to top=0 cm	3.8	0.49	2.18
Damping layer to top=5 cm	8.83	0.48	1.96
Damping layer to top=10 cm	5.13	0.48	2.11
Damping layer to top=15 cm	6.67	0.47	1.94
Damping layer to top=20 cm	4.18	0.49	2.14

Chapter 6: Design and evaluation of asphalt mixtures of the vibration-absorbing damping layer

6.1 Asphalt mixtures for damping layer

According to the analysis in Chapter 5, the vibrations of the surrounding environment and buildings can decrease by more than 20% when the damping layer is laid in the pavement structure. Such improvement is of great significance for increasing the quality of life and health of the surrounding people and it also increases the service life of surrounding buildings; in addition, according to the analysis carried out by Biligiri (2001), such a higher noise-damping response is beneficial for reducing tire-road noise. In this chapter, asphalt mixtures specifically for damping layers are designed and evaluated. In order to be used as a damping layer, besides to meet basic requirements for road pavements,

1) the asphalt mixtures must have enough high damping properties. According to the analysis in Chapter 5, its energy dissipation capacity should be 3-4 times higher compared to conventional AC or 2 times higher compared to RMAC in order to obtain sufficient vibration reduction;

2) the asphalt mixtures must have enough water resistance. This is because, in order to be designed as LNPs, the upper layer or surface layer will be a gap-graded asphalt mixture and rainwater may seep and flow from the upper layer;

3) the asphalt mixtures must have enough rutting resistance. This property must be taken seriously in the design process. Generally speaking, rutting resistance and damping property are often the opposite parameters (Ye et al. 2009). E.g. Higher rutting parameter $G^*/\sin\varphi$, means a lower tan φ thus the lower damping;

4) the asphalt mixtures should have a good ability to work together with the upper and lower structures.

6.2 Mix design

Damping is intended as the capacity of (viscoelastic) materials to dissipate mechanical energy (Zinoviev and Ermakov, 1994; Inaudi and Kelly, 1995; Feriani and Perotti, 1996; Michaels, 2008; Phillips and Hashash, 2008).

A critical distinction is made between damping of a composite structure, and damping as a material property (i.e., intrinsic damping). The first entails hysteresis, friction at joints, and other phenomena occurring the structure that causes energy dissipation. Friction between two surfaces is a clear example of this. Damping of structures depends on multiple phenomena that affect the overall dynamic response (Bergman and Hannibal 1976; Bishop 1955; Lazan 1968; Ungar 1992). For this reason, this type of damping is not modeled at the constitutive level of the materials that compose the structure.

On the other hand, the intrinsic damping is a material property and it is typically modeled considering constitutive relations and rheological properties of materials as road bitumens (Dos Reis et al., 1999; Wang et al., 2008; Gudmarsson et al., 2013).

According to many authors (Lazan 1968; Nashif et al., 1985), the loss factor (η) is the viscoelastic function most representative of intrinsic damping. It can be successfully applied to nonlinear systems, used in material testing or in evaluating composite structures. The loss factor measures the energy dissipation irrespective to the physical mechanisms involved.

The original definition of η refers to the time lag between stress and strain under sinusoidal cyclic loadings. This is a measure of the dissipative mechanisms in the materials. The higher is the loss factor, the more the material dissipates energy under loading. Asphalt mixtures are composite in nature and cannot be truly defined as structures. However, despite the presence of different constituents, their viscoelastic and damping properties, depending on the presence of bitumen, which is responsible for the energy dissipations that have challenged pavement engineers for decades. Therefore, the optimization of the damping properties of asphalt mixtures requires increasing the bitumen as a unique constituent that provides energy dissipation. However, this is not an easy task.

In fact, asphalt mixtures have been traditionally designed to be rutting and fatigue cracking resistant (Bahia et al., 2001; Witczak, 2002). These properties were truly challenged by the viscoelastic nature of bitumens that causes energy dissipation and consequent failure. Considering this, increasing the damping properties of mixtures could be literally seen as something that is against the adopted criteria for the design of asphalt mixtures. Therefore, mixes for damping layers shall be designed to mitigate vibrations under the constraints of adequate performances and durability.

The optimization of the damping properties of pavements is quite novel if compared with other traditional criteria (Kuo & Tsai, 2014). Therefore, if rutting resistance and fatigue cracking resistance can be balanced, the effects of optimized damping properties on them require still investigation. Therefore there is a need for more advanced analytical and experimental tools to enable designers to account for damping properties in pavement materials.

This work includes the findings of a wide laboratory investigation of mixes for the damping layer in the attempt to enhance the methodology for their design.

6.2.1 Materials

(1) Rubberized binder

The rubberized binder was supplied by a local manufacturer in Tuscany. The binder was produced according to the wet process by mixing a Pen 50-70 base bitumen with 20% of crumb rubber. The gradation of the rubber particles is given in Figure 6.1.
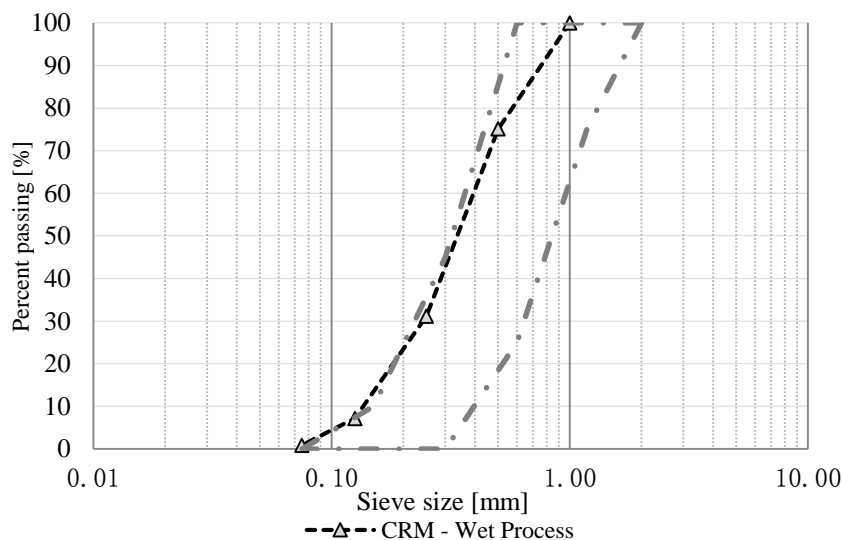
Figure 6.1 Gradation of rubber particles

(2) Aggregates

The dry mix was constituted of basalt coarse aggregates, natural sand, and mineral filler. The physical properties of the aggregates are given in Table 6.1.

Table 6.1 Physical properties of aggregates

Properties	Basalt	Sand	Mineral Filler
Bulk Specific Gravity (G_{sb})	2.753	2.629	2.650
Water Absorption (%)	1.39	0.86	-

6.2.2 Design of mixtures

Increasing damping properties of asphalt mixtures requires the use of higher volumes of (rubberized) binder compared to traditional rubberized hot mix asphalt. For this reason, the mix design has the scope to accommodate a sufficient volume of rubberized binder to increase damping while maintaining an adequate aggregate structure.

The use of an open-graded (OG) mix meets these requirements since it has a large volume of voids in mineral aggregates (VMA), and the aggregate interlock is provided by angular tough basalt aggregates. Traditionally, this mix is designed to achieve the volume of air voids in compacted mixtures between 20 and 25% with the scope of providing adequate drainage and noise absorption. In the damping layers, the large VMA available needs to be filled with rubberized asphalt to increase the volume of effective bitumen (V_{be} – bitumen not absorbed in mineral aggregates), the film thickness of the mortar (bitumen + filler) that coats the mineral coarse and fine aggregates (Underwood & Kim, 2013).

Higher values of VMA and V_{be} are likely to increase the durability of mixtures providing a higher fatigue resistance and a lower oxidative susceptibility (Kandhal & Chakraborty, 1996). However, the excessive binder content could affect the stability of the mixtures at high temperatures worsening their rutting resistance (Christensen & Bonaquist, 2005). The large film thickness of mortar coating the aggregates could reduce the grain-to-grain contact in the aggregates skeleton reducing the stability of the mixture. This type of consideration applies to mixtures used in road pavements to be durable and rutting resistant. In the case of mixtures for the damping layer, the scope is

to maximize damping, therefore the higher volume of bitumen that is used is not representative of "traditional mixtures". However, the optimization of the damping properties cannot affect the rutting resistance of mixtures. Therefore, the basic criteria behind their design are to increase damping maintaining an acceptable rutting resistance. To do this, it is necessary to stiffen the mastic coating the aggregates by increasing the volume of filler in the mastic. In other words, the amount of binder shall be increased contextually with the amount of filler.

6.2.2.1 Reference mixture

An Open-Graded (0-8 mm) mixture was selected as the reference mixture (Mix_{ref}). This mix design was optimized in a previous project where showed satisfactory functional and mechanical performances (Losa & Leandri, 2012). The mixture was prepared in the Superpave Gyratory Compactor (SGC) according to the EN 12697 – Part 10, and using mixing and compaction temperatures equal to 180°C under the recommendation of the bitumen supplier. The mix was compacted at 50 gyrations. The gradation of Mix_{ref} is given in Figure 6.2.
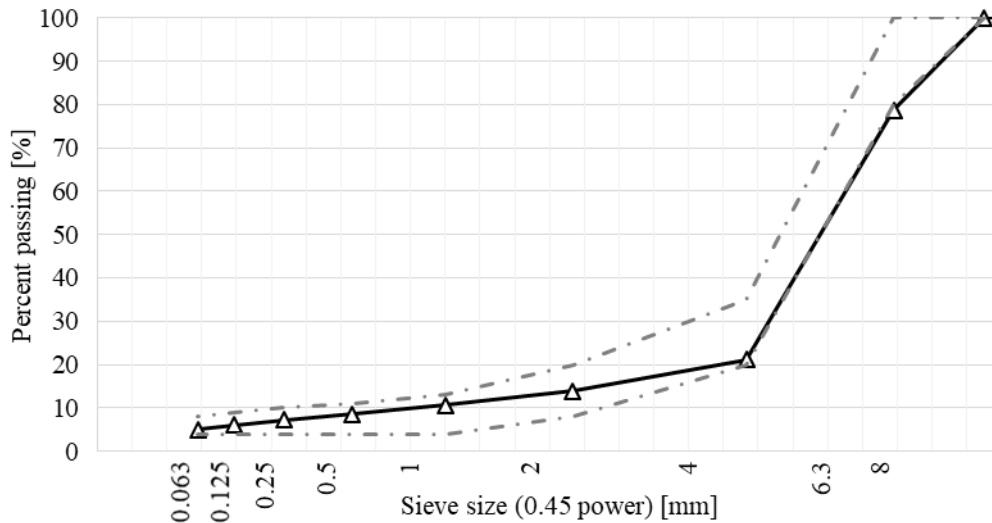
Figure 6.2 Gradation of Reference Mixture (Mixref)

The volumetric properties are given in Table 6.2.

Table 6.2 Volumetric properties (by weight and by volume) of reference mixture
(UNI EN 12697 – Part 5, 6 and 7)

Composition	Aggregate [%]	Filler [%]	Binder [%]	N_{des}	AV[%]	VMA [%]	VFA [%]	D/P
Weight (W)	90.4	4.8	4.8		-			
				50		36.1	22.9	0.95
Volume (V)	60.7	3.2	8.3		27.8			

(N_{des} – Design gyrations number of SGC; AV – Air Voids; VMA – Voids in Mineral Aggregates; VFA – Voids filled with Asphalt; D/P – Dust to binder ratio).

The mixtures for damping layers are designed starting from this mix.

6.2.2.2 Mixtures for damping layer (Mix 1 and Mix 2)

The mixtures were prepared in the SGC at the same mixing and compaction temperatures of the reference mixture. The gradations and volumetrics of the mixtures for damping layers are shown respectively in Figure 6.3.
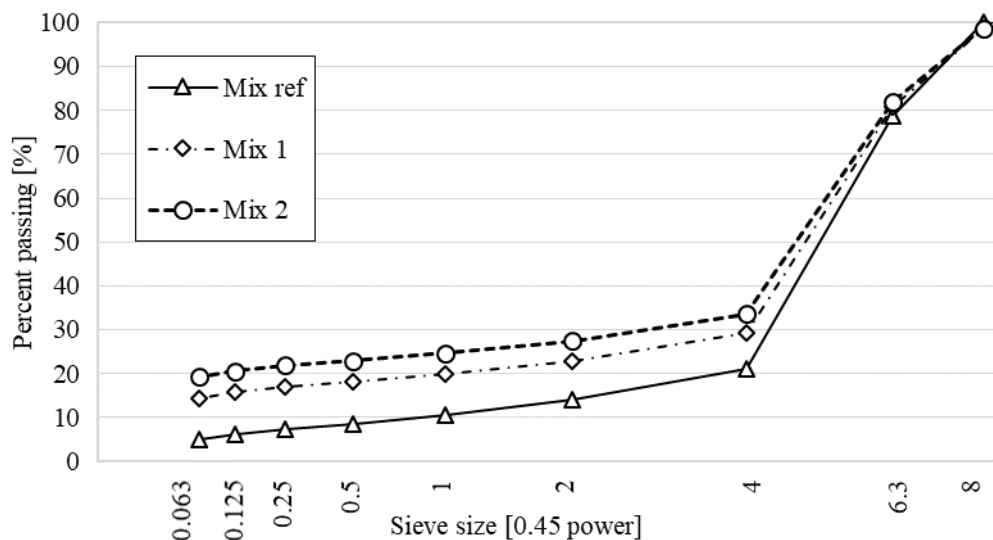
Figure 6.3 Gradations Mix 1 and Mix 2

Volumetrics for mix design were calculated on compacted 100 mm diameter mixtures (Table 6.3).

Table 6.3 Volumetric properties Mix 1 and Mix 2 (UNI EN 12697 – Part 5, 6 and 7)

Mix		Aggregates [%]	Filler [%]	Binder [%]	N_{des} [1]	AV[%]	VMA [%]	VFA [%]	D/P [1]
Mix 1	W	77.2	9.9	12.9	50	-	29.8	90.3	0.97
	V	63.2	7.1	26.9		2.8			
Mix 2	W	68.3	15.0	16.7	50	-	35.9	92.2	0.97
	V	54.5	9.6	33.0		2.9			

The mixtures contain a higher bitumen content compared to the reference mixture (Mix 1 + 8.1% by weight); Mix 2 + 11.9% by weight). However, it is known that the fraction in the mix that coats the coarse and fine aggregates is not represented by the binder alone, but it consists of the mastic formed by binder + filler. Therefore, the amount of binder in the mix has been increased as long as the amount of filler. Table 6.3 shows that Mix 1 and Mix 2 have a higher amount of filler compared to the reference mixture (Table 6.2) (Mix 1 +5.1%; Mix 2 +10.2%). It has to be noted that the filler and binder have been increased by maintaining the same D/P proportion (~1) of Mix_{ref}. This aspect is relevant since it indicates that the amount of binder has been maximized by maintaining the same volume fraction of filler in the mastic. For this reason, the mastics in the three mixtures are expected to have similar levels of stiffness preventing them from losing stability and from becoming rutting susceptible due to the high binder content. This aspect is common in the design of both Mix 1 and Mix 2, however, the two mixtures have different binder content.

In Mix 1 the amount of extra filler and extra bitumen added by following two criteria. The first was to maintain the same D/P of the reference mixture (~1.0). The second was that the volume of the VMA calculated considering the volume of Air Voids (AV), absorbed binder (V_{be}) and filler (V_f) was approximately equal to the VMA of the reference mixture. Considering this, the amount of extra binder (ΔP_b) and extra filler (Δf) were calculated by solving the following system of Eq. (6.1) and Eq. (6.2),

$$\begin{cases} \dfrac{P_{f_i} + \Delta P_f}{\left(P_{be_i} + \Delta Pb_e\right)} \cong 1.0 & (6.1) \\[2em] \dfrac{AV + \left(V_{be_i} + \Delta V_{be}\right) + \left(V_{f_i} + \Delta V_f\right)}{V_{agg} + V_b + AV} \cong 36.1\% & (6.2) \end{cases}$$

where, P and V refer to the % weight and % volume of:

- f_i – of particles passing #0.063 (filler) mm sieve in Mix$_{ref}$;

- be_i – effective binder in Mix$_{ref}$;

and where:

- ΔP_f – %weight extra-filler;

- ΔPb_e - %weight of extra effective bitumen;

- AV – represents the air voids in the compacted mix [%];

- V_{agg} – represents the volume of aggregates in the mix [%];

- V_b – represents the volume of binder in the mix [%];

Eq. (6.1) comprises the criteria of the stiffness of the mastic included above. Equation Eq. (6.2) indicates that in Mix 1 the entire VMA in the reference mixture has been filled with the rubberized mastic to maximize the damping. The comparison of the VFA of Mix$_{ref}$ (Table 6.2 – 22.9%) with those of Mix 1 (Table 6.3 – 90.3%), shows that in the latter almost all the VMA available were saturated with the mastic. The volume of mastic in Mix 1 was limited by the VMA of Mix$_{ref}$ to preserve a sufficient level of aggregates interlock.

Mix 2 was prepared by following the same considerations if Mix 1 (Eq. (6.1) and Eq. (6.2)) but an extra amount of binder (5% in weight) was added to go beyond the saturation of the VMA in the Mix$_{ref}$ to increase further the damping of the mixture. In this case, the results of Eq. (6.2) show that the VMA filled with mastic is equal to 45.5% with the VFA in the mix equal to 92.2%.

The behavior of the mixtures under compaction is discussed in the following parts.

6.3 Methods of laboratory tests

The test methods used in this work are given in Table 6.4.

Table 6.4 Test methods

Test method	Scope
Indirect Tensile Test (ITT) *EN 12697-23*	Measure the stability and the moisture susceptibility of the mixtures.
Dynamic Modulus ($|E^*|$), Phase Angle and Loss Factor (η) *AASHTO TP-79,* ISO 6721-3	Measure the stiffness ($|E^*|$), the internal dissipative mechanisms of the mixtures as a function of the phase angle (δ), and the intrinsic damping as a function of the loss factor (η).
Hamburg Wheel Tracking (HWT) test *AASHTO T324*	Measure the rutting resistance and the moisture susceptibility of the mixtures.

Some details of each test method are given below.

6.3.1 Indirect tensile test (ITT)

The test was conducted on 100 mm diameter compacted samples (SGC according to EN 12697 – 10). Mixing and compaction temperatures were kept at 180°C, and the number of gyrations for each mix is given in Table 6.2 (Mix_{ref}) and Table 6.3 (Mix 1 & 2). The samples were tested at two conditions by using three replicates for each condition. The first is the dry condition, which is conducted on dry samples conditioned at 25°C. The second is the wet condition that is conducted at 25°C on samples conditioned in the water bath at 40°C for 72 hours.

The Indirect Tensile Strength (ITS) is calculated according to Eq. (6.3).

$$ITS = \frac{2P}{\pi DH}[MPa] \tag{6.3}$$

where:

- P is the peak load [N];

- D is the sample diameter [mm];

- H is the sample height [mm].

The ITS is measured in dry (ITS$_d$) and wet (ITS$_w$) conditions. The ratio between the values at the two conditions is measured of the moisture susceptibility of the mixture intend as the loss in tensile strength due to the effects of water (Indirect Tensile Strength Ratio – ITSR, Eq. (6.4)).

$$ITSR\ [\%] = \frac{ITS_w}{ITS_d} \times 100 \tag{6.4}$$

6.3.2 Dynamic modulus |E*| and phase angle (δ)

The viscoelastic properties of the different mixtures were measured according to the AASHTO TP 79-12 standard. For each mixture, two 150 mm diameter samples were prepared in the SGC according to the AASHTO PP60-09 standard. The samples were compacted to a height of 175 mm. After compaction and cooling at room temperature, the samples were cored to a diameter of 100 mm and cut at the height of 150 mm. An example is shown in Figure 6.4 (a).

(a) (b) (c)
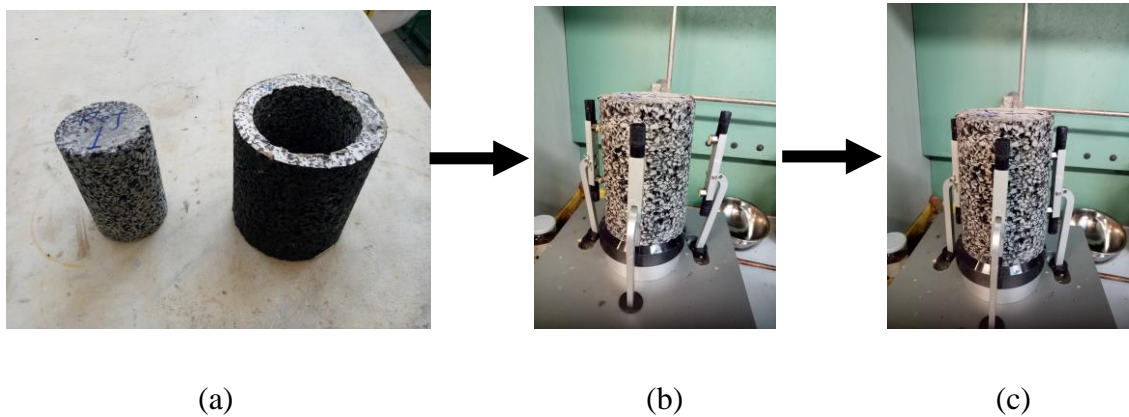
Figure 6.4 Dynamic modulus and phase angle test sample (a), and test set-up (b,c)

Three strain gauges were attached at intervals of 120°C considering the cross-section of the sample. The gauge length is 70 mm measured center-to-center of the gauge point (Figure 6.4 - b). Teflon sheets were used at the top and bottom edges of the sample to avoid friction with the loading plates (Figure 6.4 - c). The test conditions are reported in Table 6.5.

Table 6.5 Test conditions for dynamic modulus, phase angle and loss factor test

Test conditions	Configuration
Test temperature [°C]	5, 20, 31
Loading frequency [Hz]	0.1, 0.5, 1, 2, 5, 10, 20, 25
Strain level	100 µs
Confinement	Unconfined conditions

The master curves of the Dynamic Modulus (|E*|) and the phase angle (δ) were developed under the applicability of the time-temperature superposition principle (TTSP) (Ferry, 1980).

Horizontal shift factors were calculated by the William-Landel-Ferry (WLF), as shown in Eq. (6.5).

$$\log \alpha_T = -\frac{C_1 \cdot \left(T - T_{ref}\right)}{C_2 + \left(T - T_{ref}\right)} \tag{6.5}$$

where:

a_T − is the shift factor;

C_1 and C_2 − are model parameters whose values are determined fitting the data;

T_{ref} − is the reference temperature;

T − is the testing temperature.

The dynamic modulus (|E*|) and the phase angle data were modeled by using the Modified Christensen-Anderson-Marasteanu (CAM) model (Zeng et al, 2001).

The |E*| master curve of the CAM model is given by Eq. (6.6).

$$|E^*| = E_e + \frac{E_g - E_e}{\left[1 + \left(\frac{f_c}{f_r}\right)\right]^{\frac{m_e}{k}}} \tag{6.6}$$

where:

$|E^*|$ - is the dynamic modulus;

E_e – is the Equilibrium Modulus, which represents the value of stiffness at f→0. Its value represents the horizontal asymptote in the low frequencies region. In the case of mixtures, its value is considered to depend on the ultimate aggregate interlock when the contribution of the binder (or the mastic) results negligible.

E_g – is the Glassy Modulus, which represents the value of stiffness at f→∞. Its value represents the horizontal asymptote in the high frequencies region.

f_r - is the reduced frequency;

f_c – it is a location parameter that has the dimension of frequency. It is known as crossover frequency, which is the frequency where the storage modulus (E') is equal to the loss modulus (E").

m_e, k – shape dimensionless parameters.

The CAM model equation of the phase-angle master curve is given by Eq. (6.7).

$$\delta = 90I - (90I - \delta_m)\left[1 + \left(\frac{\log(f_d / f_r)}{R_d}\right)^2\right]^{-\frac{m_d}{2}}$$

$$\begin{cases} I = 0 \; for mixes \\ I = 0 \;\; if \;\; f_r > f_d \\ I = 1 \;\; if \;\; f_r < f_d \end{cases}$$

(6.7)

where:

δ – is the phase angle;

δ_m – is the phase-angle value at f_d. In the case of mixtures, it represents the maximum phase-angle value;

f_d – it is a location parameter with the dimension of frequency. It is the frequency at which δ_m occurs;

f_r – is the reduced frequency.

In damping materials, the measure of the phase angle is critical because it represents a measure of the internal damping of the material. High values of phase angle imply high internal friction and therefore more dissipative behavior under loading (a more viscous behavior). On the other side, lower values of phase angle denote a more elastic response of viscoelastic materials, which indicates the higher capacity of storing energy under loading cycles.

Therefore, the loss factor ($\tan \delta$), has been selected as a measure of the intrinsic damping of the materials.

6.3.3 Hamburg wheel tracking (HWT) test

The Hamburg Wheel Tracking test was conducted at wet conditions to evaluate the rutting resistance of mixtures and to substantiate the results if the TSR test on the moisture susceptibility. The test was conducted according to the AASHTO T324 standard at a temperature of 50°C. Four mixture "configurations" were used in the test (Figure 6.5).
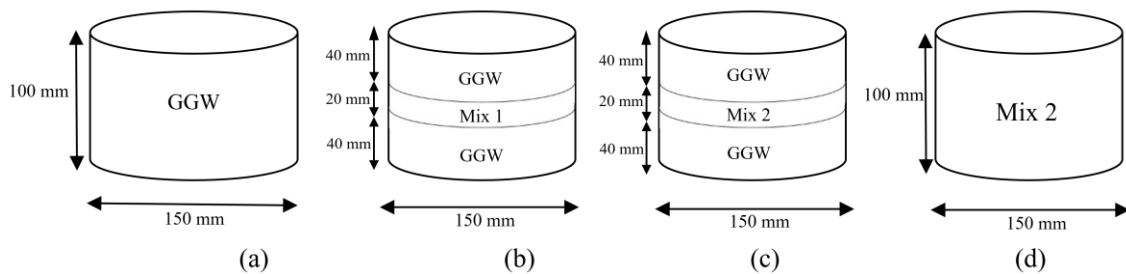
Figure 6.5 Mixture configurations used in the HWT test

The control mix is a Gap Graded Wet Rubberized Mixture (GGW) traditionally used in wearing course layers to optimize friction and acoustic performances (Figure 6.5 - a). Details on the mix design of this mixture can be found in Losa et al., 2012.

Mix 1 and Mix 2 were used as the interlayer between two "slices" of the GGW mixture as shown in Figure 6.5 (b) and (c). These layered samples were prepared directly in the SGC according to the following method:

- The mixture for the bottom slice was compacted firstly at one gyration to flatten the top surface;

- Then, the middle slice mixture was introduced in the mold and compacted at one gyration for the same scope.

- Then the top slice mixture was introduced in the mold, and the whole layered system was compacted to achieve a thickness of 100 mm (50 gyrations).

An image of the longitudinal section of a layered sample is given in Figure 6.6.
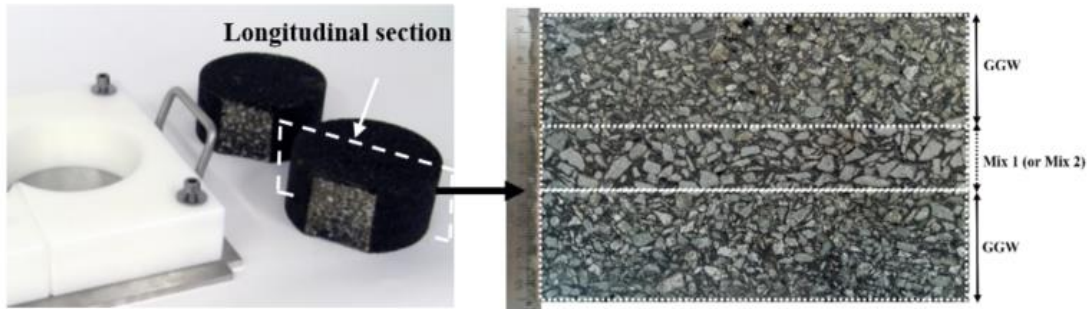
Figure 6.6 Longitudinal Section of HWT layered samples (GGW + Mix 1 & GGW + Mix 2)

Two specimens of Mix 2 were prepared according to the AASHTO T 312 (Figure 6.5 - d). Based on what shown in Table 6.3, the air void levels recommended in the AASHTO T 324 (7.0% ± 2.0%) although the mixtures were laboratory-prepared. In the case of Mix 2 due to the significant binder content, the air voids collapsed below 3.% after 2 gyrations. On the other hand, Miref and Mix 1 show significantly different volumes of air voids under the same compaction effort (50 gyrations –Table 6.3). For this reason, the mixtures were tested under equal initial thickness (100 mm).

Results were analyzed according to the Texas DOT (TEX-242-F) by considering the rut depth measured after 10,000 cycles as the test result.

6.4 Results and analysis

6.4.1 Workability

The compaction performances of the asphalt mixture refer to the change and stability of the volume parameters during the construction rolling. As far as Mix 1, a large amount of binder is used to replace the volume of VA in Mix ref, which is a typical porous

asphalt mixture. For Mix 2, apart from the binder which occupies the space of air voids, an additional 5% binder is added. It can be speculated that Mix 1 and Mix 2 should have a higher initial density because of the higher content of binder. However, it is called into question that if it is easy to compact from initial density to the required density. Hence, it is very important to evaluate the compaction performance firstly.

In the laboratory scale, the compactness of the asphalt mixture is analyzed using a gyratory compactor, and three samples with a diameter of 100 mm are produced for each mixture. The ease of compaction is measured by the densification curve plotted from the results obtained during the compaction according to the gyration numbers, as shown in Figure 6.7. According to the study of Hanz et al. (2012), the N_w was proposed to evaluate the asphalt mixture workability using volumetric data routinely collected during the current mix design and quality control testing. The N_w is defined as the number of gyrations required to reach w%·G_{mm} corresponding to w% air voids, where w% is the mean percentage of the voids at $N_{initial}$ and N_{design}. A mixture with lower N_w is characterized by better performance in terms of volumetric characteristics and workability. The N_w values of Mix ref, Mix 1 and Mix 2 are shown in Table 6.6. It can be observed that all asphalt mixtures exhibit a low value of N_w, demonstrating the ease of compaction and good workability.

Table 6.6 N_w values of Mix ref, Mix 1 and Mix 2

Type of mixtures	VA at $N_{initial}$ (%)	VA at N_{design} (%)	w (%)	N_w [n]
Mix ref	42.23	28.51	35.37	6
Mix 1	20.48	2.21	11.36	7
Mix 2	3.37	2.41	2.89	2
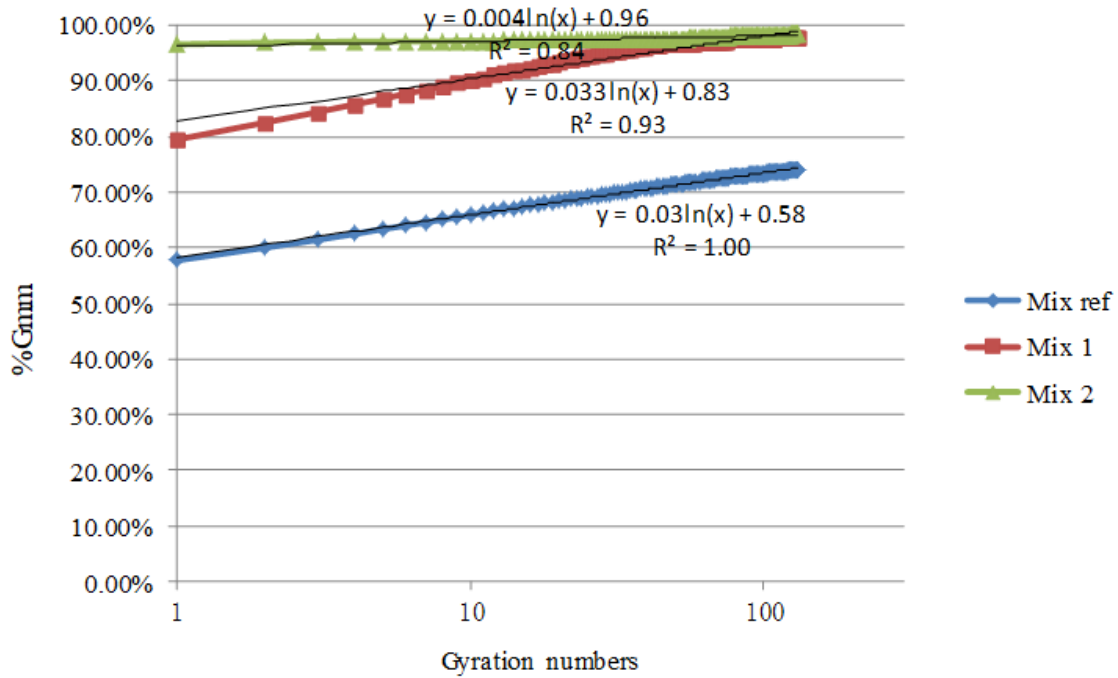
Figure 6.7 Compaction curve of Mix ref, Mix 1 and Mix 2

6.4.2 Indirect tensile strength (ITS) and water sensitivity

The indirect tensile strength test is performed on all the mixtures and the results are shown in Table 6.7. As far as ITS_d is concerned, Mix ref, Mix 1 and Mix 2 meet the specification requirements ($ITS_d \geq 0.4$ MPa), indicating that all mixtures show better performance of withstanding higher strains before failure. It can also be found that all the ITSR values are higher than 80%, so there is no water sensitivity issue associated with the three asphalt mixtures. Figure 6.8 is the results of ITS_{dry} with the varying AR content. It can be observed that with the increase of AR content, ITS_{dry} decrease. This is because the content of the binder determines the asphalt mixture porosity and cohesive force, but when the content of the binder is high, too much bitumen is dispersed between the aggregates, resulting in a lubricating effect and a decrease of the strength of the mixture.

Figure 6.9 shows the effect of AR content on the ITSR. With the increase of binder content, the value of ITSR improves, indicating that its resistance ability to moisture damage improves. In this case, for Mix 2 with AR content of 20%, the ITSR value is 6% higher compared to Mix ref.

Table 6.7 Results of indirect tensile strength for all mixes

	Mix ref		Mix 1		Mix 2		Mean		
	ITS_d /MPa	ITS_w /MPa	ITS_d /MPa	ITS_w /MPa	ITS_d /MPa	ITS_w /MPa	ITS_d /MPa	ITS_w /MPa	ITSR
Mix ref	0.62	0.44	0.66	0.60	0.58	0.50	0.62	0.51	82.3%
Mix 1	0.52	0.46	0.58	0.47	0.55	0.51	0.55	0.48	87.3%
Mix 2	0.41	0.36	0.41	0.37	0.40	0.36	0.41	0.36	87.8%
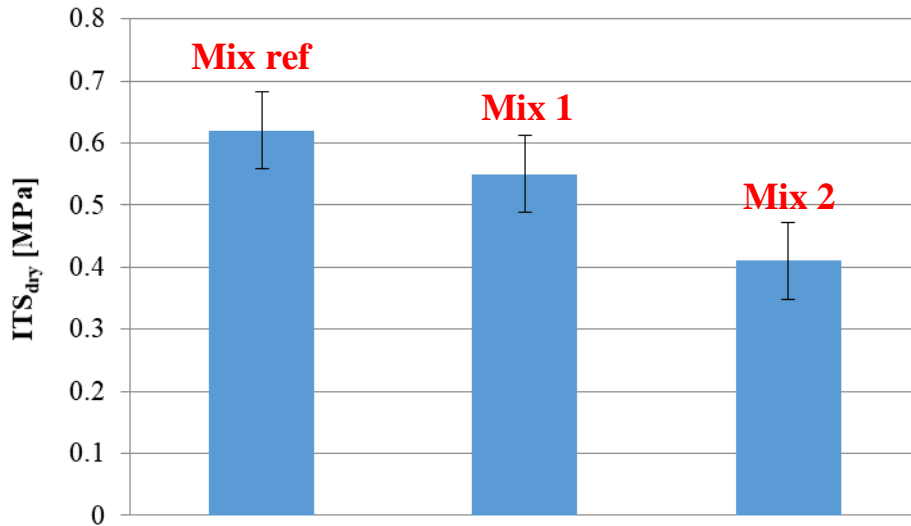
Figure 6.8 ITS results for the three asphalt mixtures
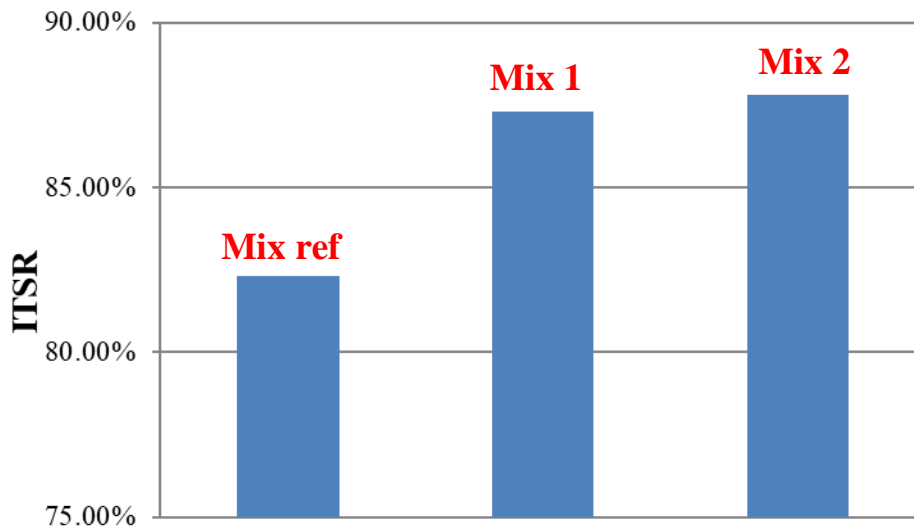
Figure 6.9 ITSR results for the three asphalt mixtures

6.4.3 Dynamic modulus and phase angle

The master curves of the dynamic modulus ($|E^*|$) and the phase angle (δ) of the mixtures are given in Figure 6.10 and Figure 6.11.
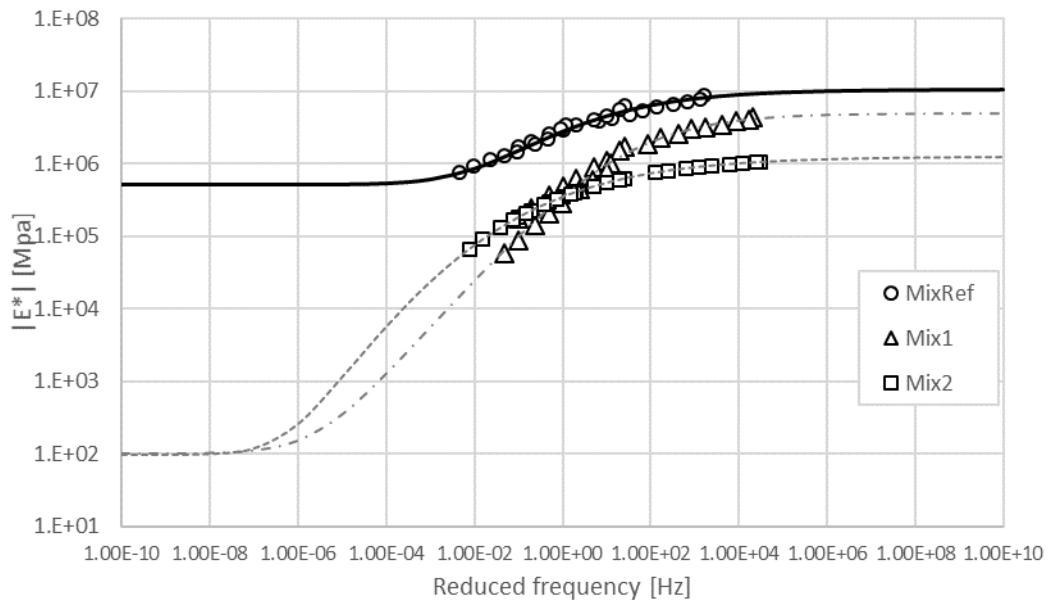
Figure 6.10 Dynamic modulus master curves
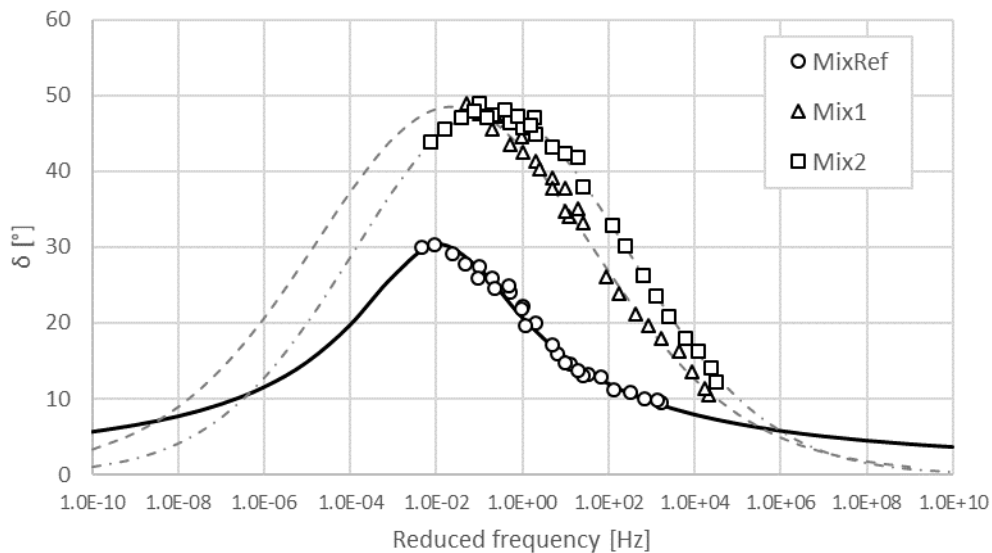
Figure 6.11 Phase angle master curves

The master curves were developed on two replicates. Results show an acceptable variability with the coefficient of variation of the average between two samples below 10% for all the cases. The shift factors were optimized on the dynamic modulus master curve and were then applied to the phase angle master curve. The CAM model provides an adequate accuracy in modeling the raw data with the R^2 coefficient being above 97% (for modulus) and 95% (for phase angle) for all mixtures.

The reference mixture shows the highest levels of stiffness (Figure 6.10) and the lowest values of phase angle (Figure 6.11) in the range of reduced frequency considered. This

aspect was expected due to the differences in the composition between the mixtures. The higher stiffness of the OG mixture is in agreement with the tensile strength values (Figure 6.8) and depends on the higher aggregate interlock provided a thinner film of mastic. The difference between Mix_{ref} and the two damping mixtures is marked in the low-frequencies region where the aggregate structure is more significant than the mastic. The difference between horizontal asymptotes in this region is of multiple orders of magnitudes. Mix 1 and Mix 2 show similar levels of stiffness in the intermediate and low range of frequencies with Mix 1 becoming stiffer at lower temperatures (higher frequencies) and Mix 2 stiffer at higher temperatures (lower frequencies).

The shape of the δ master curves is typical of mixtures. At low frequencies, the response is more controlled by the aggregate skeleton, and thus, it is more elastic. At the very high frequencies, the mastic becomes stiffer and more elastic lowering the phase angle. While at the intermediate region, the response is controlled by both the constituents (aggregate and binder) showing visible viscoelastic behavior. The values of the phase angle support what was the main scope of the mix design that is, increasing the damping response of mixtures - Mix 1 and Mix 2 show consistently higher phase angle values than the reference mixture. Higher phase angle values indicate a more viscous response under loading with a consequent higher dissipation of energy dissipation. Although the phase angle is representative of the damping properties, the comparison between the damping properties of mixtures is given in the next section in terms of loss factor.

6.4.4 Damping property

The damping property is characterized by the loss factor, which is calculated by the Eq. (6.8),

$$\eta = \tan \delta = \frac{E''}{E'} \qquad (6.8)$$

where:

δ – is the phase angle;

E'' – is the loss modulus;

E' - is the storage modulus.

High values of loss factor indicate a higher level of energy dissipation under loading. The values of the loss factors of Mix 1 and Mix 2 of the mixtures were normalized versus those of Mix_{ref}. The results are given in Table 6.8.

Table 6.8 Normalised loss factors

Temperatures	Mixtures	Frequency (Hz)							
		0.1	0.5	1	2	5	10	20	25
5 °C	Mix ref	1							
	Mix 1	1.25	1.16	1.36	1.39	1.38	1.26	1.20	1.22
	Mix 2	1.45	1.45	1.65	1.54	1.62	1.54	1.53	1.60
20 °C	Mix ref	1							
	Mix 1	5.06	4.27	3.25	3.05	2.84	2.69	2.55	2.37
	Mix 2	5.90	5.43	3.81	3.50	3.21	3.00	2.83	2.61
31 °C	Mix ref	1							
	Mix 1	1.78	1.64	1.60	1.77	2.06	2.07	2.16	2.10
	Mix 2	2.49	2.52	2.78	2.53	2.46	2.36	2.28	2.08

At 5°C, damping is mitigated since the response of bitumens is more elastic and the loss factors of Mix 1 and 2 are closer to the one of Mix_{ref}. In other words, in this range of temperature, although Mix 1 and 2 include a higher binder content, the viscoelastic effects are limited by the temperature. Furthermore, the more elastic response is visible also in the lower susceptibility to frequency, which indicates a reduced time dependency.

At 20°C, the viscoelasticity of the material is very visible with the response becoming more elastic with the increase of frequency. At this temperature, Mix 1 and 2 show the highest damping effects (particularly at low loading frequencies) in the response with the loss factor that decreases at higher frequencies. If in terms of resistance, this effect is beneficial, but for reducing vibrations, it is not. Traffic-induced vibrations increase with the traffic speed; therefore, higher damping at higher frequencies would be preferable but this is not in the nature of bituminous materials. However, Mix 1 and Mix 2 provide sensibly higher damping to the traditional OG mixture.

Rations like those in Table 6.8 can be used as the basis for judging the mitigation efficiency of pavements under different traffic environmental conditions.

At 31°C the loss factors of Mix_{ref} and Mix 1, decrease with the increase in frequency (typical viscoelastic behavior). On the other hand, Mix 2 shows more complex behavior with the loss factor that increases between 0.5 and 1.0 Hz (Table 6.8) and decreases afterward. At low frequencies, the consistency of the mastic is low and the aggregate skeleton influence more the response that becomes more elastic as much as the mastic becomes softer (lowering the frequency). On the other hand, at high frequencies, the mastic recover consistency affecting more the response, which becomes more elastic with the increase in frequency. This behavior is visible in the δ-master curves that show a peak as well (Figure 6.11). It is true that the master curves were developed at the reference temperature of 20°C, but what has to be noticed is that Mix 2 shows the peak at higher frequencies that Mix 1 and Mix_{ref}. In this mix, the transition described above (between the skeleton and the mastic controlling the response), occurs at a lower temperature than the other two mixes. That is, Mix 2 is more temperature susceptible due to the very high level of binder content.

To conclude, these preliminary findings are indicative of the fact that rubberized asphalt mixtures that have 13% or 17% asphalt binder content (with respect to the weight of mix), along with CR inclusions provide higher damping response than the conventional rubberized asphalt mixtures.

6.4.5 Hamburg wheel tracking (HWT) test

Results of the Hamburg wheel Test are given in Figure 6.12.
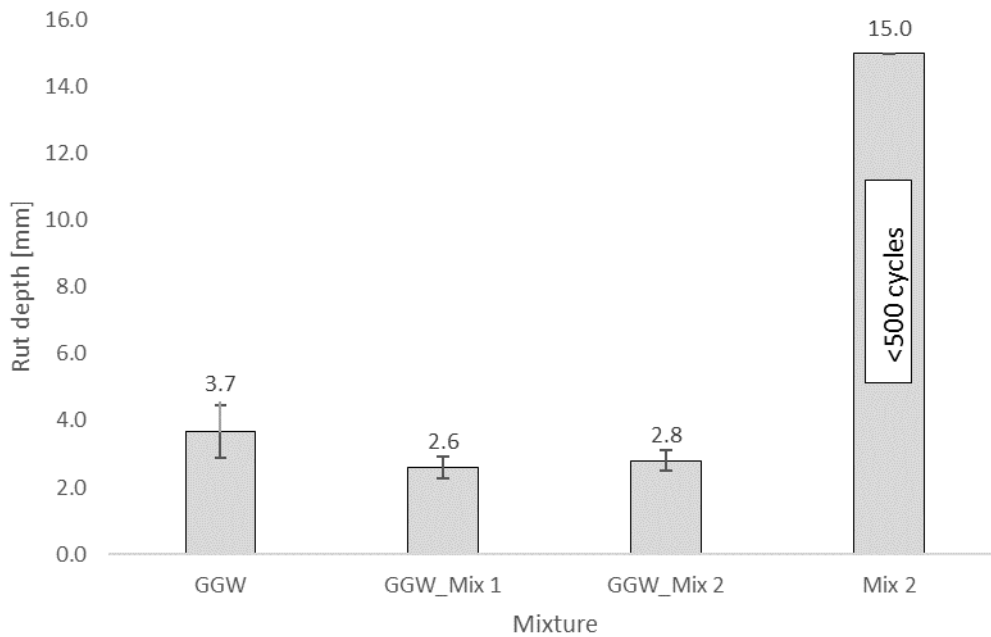
Figure 6.12 Hamburg Wheel Test results: rut depth after 10,000 cycles

The values of the creep slope are given in Table 6.9.

Table 6.9 Values of Creep slope

Mixture	Creep Slope (x1000) [mm/pass]
Mix_{ref}	0.197
GGW_Mix 1	0.144
GGW_Mix 2	0.159

In the case of the Mix 2 test was interrupted after 500 cycles since the rut depth was higher than 15 mm already within this number of passes. The rutting susceptibility of Mix 2 was observed also during compaction (Chapter 6.4.1).

Prior to discussing the other mixtures, it is worth to recall that since Mix 1 and Mix 2 are meant to be used as the interlayer. Therefore, their rutting resistance has been evaluated with them being used in layered samples shown in Figure 6.5 and labeled in Figure 6.12 as GGW_Mix 1 (GGW + Mix 1 + GGW) and GGW_Mix 2 (GGW + Mix 2 + GGW).

The final rut depths of the layered mixtures are similar and are lower than the one of a traditional Gap Graded mixture prepared with the rubberized binder (wet method - GGW) (Figure 6.12). This aspect indicates that the use of Mix 1 and Mix 2 as an

interlayer does not worsen the rutting resistance, but on the contrary, it provides a beneficial effect. The higher rutting resistance of the layered mixtures is confirmed by the values of the creep slope in Table 6.9.

This result can be explained as follows. The GGW mix incorporates a volume of voids approximately of 9%. For this reason, part of the volume of such a mixture is prone to reduce under the effect of the loading wheel. On the other hand, once a slice of Mix 1 or Mix 2 is in the sample, an important part of the bulk volume is occupied by a region where the air is around 2% or lower. The presence of such a dense region makes the mixture less prone to accumulate deformation (densification and shear failure) than the sole GGW mix.

Concerning the moisture susceptibility, results from the HWT confirm the results of the ITSR (Chapter 6.4.2) with the mixtures that do not show stripping during the test.

In order to better understand the above conclusion, the internal structures of 'GGW + Mix 2 + GGW' and 'Mix 2' before and after the HWT test are evaluated. The longitudinal tangent planes are taken photos before and after the HWT test. By using ImageJ software, planes with the size of 100 mm*70 mm are obtained, and then through thresholding processing of ImageJ software, the final binary images are obtained. The thresholding processing is shown in Figure 6.13.

Figure 6.13 Longitudinal section of the HWT sample

In order to measure the deformation of various layers ('GGW upper layer', 'Mix 2 layer', 'GGW downer layer', 'all Mix 2 layer'), the binary images are set at the same scale. As far as the sample of 'GGW + Mix 2 + GGW', twelve random points at the boundary of each layer are selected, as shown in Figure 6.14. The positions (x, y) of these twelve points before and after the test are recorded, as shown in Table 6.10. In this way, the average vertical displacement of the boundary of each layer can be calculated. Thereby, the deformation of each layer can be calculated, as shown in Figure 6.16. A

similar method is also conducted for 'Mix 2': ten random points are selected in accordance with the intervals of 20 mm, as seen in Figure 6.15. The positions (x, y) of the ten points before and after the test and the average vertical displacements of the boundary are shown in Table 6.11 and Figure 6.17, respectively.

(1) Before   (2) After
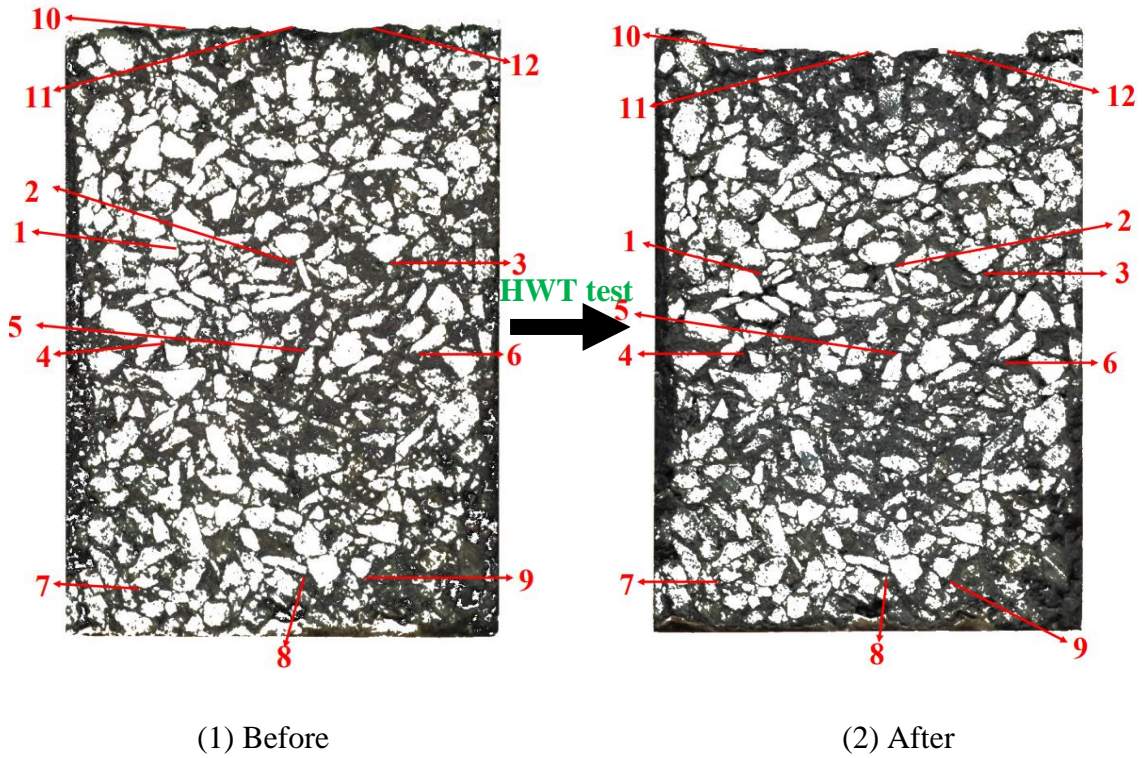
Figure 6.14 Binary images of GGW + Mix 2 + GGW before and after HWT test

(1) Before   (2) After
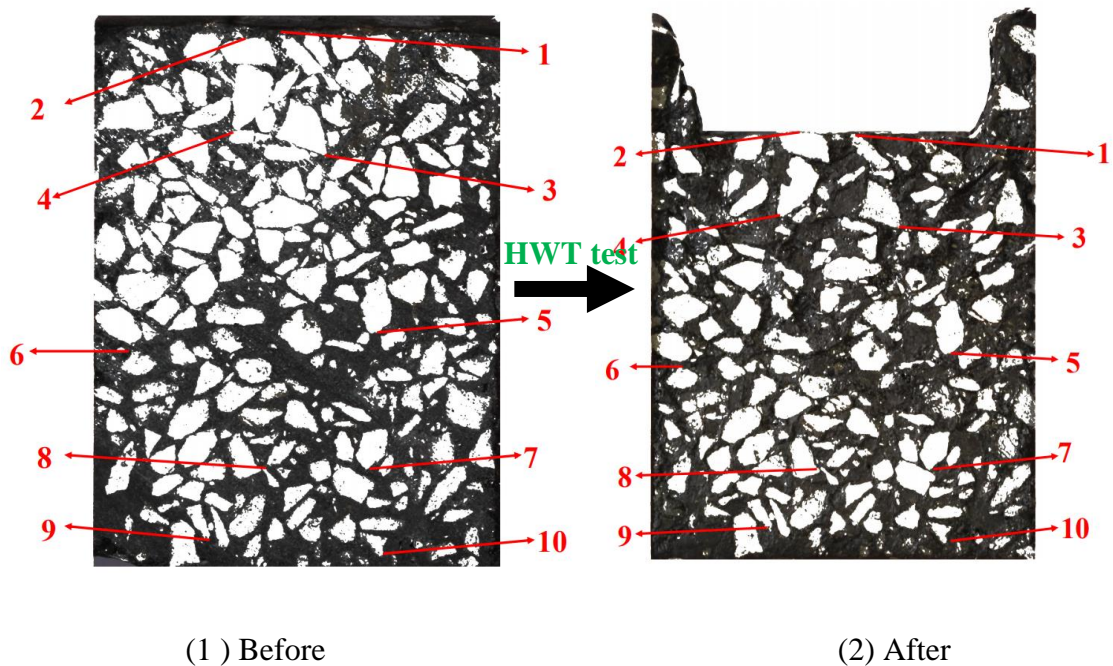
Figure 6.15 Binary images of Mix 2 before and after HWT test

Table 6.10 Positions of selected points in GGW + Mix 2 + GGW before and after HWT test

Point	x (before) [mm]	y (before) [mm]	x (after) [mm]	y (after) [mm]	Vertical displacement [mm]	Average value of vertical displacement [mm]
1	18.560	63.088	18.394	61.612	1.476	
2	38.378	61.433	38.46	59.298	2.135	2.118
3	51.981	60.757	52.609	58.012	2.745	
4	16.202	47.526	15.719	45.922	1.604	
5	40.101	46.851	39.746	44.992	1.859	1.934
6	55.491	46.074	56.082	43.733	2.341	
7	13.232	8.854	11.962	8.232	0.622	
8	38.615	10.093	38.332	9.16	0.933	0.874
9	47.796	9.316	47.336	8.247	1.069	
10	15.518	98.776	15.518	96.099	2.677	
11	37.041	98.776	37.041	95.327	3.449	3.368
12	52.357	99.721	55.000	95.742	3.979	

Table 6.11 Positions of selected points in GGW + Mix 2 + GGW before and after HWT test

Point	x (before) [mm]	y (before) [mm]	x (after) [mm]	y (after) [mm]	Vertical displacement [mm]	average value of vertical displacement [mm]
1	31.900	91.413	37.219	76.833	14.580	14.304
2	25.899	91.710	26.807	77.682	14.028	
3	39.747	71.198	44.732	60.097	11.101	12.151
4	24.872	75.005	23.561	61.804	13.201	
5	47.822	40.385	53.439	37.391	2.994	2.651

6	7.308	36.796	4.954	34.488	2.308	
7	47.054	16.667	50.885	15.879	0.788	0.553
8	28.974	16.538	30.049	16.219	0.319	
9	19.487	4.615	24.415	4.239	0.376	0.980
10	43.718	3.974	53.780	2.390	1.584	
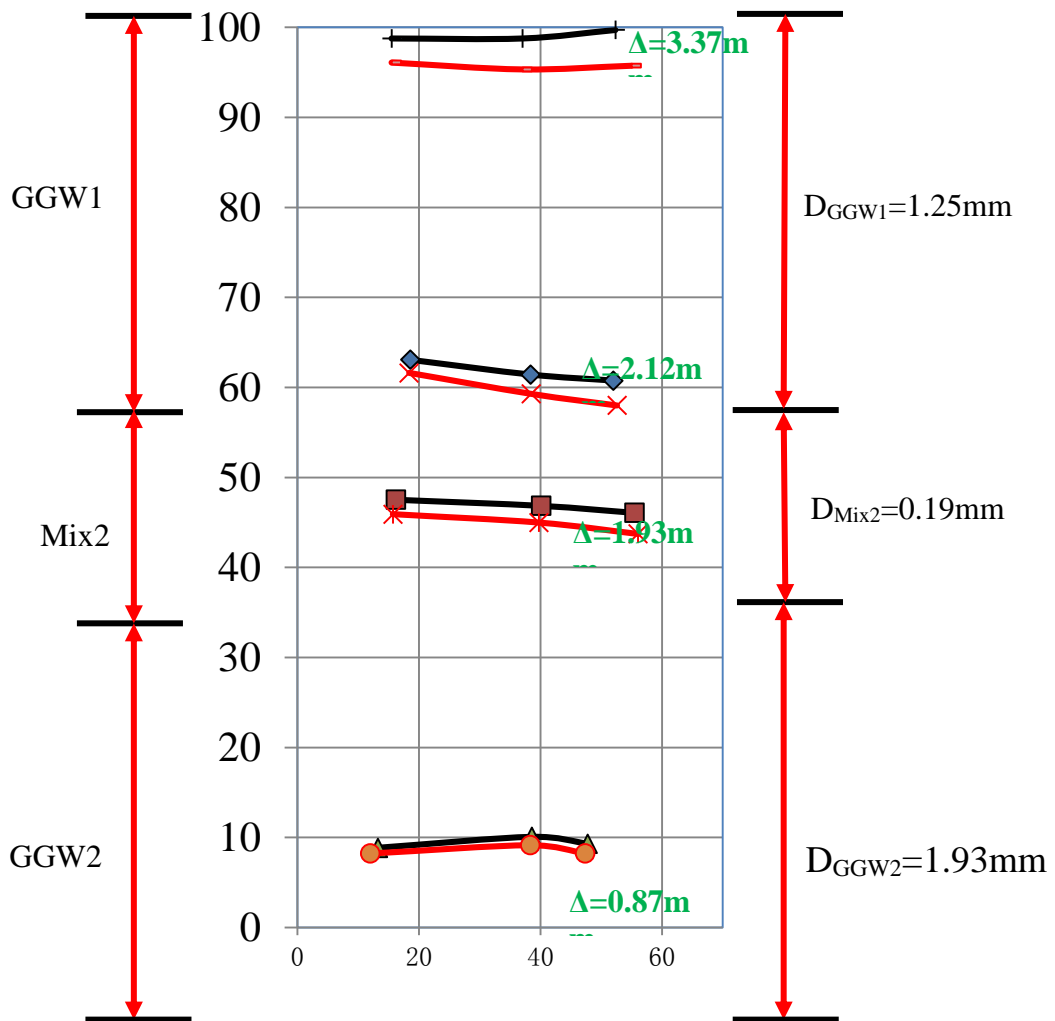
(Notes[*]: blackline means the position before HWT; red line means the position after HWT)

Figure 6.16 Contributions of each layer to the total deformations (GGW + Mix 2 + GGW)

122
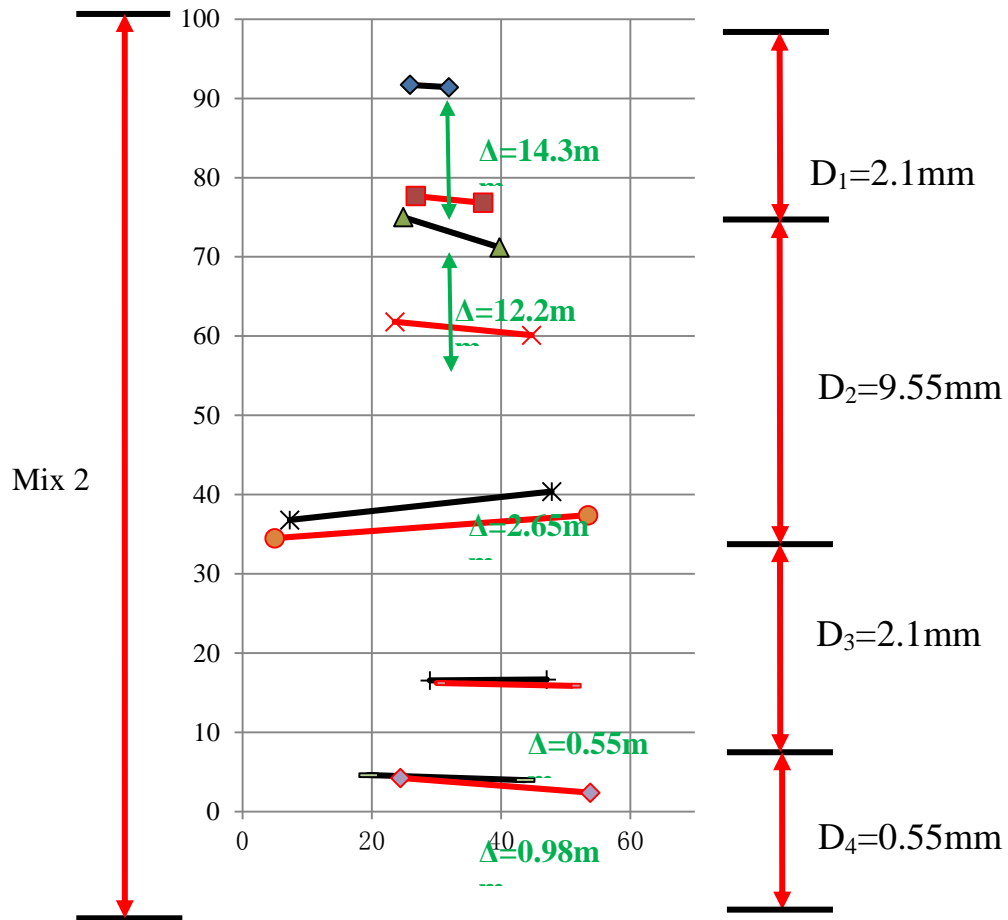
Figure 6.17 Contributions of each layer to the total deformations (Mix 2)

It can be found from Figure 6.17 that the contribution of the downer part (D_3+D_4= 2.65 mm) is much lower than that of the upper part (D_1+D_2=12 mm), demonstrating that the "aggregate-mastic-aggregate" internal structure has a lower resistance to rutting deformation. However, it is found from Figure 6.16 that the deformation value of the Mix 2 layer is lowest, only about 0.19 mm, demonstrating that Mix 2 layer has the lowest contribution to deformation. Nevertheless, the upper and downer layer have similar and relatively large deformations (1.3 mm and 2 mm). This proves that the Mix 2 layer has a good ability to coordinate deformation and ensures the stress transmission from the upper to lower structural layer. At the same time, it verifies the explanation that the lower deformation is caused by the lower VA of Mix 1 and Mix 2, is reasonable. By using mix 2 as the interlayer, the pavement improves not only the ability of the upper and lower layers to work together but also its ability to resist permanent deformation.

6.5 Field tests of pavement with a damping layer

In order to verify the construction feasibility and the vibration-absorbing effects of the damping layer, the field trial test is carried out, as shown in Figure 6.18. The field test road is located in Via Francesco Ferrucci, Agliana, Pistoia (PT). The experiment plan is to overlay a new asphalt pavement with a damping layer by milling 8 cm of the existing old asphalt pavement. Figure 6.19 shows the old asphalt pavement, which has been milled, cleaned and leveled. The length and width of the field test road are 30 m and 6 m, respectively.

Figure 6.18 Construction bulletin board

Figure 6.19 The old asphalt pavement

6.5.1 Construction feasibility

The new asphalt pavement consists of two layers, a damping layer and a surface layer with a thickness of 3 cm and 5 cm, respectively, as shown in Figure 6.20.

Mix 1, designed in this study, is used as the material for the damping layer because of its good mechanical and damping properties, which have been verified in previous chapters. The experimental process is carried out as follows; first, Mix 1 is mixed and paved to a thickness of 3 cm, which is optimized in the previous chapters. Then, the damping layer is manually laid and leveled to the design thickness. Since Mix 1 contains a large amount (15%) of asphalt binder, a small vibratory roller instead of a heavy-weight roller is used to avoid over-crushing and causing the asphalt to seep out, as shown in Figure 6.21. The mixing, laying and rolling processes show that the mineral materials are embedded and stabilized, and the asphalt is evenly distributed, demonstrating that the Mix1 has the good working ability and compaction performance similar to traditional asphalt mixture.

Figure 6.20 Pavement structure with a damping layer

Figure 6.21 Paving process of the damping layer

The conventional dense-graded asphalt mixture is used as the surface layer to verify the ability of the damping layer to work in conjunction with conventional asphalt mixtures.

The wheel type asphalt paver is used for the leveling and paving process and the small vibratory roller is used for the compaction process in order to prevent over-compacting of the damping layer, as shown in Figure 6.22. The laying and compaction process shows that the surface layer and the damping layer have good bonding properties, and the thickness, compactness, and flatness of the newly laid pavement meet the design requirements. The whole construction process is simple and not much different from the traditional laying. The good performance of the field tests demonstrating the anti-absorbing pavement has high practicability and has good promotion prospects.
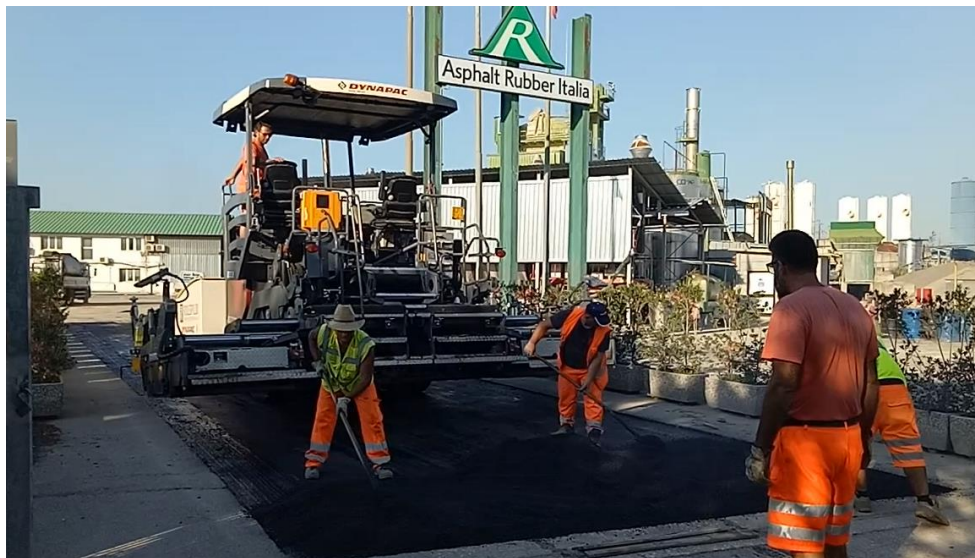
Figure 6.22 The paving process of the surface layer

6.5.2 Vibration-absorbing effects

The vibration-absorbing effects are evaluated by the means of the field FWD tests 2 months after the constructions, as shown in Figure 6.23. The in-situ pavements are divided as the part with the damping layer and the one without damping layer in order to evaluate the effect of vibration-absorbing. 6 points near the edge of the pavement are selected as the loading points for the FWD tests, named as P_1, P_2…P_6, the detailed positions of which are shown in Figure 6.23. The time-history deflections of the 4 sensors (D_1, D_2, D_6, D_9) in each test are recorded and compared.
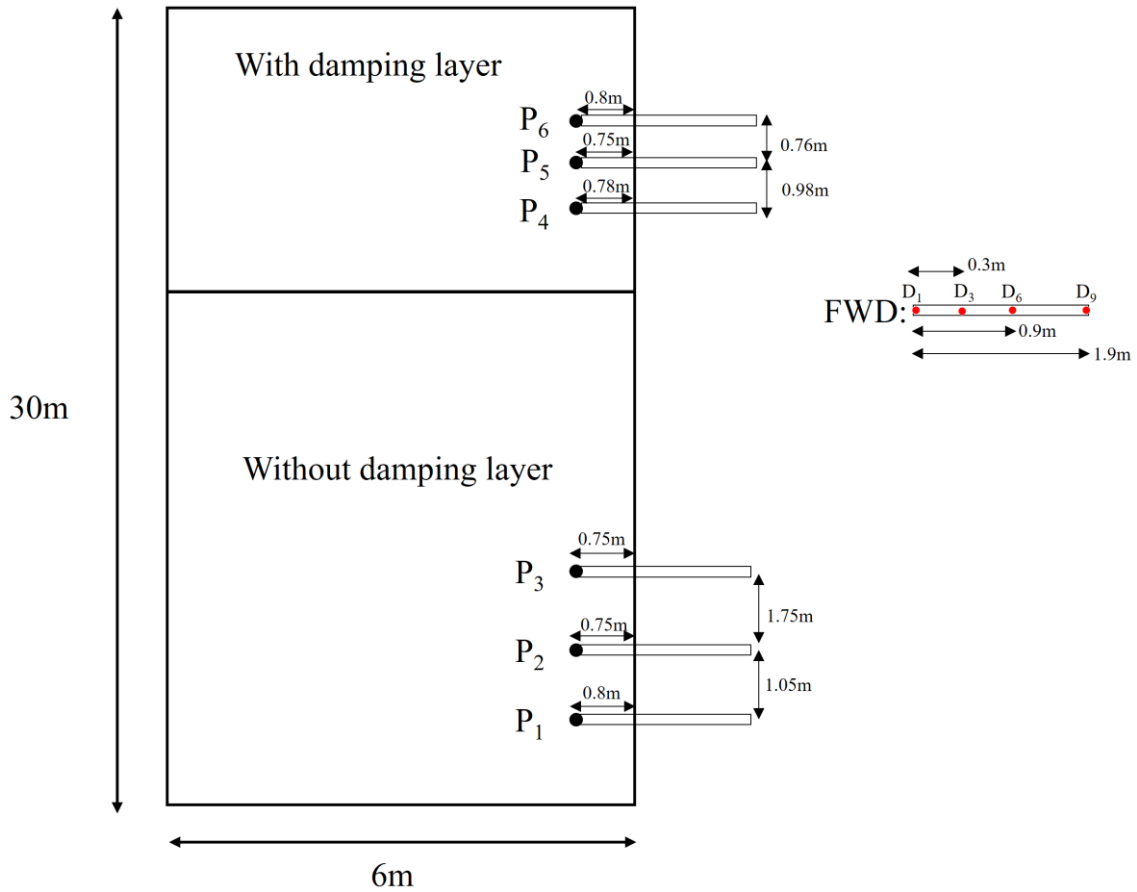
Figure 6.23 Field FWD tests to evaluate the vibration-absorbing effects

The time-history deflections of the 6 FWD tests at D_1, D_3, D_6, and D_9 are shown in Figure 6.24 (1)-(4).
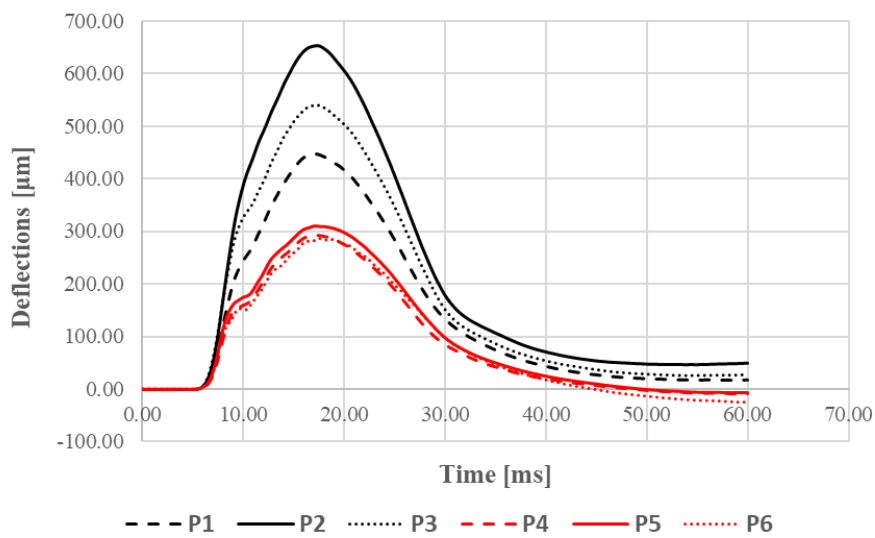
(1) D_1=0m
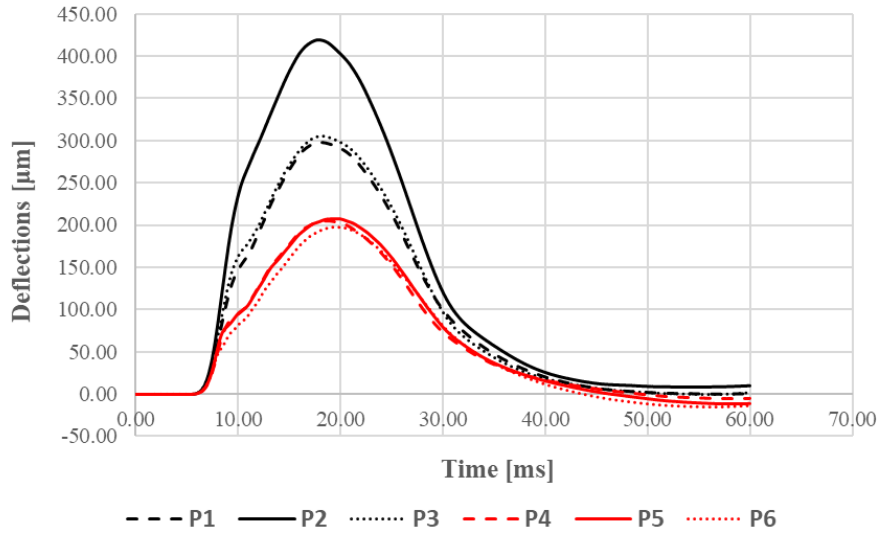
(2) D$_3$=0.3m
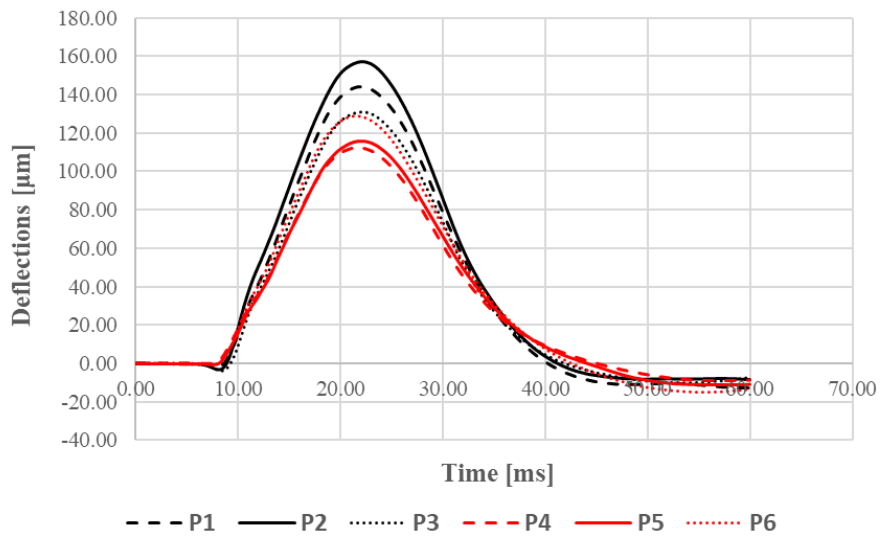
(3) D$_6$=0.9m
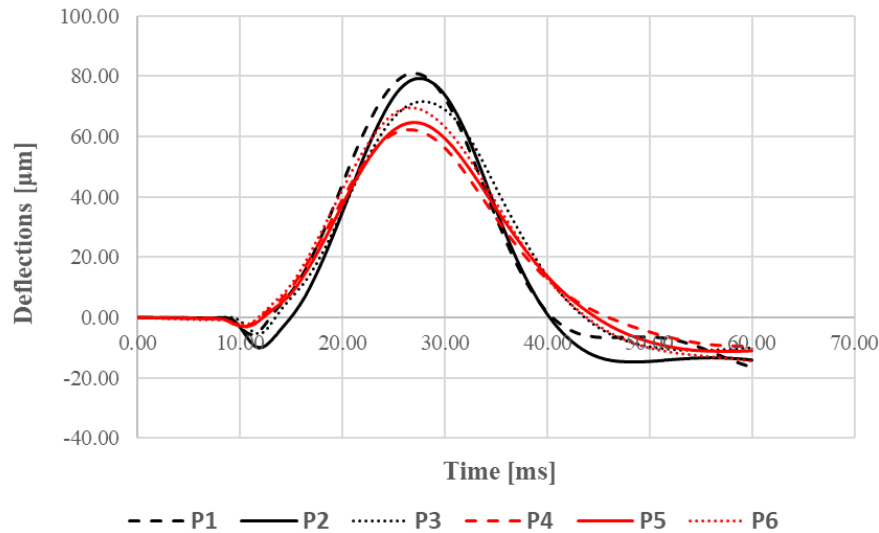
(4) D_9=1.9m

Figure 6.24 Time-history deflections of the FWD tests at D_1, D_3, D_6, and D_9

Overall, from the time-history deflections at D_1, D_3, D_6, and D_9, much lower deflection values are found for the pavement with the damping layer, demonstrating its great effect on the vibration-reduction. As the monitoring point becomes farther away from the loading center, its damping effect is weakening. However, It should be noted that even at a distance of 1.9 meters (D_9) from the loading center, the damping effect is still very obvious. It can be foreseen that when the monitoring point is far enough from the loading center position, the damping effect can become so weak that it disappears.

It should be noted that the vibration response of monitoring points D_1 will be related to the low-frequency noise generated by tire tread-impact, and the vibration response of monitoring points D_6 and D_9 will determine the impact of traffic loads on the surrounding environment. Therefore, it can draw the conclusions that by laying the damping layer in the road structure, the rebound amplitude at the loading center will be reduced by nearly 50% and will greatly reduce the tread-impact noise. The deflections at the surrounding environment of the road can be reduced by 20% to 30% and thus greatly reduce the impact of the traffic loads.

For the monitoring points D_1 and D_3, the pavements with the damping layer (P4, P5, and P6) show relative stable values of deflections, as shown in (1) and (2) of Figure 6.24. However, when the vibration waves induced by the pulse load arrive D_6 and D_9, a

relative difference can be found. This can be explained by the heterogeneity of the subgrade or the surrounding environment of the road.

Chapter 7: Conclusions and future works

7.1 Study overview

Nowadays, a complex transportation network has been a symbol of urbanization development and convenient transportation enriches people's life. However, traffic noise and vibrations from the transportation network are around everyone in the city, which affect the living condition of urban residents and could result in a sleeping disorder. Such induced vibration may cause some fatigue damage of surrounding buildings as well; on the other hand, the indirect impact of the more convenient transportation network is the recycling of end-of-life tires from increasing numbers of vehicles. In order to solve the above problems, this study is trying to refine and optimize a new noise and vibration absorbing system for road pavements while complying with the requirement of sustainability by the use of crumb rubber from end-of-life tires. The noise and vibration absorbing system is composed of a gap graded asphalt surface layer, containing a large amount of crumb rubber, and a lower vibration-absorbing layer with higher damping property.

As far as the surface layer, two gap-graded asphalt mixtures with a high content of crumb rubber by the different adding process (wet process and dry process) were designed and analyzed, with a comparison of two conventional asphalt mixtures, which are commonly used as low noise pavements in Europe. Based on the database from the project "Leopoldo", the noise reduction mechanism of rubberized LNPs can be drawn.

As far as the damping layer, the effect on vibration-absorbing was evaluated firstly, because if the damping layer has no or weak effect for reducing the vibration, the study of designing such a damping layer was obviously not desirable. In this study, the methods commonly used in the field of road engineering to characterize damping property were reviewed, and the shortcomings of these methods, when applied to this study, were summarized. Based on this consideration, a uniform method for solving the Rayleigh damping coefficient in the field of road engineering was proposed and it was proved to be applicable not only to roads composed of materials with close damping properties but also to the ones composed of materials with large different damping. The accuracy of the method was verified by comparing the simulation results obtained by

the finite element model based on the proposed method to the results of the field test. In the second phase, based on the proposed method, this study verified that the effect of laying a damping layer in the pavement structure to reduce the traffic-induced vibration was significant. Additionally, a parametric study of the damping layer was performed, including different damping layer locations, thicknesses, and damping ratios, by which the optimized pavement structure was determined.

In the last step, considering the materials specifically for the damping layer, this study designed the asphalt mixtures with high binder content as well as high crumb rubber content in order to improve the damping property. The asphalt mixtures were verified by laboratory tests and proved to have sufficient strength to meet the requirements of the specification and much higher damping capacity than conventional asphalt mixtures. It can also work together well with the upper and lower asphalt layers as well as providing enough ability to resist rutting according to the results of the special HWT tests. At the same time, an experimental road with a damping layer was carried out in the field to verify the construction feasibility of the asphalt mixture.

The main conclusions from this study can be concluded as follows:

(1) A new noise and vibration system absorbing system is developed. This system consists of a noise and vibration reduction layer and a vibration-absorbing layer. The surface layer will work as a noise and vibration reduction layer, which is composed of gap-graded asphalt mixtures with CR by a wet process. The interlayer placed in the middle of the asphalt layer will work as a vibration-absorbing layer, which is composed of specific asphalt mixtures with high damping properties.

(2) The noise absorbing is beneficial from two parts: the first one is the low-noise surface layer by the optimized pavement texture and the adding of CR; the other one is the high damping of the vibration-absorbing layer to reduce tire/pavement vibration, and then reduce the tire/pavement noise. The vibration absorbing is beneficial from the reduction in the generation of vibration waves and weakening the propagation of vibrational waves by absorbing energy. As far as the reduction in the generation of vibration waves, the optimized pavement texture and the adding of CR by the wet process (wet process has been confirmed to have better vibration-reduction performance than the dry process in this study) will be used. The

vibration-absorbing layer will be used against the vibration propagation between the source and receiver.

The following are some of the conclusions that may also be drawn:

1. Adding crumb rubber particles in asphalt mixtures by DP or WP can improve the acoustic absorption performance of asphalt mixtures since the rubber particles can use their viscous energy dissipation, that is, the damping mechanism, to convert the acoustic energy or mechanical energy to heat dissipation.

2. The mechanism of reducing the tire/pavement noise by adding the rubber particles to the asphalt mixture by WP is that it can effectively reduce the noise generated by the vibration. The mechanism by DP is that it can effectively improve the sound absorption coefficient of the asphalt mixture, thereby reducing the noise generated by the aerodynamic mechanism. Therefore, from the perspective of designing anti-vibration pavement, rubberized mixture by WP is more suitable for the surface layer compared to the one by DP because it can reduce the generation of vibration waves more effectively.

3. Based on the idealized shear beam model, a more reasonable method to calculate natural frequencies of different layers is proposed, by which the nonclassical damping matrix of a road system can be assembled. FEM simulations and in-situ field tests are performed to validate the accuracy of this method. Good agreements are achieved between simulation and field test results demonstrating that this method can provide a more accurate basis for future dynamic modeling and back-calculation in road engineering.

4. A parametric study of the damping layer shows that, by laying a damping layer with a damping ratio of 0.2 into a road structure, the traffic-induced vibration of the surrounding environment can reduce 15%-20%. With the increase of distance from the monitoring point to the loading point, the vibration reduction increases firstly and then decreases; the maximum value of vibration reduction appears at a distance of 5-6 meters. When the distance is enough far, the effect of vibration reduction may decrease until it vanishes; with different loading frequency, the maximum vibration reductions appear at different distances but are showing a very similar trend.

5. With the increasing of damping ratio, the A_{RMS} of monitored positions reduce. In addition, this reduction has obvious linearity, demonstrating the damping layer is playing a predominant role to characterize the damping property of the whole system. To optimize the damping layer position is useful to reduce the vibration at Point A (representing the place on the pavement) and Point E (representing the place far from the pavement), but almost useless at Point C (representing the place close to the pavement).

6. When the thickness of the damping layer is equal to 30 mm and the damping ratio increases from 0.02 to 0.2, the vibration at 10 m away from the pavement can reduce about 20% and the one at 30 m away from the pavement can reduce about 15%, demonstrating that such vibration reduction can lead to significant benefits in reducing the impact of traffic-induced vibration on the surrounding environment and building. Considering the effects of the damping layer on functional characterization and mechanical response as well as pavement performance, the optimized position of the damping layer is in the middle of the AC layer and the optimized thickness is 30 mm.

7. Mix 1 and Mix 2, with 15% and 20% (by weight of aggregate) asphalt rubber content, are designed in the study in order to meet the special target of high damping. There is no water sensitivity issue associated with Mix ref, Mix 1 and Mix 2. For ITS, all the mixtures meet the specification requirements of standards ($ITS_d \geq 0.4$ MPa). With the increase of AR content, ITS_{dry} decreases. The reason is that the content of the binder determines the asphalt mixture porosity and cohesive force. When the content of the binder is too high, bitumen is dispersed between the aggregates, resulting in a lubricating effect and the decrease of strength. With the increase of binder content, the value of ITSR improves, demonstrating that the resistance to moisture damage is improving.

8. When the experimental temperature is 20°C, the estimated critical damping ratios of Mix1 and Mix2 are almost 3 times higher compared to conventional rubberized asphalt mixtures, so they can meet the proposed design targets for the "damping layer". By laying Mix 1 or Mix 2 in the road structure, the design of the "anti-vibration" pavement can be achieved while reducing the tire/pavement noise generated by vibration mechanism.

9. Using Mix 1 or Mix 2 as a thin interlayer, will not decrease the resistance to permanent deformation of the pavement, and can even improve to a certain extent. However, by using Mix 1 or Mix 2 as a thick structure layer, the pavement can lose the resistance to permanent deformation soon. The mixing, laying and rolling processes of the experimental road with the damping layer show that the mineral materials are embedded and stabilized, and the asphalt is evenly distributed, demonstrating that the designed asphalt mixture has the good working ability and compaction performance similar to traditional asphalt mixture. By laying a damping layer in the road structure, the deflection can be reduced by almost 50% at the loading center position, while the deflection can be reduced by about 20% at the 1.9m position around the road, demonstrating the effectiveness of the damping layer.

7.2 Future developments

During the writing and the development of this thesis, several problems and questions came out. Some of these would need further investigation:

1. Explore the changing of the internal microstructure of gap-graded asphalt mixtures with crumb rubber over time, establish the relationship between internal structure and performance, and better understand the mechanism of rubber particles in asphalt mixtures.

2. Laboratory or field test of pavement structures with additional damping layer to evaluate its effect on vibration reduction.

3. In-situ tests of acoustic and vibration performance should be conducted by comparing the pavement structures with and without the noise and vibration absorbing system designed in this study.

Bibliography

1. AASHTO, T. 324-04. (2007). Standard Test Method for Hamburg Wheel Track testing of Compacted Hot-Mix Asphalt (HMA).

2. Adrienne Research Team. (1998). Test methods for the acoustic performance of road traffic noise reducing devices-Final report. European Commission-DGXII-SMT Project MAT1-CT94049.

3. Ahammed, M. A., & Tighe, S. L. (2011). Acoustic absorption of conventional pavements. International Journal of Pavement Research and Technology, 4(1), 41-47.

4. Al-Hunaidi, M. O., Rainer, J. H., & Tremblay, M. (1996). Control of traffic-induced vibration in buildings using vehicle suspension systems. *Soil Dynamics and Earthquake Engineering*, *15*(4), 245-254.

5. Al-Qadi, I. L., Wang, H., Yoo, P. J., & Dessouky, S. H. (2008). Dynamic analysis and in situ validation of perpetual pavement response to vehicular loading. Transportation research record, 2087(1), 29-39.

6. Anderson, G. A. L. (1999). An investigation into the factors which affect the acoustical characteristics of bituminous porous road surfacings (Doctoral dissertation, University of Ulster).

7. Anfosso-Lédée, F. (2004). The development of a new tire-road noise measurement device in France. In Symposium on Pavement Surface Characteristics [of Roads and Airports], 5th, 2004, Toronto, Ontario, Canada.

8. Anfosso-Lédée, F., & Brosseaud, Y. (2009). Acoustic monitoring of low noise road pavements. Noise Control Engineering Journal, 57(2), 50-62.

9. Antunes, M. L. (1991). Dynamic analysis of falling weight deflectometer test results. In Session II Proc., Forum of European National Highway Research Laboratories-Falling Weight Deflectometer (FEHRL-FWD) Seminar (pp. 1-10).

10. Arenas, J. P., & Crocker, M. J. (2010). Recent trends in porous sound-absorbing materials. Sound & vibration, 44(7), 12-18.

11. Aspro; Silence in Arizona. Official Journal of the Institute of Asphalt Technology; Institute of Asphalt Technology: Bathgate, UK, 2005.

12. Batayneh, M. K., Marie, I., & Asi, I. (2008). Promoting the use of crumb rubber concrete in developing countries. *Waste management*, *28*(11), 2171-2176.

13. Bathe, K. J. (2006). Finite element procedures. Klaus-Jurgen Bathe.

14. Bendtsen, H. (1998). Drainage asphalt and noise reduction over a long period. Proc. Inter-Noise 98, Munich.

15. Bendtsen, H., & Andersen, B. (2005). Noise-Reducing Pavement for Highways and Urban Roads-State of the Art in Denmark (With Discussion). Journal of the Association of Asphalt Paving Technologists, 74.

16. Bendtsen, H., & Larsen, L. E. (2002, August). Two-layer porous pavements and noise reductions in Denmark. In Ninth International Conference on Asphalt PavementsInternational Society for Asphalt Pavements.

17. Bendtsen, H., & Nielsen, E. (2008). DRI-DWW Thin Layer Project.

18. Bendtsen, H., & Raaberg, J. (2006). French experiences on noise reducing thin layers. Report, Denmark.

19. Bendtsen, H., Lu, Q., & Kohler, E. (2010). Acoustic aging of asphalt pavements: A Californian/Danish comparison (No. UCPRC-RP-2010-01).

20. Bendtsen, H.; Larsen, E. Two-layer porous pavements and noise reductions in Denmark. In Proceedings of the the Inter-Noise, The Hague, The Netherlands, 27–30 August 2001. Inter-Noise, The Hague, The Netherlands, 27–30 August 2001.

21. Bendtsen, H.; Lu, Q.; Kohler, E. Acoustic Aging of Asphalt Pavements: A Californian/Danish Comparison; Report No. UCPRC-RP-2010-0; California Department of Transportation: Berkeley, CA, USA, 2010.

22. Bendtsen, H.; Nielson, E. DRI-DWW Thin Layer Project—Final Report; DRI Report 159; Road Directorate, Danish Road Institute: Copenhagen, Denmark, 2008.

23. Bennett, G., King, E. A., Curn, J., Cahill, V., Bustamante, F., & Rice, H. J. (2010, September). Environmental noise mapping using measurements in transit. In Proceedings of ISMA.

24. Bernhard, J.; Sandberg, U. Tire-Pavement Noise; Where Does It Come from? Report No. 240, TR News; Transportation Research Board: Washington, DC, USA, 2005.

25. Bernhard, R. J., & Sandberg, U. (2005). Tire-Pavement Noise: Where Does It Come From?. Tr News, (240).

26. Bernhard, R., Wayson, R. L., Haddock, J., Neithalath, N., El-Aassar, A., Olek, J., ... & Weiss, W. J. (2005). An introduction to tire/pavement noise of asphalt pavement. Institute of Safe, Quiet and Durable Highways, Purdue University.

27. Bernhard, R.; Wayson, R. An Introduction to Tire-Pavement Noise; Final Research Report SQDH 2005-1; Purdue University: West Lafayette, IN, USA, 2005.

28. Bessa, I. S., Branco, V. T. C., Soares, J. B., & Neto, J. A. N. (2014). Aggregate shape properties and their influence on the behavior of hot-mix asphalt. *Journal of Materials in Civil Engineering*, *27*(7), 04014212.

29. Biligiri, K. P. (2013). Effect of pavement materials' damping properties on tyre/road noise characteristics. Construction and Building Materials, 49, 223-232.

30. Broutin, M., & Theillout, J. N. (2010). Towards a Dynamical Back-Calculation Procedure for HWD; A Full-Scale Validation Experiment. In 2010 FAA Worldwide Airport Technology Transfer ConferenceFederal Aviation AdministrationAmerican Association of Airport Executives.

31. Bucka, M. (2002). Asphalt rubber overlay noise study update. AAAI Report, 1272.

32. Cannone Falchetto, A., Montepara, A., Tebaldi, G., & Marasteanu, M. O. (2012). Microstructural characterization of asphalt mixtures containing recycled asphalt materials. *Journal of Materials in Civil Engineering*, *25*(1), 45-53.

33. Chapuis, R. P., & Gatien, A. (1995). Temperature dependent tensile strength of asphalt mixtures in relation to field cracking data. In Engineering Properties of Asphalt Mixtures and the Relationship to their Performance. ASTM International.

34. Chatti, K., & Kim, T. (2000). Effect of frequency-dependent asphalt concrete Layer moduli on pavement response. In Nondestructive Testing of Pavements and Backcalculation of Moduli: Third Volume. ASTM International.

35. Chatti, K., & Yun, K. K. (1996). SAPSI-M: computer program for analyzing asphalt concrete pavements under moving arbitrary loads. Transportation Research Record, 1539(1), 88-95.

36. Chatti, K., Ji, Y., & Harichandran, R. (2004). Dynamic time domain backcalculation of layer moduli, damping, and thicknesses in flexible pavements. Transportation research record, 1869(1), 106-116.

37. Chatti, K., Lee, H., & El Mohtar, C. (2004). Fatigue life predictions for asphalt concrete subjected to multiple axle loadings. In International Symposium on Heavy Vehicle Weights and Dimensions, 8th, 2004, Muldersdrift, South Africa.

38. Chen, S. S. (1987). The response of multi-layered systems to dynamic surface loads. University of California, Berkeley.

39. Chen, X., & Huang, B. (2008). Evaluation of moisture damage in hot mix asphalt using simple performance and superpave indirect tensile tests. *Construction and Building Materials*, *22*(9), 1950-1962.

40. Cho Y, Liu C, Dossey T, McCullough BF. Asphalt overlay design methods for rigid pavements considering rutting, reflection cracking, and fatigue cracking, Research report 987-9. Center for Transportation Research, Bureau of Engineering Research, The University of Texas at Austin; 1998.

41. Chopra, A. K. (2001). Dynamics of structures: Theory and applications.

42. Clemente, P., & Rinaldis, D. (1998). Protection of a monumental building against traffic-induced vibrations. Soil Dynamics and Earthquake Engineering, 17(5), 289-296.

43. Clough, R. W., & Penzien, J. (1995). Dynamics of Structures. Berkeley: Computers & Structures.

44. Cocurullo, A., Airey, G. D., Collop, A. C., & Sangiorgi, C. (2008, November). Indirect tensile versus two-point bending fatigue testing. In *Proceedings of the Institution of Civil Engineers-Transport* (Vol. 161, No. 4, pp. 207-220). Thomas Telford Ltd.

45. County, S. (1999). Report on the status of rubberized asphalt traffic noise reduction in Sacramento County. Sacramento County and Bollard & Brennan Inc.

46. Cox, T., & d'Antonio, P. (2016). Acoustic absorbers and diffusers: theory, design and application. Crc Press.

47. Crocker, M., Hanson, D., Li, Z., Karjatkar, R., & Vissamraju, K. (2004). Measurement of acoustical and mechanical properties of porous road surfaces and tire and road noise. Transportation Research Record: Journal of the Transportation Research Board, (1891), 16-22.

48. Daniel, E. (2007). Noise and hearing loss: a review. Journal of School Health, 77(5), 225-231.

49. Dare, T.; McDaniel, R.; Shah, A.; Bernhard, R. Hot Mix Asphalt Surface Characteristics Related to Ride, Texture, Friction, Noise and Durability; Report No. MN/RC 2014-07; Minnesota Department of Transportation: Saint Paul, MN, USA, 2014.

50. Dave Cohen and Carlos Matos. Third Year Projects – Rules and Guidelines. Royal Holloway, University of London, 2013.

51. Descornet, G. (1980). Road surface influence on tire/road noise-part II. In Proceedings of Inter-Noise Conference, Florida, December, 1980.

52. Descornet, G., Faure, B., Hamet, J. F., Kestemont, X., Luminari, M., Quaresma, L., & Sandulli, D. (2000). Traffic noise and road surfaces: state of the art. Belgian Road Research Centre, Brussels.

53. Dobry, R., Oweis, I., & Urzua, A. (1976). Simplified procedures for estimating the fundamental period of a soil profile. Bulletin of the Seismological Society of America, 66(4), 1293-1321.

54. Donavan, P. (2005). Reducing traffic noise with quieter pavements. The Journal of the Acoustical Society of America, 118(3), 1885-1885.

55. Donavan, P. R., & Rymer, B. (2003). Assessment of highway pavements for tire/road noise generation (No. 2003-01-1536). SAE Technical Paper.

56. Dondi, G., & Simone, A. (2005). Soluzioni tecniche innovative per la mitigazione del rumore e delle vibrazioni da traffico stradale. In Atti della Conferenza Nazionale sulla politica energetica in Italia.–Università di Bologna–18-19 Aprile.

57. El Ayadi, A., Picoux, B., Lefeuve-Mesgouez, G., Mesgouez, A., & Petit, C. (2012). An improved dynamic model for the study of a flexible pavement. Advances in Engineering Software, 44(1), 44-53.

58. Eslaminia, M., Thirunavukkarasu, S., Guddati, M. N., & Kim, Y. R. (2012). Accelerated pavement performance modeling using layered viscoelastic analysis. In *7th RILEM International Conference on Cracking in Pavements* (pp. 497-506). Springer, Dordrecht.

59. European Asphalt Pavement Association (EAPA). Abatement of Traffic Noise—The Arguments for Asphalt; EAPA: Brussels, Belgium, 2007

60. European Asphalt Pavement Association. (1998). Heavy duty surfaces: the arguments for SMA. EAPA.

61. European Tyre & Rubber Manufacturers' Association (Belgium), 2010a. A Valuable Resource with Growing Potential 2010 edition. Report downloaded from (May 2011).

62. European Tyre and Rubber Manufacturers' Association. (2011). End of life tyres–A valuable resource with growing potential.

63. Faure, B.; Hamet, J.F.; Kestemont, X.; Luminari, M.; Quaresma, L.; Sandulli, D. Traffic Noise and Road Surfaces: State of the Art; Belgian Road Research Centre: Brussels, Belgium, 2000.

64. Feilden, B. (2007). Conservation of historic buildings. Routledge.

65. Foss, K. A. (1956). Coordinates which uncouple the equations of motion of damped linear dynamic systems (No. MIT-TR-25-20). MASSACHUSETTS INST OF TECH CAMBRIDGE AEROELASTIC AND STRUCTURES RESEARCH LAB.

66. Frei, P., Mohler, E., & Röösli, M. (2014). Effect of nocturnal road traffic noise exposure and annoyance on objective and subjective sleep quality. International journal of hygiene and environmental health, 217(2-3), 188-195.

67. Freitas, E. F. (2012). The effect of time on the contribution of asphalt rubber mixtures to noise abatement. Noise Control Engineering Journal, 60(1), 1-8.

68. Fujikawa, T. (2006). Road texture for abating truck tire noise generation. Inter-Noise 2006.

69. Fwa, T., Tan, S., & Guwe, Y. (1999). Laboratory evaluation of clogging potential of porous asphalt mixtures. Transportation Research Record: Journal of the Transportation Research Board, (1681), 43-49.

70. Gardziejczyk, W. (2016). The effect of time on acoustic durability of low noise pavements–The case studies in Poland. Transportation Research Part D: Transport and Environment, 44, 93-104.

71. Goh, S. W., & You, Z. (2011). Mechanical properties of porous asphalt pavement materials with warm mix asphalt and RAP. Journal of Transportation Engineering, 138(1), 90-97.

72. Goh, S. W., Akin, M., You, Z., & Shi, X. (2011). Effect of deicing solutions on the tensile strength of micro-or nano-modified asphalt mixture. Construction and Building Materials, 25(1), 195-200.

73. Goubert, L. (2005). Two-layer porous asphalt: An international survey. DWW Report DWW-2005-023. RWS DWW, Delft, The Netherlands (available for download from www. innovatieprogrammageluid. nl).

74. Grandi, F. (2008). La progettazione di pavimentazioni antivibranti (Doctoral dissertation, alma).

75. HAMET, J. F., & Berengier, M. (1993). ACOUSTICAL CHARACTERISTICS OF POROUS PAVEMENTS: A NEW PHENOMENOLOGICAL MODEL. In INTER-NOISE 93: PEOPLE VERSUS NOISE.

76. Hamet, J. F., & Klein, P. (2004). Road stiffness influence on rolling noise: Parametric study using a rolling tire model.

77. Hanazato, T., Ugai, K., Mori, M., & Sakaguchi, R. (1991). Three-dimensional analysis of traffic-induced ground vibrations. *Journal of geotechnical engineering*, *117*(8), 1133-1151.

78. Hanson, D. I., & James, R. S. (2004). Colorado DOT tire/pavement noise study (No. CDOT-DTD-R-2004-5). Colorado Department of Transportation, Research Branch.

79. Hanson, D. I., Donavon, P., & James, R. (2005). Tire/Pavement Noise Characteristics of HMA Pavements (With Discussion). *Journal of the association of Asphalt Paving Technologists*, *74*.

80. Hanson, D. I., James, R. S., & NeSmith, C. (2004). Tire/pavement noise study (p. 49). The Center.

81. Hanz, A., & Bahia, H. (2013). Asphalt binder contribution to mixture workability and application of asphalt lubricity test to estimate compactability temperatures for warm-mix asphalt. Transportation Research Record: Journal of the Transportation Research Board, (2371), 87-95.

82. Hao, H., Ang, T. C., & Shen, J. (2001). Building vibration to traffic-induced ground motion. Building and Environment, 36(3), 321-336.

83. Harris, C. M., & Crede, C. E. (Eds.). (1961). Shock and Vibration Handbook Vol I Basic Theory and Measurements. McGraw-Hill Book Company Incorporated.

84. Haselbach, L. M. (2009). Potential for clay clogging of pervious concrete under extreme conditions. Journal of Hydrologic Engineering, 15(1), 67-69.

85. Henry, J. J., Abe, H., Kameyama, S., Tamai, A., Kasahara, A., & Saito, K. (2000). Determination of the international friction index (IFI) using the circular texture meter (CTM) and the dynamic friction tester (DFT). In SURF 2000: Fourth

International Symposium on Pavement Surface Characteristics on Roads and AirfieldsWorld Road Association-PIARC.

86. Hochuli, A. S., Sayir, M. B., Poulikakos, L. D., & Partl, M. N. (2001). Measuring the complex modulus of asphalt mixtures by structural wave propagation. *Journal of the Association of Asphalt Paving Technologists*, *70*(1), 6462659.

87. Hopman, P.C., 1996. The visco-elastic multilayer program VEROAD. Heron 41, 71-91.

88. HOUGHTON, J. C. (1994). ROYAL COMMISSION ON ENVIRONMENTAL POLLUTION. EIGHTEENTH REPORT. TRANSPORT AND THE ENVIRONMENT.

89. Huang, Y., Bird, R. N., & Heidrich, O. (2007). A review of the use of recycled solid waste materials in asphalt pavements. *Resources, Conservation and Recycling*, *52*(1), 58-73.

90. Hudson, M. A. R. T. I. N., Idriss, I. M., & Beikae, M. (1994). User's Manual for QUAD4M. Center for Geotechnical Modeling, Department of Civil & Environmental Engineering, University of California, Davis, California, May.

91. Hunaidi, O. (2000). Traffic vibrations in buildings. Institute for Research in Construction, National Research Council of Canada.

92. Hunaidi, O., & Tremblay, M. (1997). Traffic-induced building vibrations in Montréal. Canadian Journal of Civil Engineering, 24(5), 736-753.

93. Idriss, I. M. (1973). Quad-4: A Computer Program for Evaluating the Seismic Response of Soil Structures by Variable Damping Finete Element Procedures. University of California.

94. Imaninasab, R., Bakhshi, B., & Shirini, B. (2016). Rutting performance of rubberized porous asphalt using finite element method (FEM). Construction and Building Materials, 106, 382-391.

95. ISO 13473-1. (1997). Characterization of pavement texture by use of surface profiles–Part 1: Determination of mean profile depth.

96. Kausel, E., Park, J. 2006. Response of Layered Half-Space Obtained Directly in the Time Domain, Part II: SV-P and Three-Dimensional Sources. Bulletin of the Seismological Society of America 96, 1810–1826.

97. Kayhanian, M., Anderson, D., Harvey, J. T., Jones, D., & Muhunthan, B. (2012). Permeability measurement and scan imaging to assess clogging of pervious concrete pavements in parking lots. Journal of Environmental management, 95(1), 114-123.

98. Kim, J., Kim, K., and Sohn, H., 2013. In situ measurement of structural mass, stiffness, and damping using a reaction force actuator and a laser Doppler, vibrometer. Smart Materials and Structures 22, 1-11.

99. Kim, S., Jeong, W., Park, Y., & Lee, S. (2006). Prediction method for tire air-pumping noise using a hybrid technique. The Journal of the Acoustical Society of America, 119(6), 3799-3812.

100. Kök, B. V., & Çolak, H. (2011). Laboratory comparison of the crumb-rubber and SBS modified bitumen and hot mix asphalt. Construction and Building Materials, 25(8), 3204-3212.

101. Kragh, J. (2008). Road Surfacings-Noise reduction time history (No. 161).

102. Kragh, J.; Nielsen, E.; Olesen, E.; Goubert, L.; Vansteenkiste, S.; Visscher, J.; Sandberg, U.; Karlsson, R. Optimization of Thin Asphalt Layers; Project: ERA-NET ROAD, Project No. VV 2009/40520; European National Road Administrations: Brussels, Belgium, 2011.

103. Krivanek, V., Pavkova, A., Togel, M., Jedlicka, J., & Cholava, R. (2016). Cleaning Low-Noise Surfaces as a Basic Condition for Improving Pavement's Acoustic Absorption Capability. Arabian Journal for Science and Engineering, 41(2), 425-431.

104. Kroger, M., Lindner, M., & Popp, K. (2004, August). Influence of friction on noise and vibrations of tyres. In INTER-NOISE and NOISE-CON Congress and Conference Proceedings(Vol. 2004, No. 6, pp. 1457-1464). Institute of Noise Control Engineering.

105. Kweon, G., & Kim, Y. (2006). Determination of asphalt concrete complex modulus with impact resonance test. Transportation Research Record: Journal of the Transportation Research Board, (1970), 151-160.

106. Kwok, A. O., Stewart, J. P., Hashash, Y. M., Matasovic, N., Pyke, R., Wang, Z., & Yang, Z. (2007). Use of exact solutions of wave propagation problems to guide implementation of nonlinear seismic ground response analysis procedures. Journal of Geotechnical and Geoenvironmental Engineering, 133(11), 1385-1398.

107. Lee, H. S. (2013). Development of a New Solution for Viscoelastic Wave Propagation of Pavement Structures and Its Use in Dynamic Backcalculation. Michigan State University. Civil Engineering.

108. Lee, S. J., Akisetty, C. K., & Amirkhanian, S. N. (2008). The effect of crumb rubber modifier (CRM) on the performance properties of rubberized binders in HMA pavements. Construction and Building Materials, 22(7), 1368-1376.

109. Lesieutre, G. A., and Mingori, D. L., 1990. Finite element modelling of frequency dependent material proper-ties using augmented thermodynamic fields. Control and Dynamics 13, 1040–1050.

110. Liang, F., Chen, H., & Huang, M. (2017). Accuracy of three-dimensional seismic ground response analysis in time domain using nonlinear numerical simulations. Earthquake Engineering and Engineering Vibration, 16(3), 487-498.

111. Licitra, G., Teti, L., & Cerchiai, M. (2014). A modified Close Proximity method to evaluate the time trends of road pavements acoustical performances. Applied Acoustics, 76, 169-179.

112. LING, C., & NEWCOMB, E. (1991). Comparison of dynamic and static back calculation module for three-layer pavements.

113. Liu, W. (2008). Experimental and analytical estimation of damping in beams and plates with damping treatments (Doctoral dissertation, University of Kansas).

114. Liu, Y., Han, S., Zhang, Z., & Xu, O. (2012). Design and evaluation of gap-graded asphalt rubber mixtures. Materials & Design, 35, 873-877.

115.   Londhe, N., Rao, M. D., & Blough, J. R. (2009). Application of the ISO 13472-1 in situ technique for measuring the acoustic absorption coefficient of grass and artificial turf surfaces. Applied Acoustics, 70(1), 129-141.

116.   Losa, M., & Leandri, P. (2012). A comprehensive model to predict acoustic absorption factor of porous mixes. Materials and structures, 45(6), 923-940.

117.   Losa, M., Leandri, P., & Bacci, R. (2010). Empirical rolling noise prediction models based on pavement surface characteristics. Road Materials and Pavement Design, 11(sup1), 487-506.

118.   Losa, M., Leandri, P., & Rocchio, P. (2012). Crumb Rubber Modified Asphalt Concrete for Low Noise Surfaces. In Asphalt Rubber Conference, Munich. Retrieved from http://www. ra-foundation. org/crumb-rubber-modified-asphalt-concrete-for-low-noise-surfaces

119.   Lu, Q., & Harvey, J. (2011). Laboratory evaluation of open-graded asphalt mixes with small aggregates and various binders and additives. Transportation Research Record: Journal of the Transportation Research Board, (2209), 61-69.

120.   Magnuson, A. H. (1988). computer analysis of falling-weight deflectometer data, part I: vertical displacement computations on the surface of a uniform (one-layer) half-space due to an oscillating surface pressure distribution. Final report (no. fhwa/tx-88/1215-1f).

121.   McDaniel, R., Shah, A., Dare, T., & Bernhard, R. (2014). Hot mix asphalt surface characteristics related to ride, texture, friction, noise and durability. Final Rep, (2014-07).

122.   McTavish, D. J., and Hughes, P. C., 1993. Modeling of linear viscoelastic space structures. Transactions of ASME, Journal of Vibration and Acoustics 115, 103–110.

123.   Meier, R.W., Alexander, D.R., Freeman, R.B., 1997. Using artificial neural networks as a forward approach to back calculation. Transportation Research Record 1570, 126-133.

124. Michalak, C.H. and Scullion, T., 1995. MODULUS 5.0: user's manual, Research Report 1987-1 of Texas Transportation Institute. College Station, Texas.

125. Miljković, M., Radenberg, M., & Gottaut, C. (2013). Characterization of noise-reducing capacity of pavement by means of surface texture parameters. Journal of Materials in Civil Engineering, 26(2), 240-249.

126. Miller, G.F and Pursey, H., 1954. The field and radiation impedance of mechanical radiators on the free surface of a semi-infinite isotropic solid. Proceedings of the Royal Society A 223, 521-541. 198

127. Miller, J. D. (1974). Effects of noise on people. *The Journal of the Acoustical Society of America*, *56*(3), 729-764.

128. Milne, G. (2006). Your Home Technical Manual 2.7 Noise Control, Department of Climate Change and Energy Efficiency, Australia.

129. Milne, G., & Reardon, C. (2007). Your Home Technical Manual–3.1 Embodied Energy.

130. Mo, L.T., Huurman, M., Wu, S.P., Molenaar, A.A.A., 2008. 2D and 3D mesoscale finite element models for raveling analysis of porous asphalt concrete. Finite Elements in Analysis and Design 44, 186–196.

131. Morgan, P. (Ed.). (2006). Guidance manual for the implementation of low-noise road surfaces. benefits, 769, 66.

132. Morgan, P. A. (2008). IPG Research Report-Innovative mitigation measures for road traffic noise. DVS Project Report DVS-2008-018, Centre for Transport and Navigation of Rijkswaterstaat, Delft.

133. Morgan, P. A., & Watts, G. R. (2003). A novel approach to the acoustic characterisation of porous road surfaces. Applied Acoustics, 64(12), 1171-1186.

134. Motamed, A., Bhasin, A., and Liechti, K. M., 2013. Constitutive modelling of the nonlinearly viscoelastic response of asphalt binders; incorporating three dimensional effects. Mechanics of Time-Dependent Materials, 17, 83–109. Nazarian,S., Stokoe, K.H., Briggs, R.C., 1987. Non-destructively delineating changes in modulus profiles of secondary roads, Transportation Research Record:

Journal of the Transportation Research Board 1136, 96-107. Nocedal, J. and Wright, S.J., 2006. Numerical Optimization, second edition, Springer-Verlag.

135. Nilsson, N. A. (1982, May). Principles in the control of external tire/road noise. In INTER-NOISE and NOISE-CON Congress and Conference Proceedings (Vol. 1982, No. 2, pp. 123-126). Institute of Noise Control Engineering.

136. Nilsson, N. A., Bennerhult, O., & Soderqvist, S. (1980). External tire/road noise: its generation and reduction. In Proceedings of the International Conference Noise Control Engineering, Noise Control for the 80's, Inter-Noise 80, Vol. 1, Miami, Florida, December 8-10, 1980..

137. Ohiduzzaman, M. D., Sirin, O., Kassem, E., & Rochat, J. L. (2016). State-of-the-art review on sustainable design and construction of quieter pavements—Part 1: traffic noise measurement and abatement techniques. Sustainability, 8(8), 742.

138. Omez-Ramirez, F., and Thompson, M. R., 2001. Characterizing Aircraft Multiple Wheel Load Interaction for Airport Flexible Pavement Design. University of Illinois at Urbana-Champaign, IL.

139. Ongel, A., Kohler, E., & Nelson, J. (2007). Acoustical absorption of open-graded, gap-graded, and dense-graded asphalt pavements. *Report prepared for the Caltrans (California Department of Transportation)*.

140. Ongel, A., Kohler, E., Lu, Q., & Harvey, J. (2008). Comparison of surface characteristics and pavement/tire noise of various thin asphalt overlays. Road Materials and Pavement Design, 9(2), 333-344.

141. Oppenheim, A.V. and Schafer, R.W., 1975. Digital Signal Processing. PrenticeHall, Inc., Englewood Cliffs, New Jersey.

142. Pacheco, J. E. L., Bavastri, C. A., & Pereira, J. T. (2015). Viscoelastic relaxation modulus characterization using Prony series. Latin American Journal of Solids and Structures, 12(2), 420-445.

143. Paje, S. E., Bueno, M., Terán, F., Miró, R., Pérez-Jiménez, F., & Martínez, A. H. (2010). Acoustic field evaluation of asphalt mixtures with crumb rubber. Applied Acoustics, 71(6), 578-582.

144.	Paje, S. E., Luong, J., Vázquez, V. F., Bueno, M., & Miro, R. (2013). Road pavement rehabilitation using a binder with a high content of crumb rubber: Influence on noise reduction. *Construction and building materials*, *47*, 789-798.

145.	Pan, E., Han. F., 2005. Green's functions for transversely isotropic piezoelectric functionally graded multilayered half spaces. International Journal of Solids and Structures 42, 3207-3233.

146.	Park, D., & Hashash, Y. M. (2004). Soil damping formulation in nonlinear time domain site response analysis. Journal of Earthquake Engineering, 8(02), 249-274.

147.	Park, S. W., & Schapery, R. A. (1999). Methods of interconversion between linear viscoelastic material functions. Part I—A numerical method based on Prony series. International Journal of Solids and Structures, 36(11), 1653-1675.

148.	Park, S. W., Kim, Y. R., & Schapery, R. A. (1996). A viscoelastic continuum damage model and its application to uniaxial behavior of asphalt concrete. Mechanics of Materials, 24(4), 241-255.

149.	Park, S.W., Schapery, R.A., 1999, Methods of interconversion between linear viscoelastic material functions. Part I—a numerical method based on Prony series, International Journal of Solids and Structures 36, 1653-1675.

150.	Paulo, J. P., Coelho, J. B., & Figueiredo, M. A. (2010). Statistical classification of road pavements using near field vehicle rolling noise measurements. The Journal of the Acoustical Society of America, 128(4), 1747-1754.

151.	Pellinen, T.K., 2001. Investigation of the Use of Dynamic Modulus as Indicator of Hot-Mix Asphalt Performance. Ph.D. Dissertation, Arizona State University.

152.	Plotkin, K. J., Montroll, M. L., & Fuller, W. R. (1980). Generation of Tire Noise by Air Pumping and Carcass Vibration. In Proceedings of the International Conference Noise Control Engineering, Noise Control for the 80's, Inter-Noise 80, Vol. 1, Miami, Florida, December 8-10, 1980..

153.	Praticò, F. G., Fedele, R., & Vizzari, D. (2017). Significance and reliability of absorption spectra of quiet pavements. Construction and Building Materials, 140, 274-281.

154. Praticò, F. G., Vaiana, R., & Fedele, R. (2015). A study on the dependence of PEMs acoustic properties on incidence angle. International Journal of Pavement Engineering, 16(7), 632-645.

155. Presti, D. L. (2013). Recycled tyre rubber modified bitumens for road asphalt mixtures: a literature review. *Construction and Building Materials*, *49*, 863-881.

156. Puthanpurayil, A. M., Dhakal, R. P., & Carr, A. J. (2011, April). Modelling of In-Structure Damping: A Review of the State-of-the-art. In Proc. Ninth Pacific Conf. Earthquake Engineering,[Online]. Paper (No. 091).

157. Ranieri, V. (2005). The Development in the use of Porous Asphalts in Europe. In Proceedings of the XV SIIV Congress. Palermo: SIIV.

158. Rasband, W. S. (1997). ImageJ software. National Institutes of Health: Bethesda, MD, USA, 2012.

159. Rasmussen, R.; Bernhard, R.; Sandberg, U.; Mun, E. The Little Book of Quieter Pavements; Report No. FHWA-IF-08-004; Federal Highway Administration: Washington, DC, USA, 2007.

160. Ray, L. R. (1997). Nonlinear tire force estimation and road friction identification: Simulation and experiments1, 2. *Automatica*, *33*(10), 1819-1833.

161. Rayleigh, J. W. S., & Lindsay, R. B. (1945). The theory of Sound,(1945).

162. Region, Tuscany. "LEOPOLDO" project." il controllo delle pavimentazioni stradali per la viabilita ordinaria. URL: http://Ieopoldo. pj xp. com.

163. Ripke, O., Andersen, B., Bendtsen, H., & Sandberg, U. (2005). Report of promising new road surfaces for testing.

164. RMA – Rubber Manufacturers Association (USA), 2009. Scrap Tire Markets in the United States 9th Biennial Report

165. Roesset, J. M. (1987). Computer program UTFWIBM. University of Texas, Austin, TX.

166. Royal Commission. (1994). Royal Commission on Environmental Pollution, Eighteenth Report: Transport and the Environment.

167. Ruhala, R. J. (1999). A study of tire/pavement interaction noise using near-field acoustical holography.

168. Rutherford, T., Wang, Z., Shu, X., Huang, B., & Clarke, D. (2014). Laboratory investigation into mechanical properties of cement emulsified asphalt mortar. Construction and Building Materials, 65, 76-83.

169. Sandberg U., Ejsmont J.A., Tyre/road noise reference book, Kisa, Sweden, Informex, 2002

170. Sandberg, U. (1987). Noise and the road: Is there a conflict between requirements for safety and noise?. Statens Väg-och Trafikinstitut. VTI särtryck 120.

171. Sandberg, U. (2001). Noise emissions of road vehicles effect of regulations: Final Report 01-1. Noise News International, 9(3), 147-203.

172. Sandberg, U. (2009). The global experience in using low-noise road surfaces: A benchmark report. Hong Kong Environmental Protection Department, Hong Kong.

173. Sandberg, U. The Global Experience in Using Low-Noise Road Surfaces: A Benchmark Report; Report Made in Response to 'Hong Kong Environmental Protection Department' Project No. AN 06-004; Hong Kong Environmental Protection Department: Hong Kong, China, 2009

174. Sandberg, U. Tire-road noise-myths and realities. In Proceedings of the Inter-Noise, The Hague, The Netherlands, 27–30 August 2001.

175. Sandberg, U., & Descornet, G. (1980). Road surface influence on tire/road noise.

176. Sandberg, U., & Ejsmont, J. (2002). Tyre/Road Noise Sources and Generation Mechanisms. Tire/Road Noise Reference Book.

177. Sandberg, U., & Gucbert, L. (2011, July). Pooelastic road surface (PERS): A review of 30 years of R and D work. In Inter-noise and Noise-con Congress and

Conference Proceedings (Vol. 2011, No. 4, pp. 3014-3021). Institute of Noise Control Engineering.

178.   Sandberg, U., & Mioduszewski, P. (2015). Reduction of noise and rolling resistance by horizontal grinding of asphalt pavements. In 44th International Congress and Exposition on Noise Control Engineering, INTER-NOISE 2015, 9 August 2015 through 12 August 2015. The Institute of Noise Control Engineering of the USA, Inc..

179.   Sandberg, U., Kragh, J., Goubert, L., Bendtsen, H., Bergiers, A., Biligiri, K. P., ... & Vansteenkiste, S. (2011). Optimization of thin asphalt layers. ERA-NET ROAD Project, Swedish National Road and Transport Research Institute (VTI), Danish Road Institute (DRI) and Belgian Road Research Centre (BRRC), 30.

180.   Sandberg, U.; Ejsmont, J. Tire-Road Noise Reference Book; Informex: Kisa, Sweden, 2002

181.   Sandberg, U.; Goubert, L. Poroelastic Road Surface (PERS): A review of 30 years of R&D work. In Proceedings of the Inter-Noise 2011, Osaka, Japan, 4–7 September 2011.

182.   Sandberg, U.; Kragh, J.; Goubert, L.; Bendtsen, H.; Bergiers, A.; Biligiri, K.; Karlsson, R.; Nielsen, E.; Olesen, E.; Vansteenkiste, S. Optimization of Thin Asphalt Layers—State of the Art Review; Project: ERA-NET ROAD; European National Road Administrations: Brussels, Belgium, 2011.

183.   Sangiorgi, C., Tataranni, P., Simone, A., Vignali, V., Lantieri, C., & Dondi, G. (2018). Stone mastic asphalt (SMA) with crumb rubber according to a new dry-hybrid technology: A laboratory and trial field evaluation. *Construction and Building Materials*, *182*, 200-209.

184.   Schapery, R. A. (1961). Two simple approximate methods of Laplace transform inversion for viscoelastic stress analysis.

185.   Schubert, S., Gsell, D., Steiger, R., & Feltrin, G. (2010). Influence of asphalt pavement on damping ratio and resonance frequencies of timber bridges. Engineering Structures, 32(10), 3122-3129.

186. Sefidmazgi, N. R. (2011). Defining effective aggregate skeleton in asphalt mixture using digital imaging. University oF Wisconsin.

187. Sefidmazgi, N. R., Tashman, L., & Bahia, H. (2012). Internal structure characterization of asphalt mixtures for rutting performance using imaging analysis. Road materials and pavement design, 13(sup1), 21-37.

188. Sezen, H., & Fisco, N. (2013). Evaluation and comparison of surface macrotexture and friction measurement methods. Journal of Civil Engineering and Management, 19(3), 387-399.

189. Siddharthan, R. V., Sebaaly, P. E., El-Desouky, M., Strand, D., & Huft, D. (2005). Heavy off-road vehicle tire-pavement interactions and response. *Journal of Transportation Engineering*, *131*(3), 239-247.

190. Siddharthan, R. V., Yao, J., & Sebaaly, P. E. (1998). Pavement strain from moving dynamic 3D load distribution. Journal of Transportation Engineering, 124(6), 557-566.

191. Sienkiewicz, M., Kucinska-Lipka, J., Janik, H., & Balas, A. (2012). Progress in used tyres management in the European Union: a review. Waste Management, 32(10), 1742-1751.

192. Sotil, A., Kaloush, K. E., Biligiri, K., & Golden, J. (2006). Dynamic Complex Modulus (E*) Test as Potential Indicator for Asphalt Mixture Tire-Road Noise Characteristics (No. 06-3088).

193. Soto, F. M., & Di Mino, G. (2017). Procedure for a Temperature-Traffic Model on Rubberized Asphalt Layers for Roads and Railways. Journal of Traffic and Transportation Engineering, 5(4), 171-202.

194. Subhy, A., Airey, G., & Presti, D. L. (2017). An investigation of the mechanical properties of rubber modified asphalt mixtures using a modified dry process. In Conference proceedings BCRRA.

195. Sun, L., & Duan, Y. (2013). Dynamic response of top-down cracked asphalt concrete pavement under a half-sinusoidal impact load. Acta Mechanica, 224(8), 1865-1877.

196.   Tan, S. A., Fwa, T. F., & Guwe, V. Y. (2000). Laboratory measurements and analysis of clogging mechanism of porous asphalt mixes. *Journal of testing and evaluation*, *28*(3), 207-216.

197.   Tang, X. C., Stoffels, S. M., & Palomino, A. M. (2013). Evaluation of pavement layer moduli using instrumentation measurements. *International Journal of Pavement Research and Technology*, *6*(6), 755-764.

198.   TANIGUCHI, E., & Sawada, K. (1979). Attenuation with distance of traffic-induced vibrations. *Soils and foundations*, *19*(2), 15-28.

199.   Tehrani, F. (2014). Noise abatement of hot mix asphalt: A brief review. Int. J. Pavement Res. Technol, 8, 58-61.

200.   Thomsen, S.; Bendtsen, H.; Andersen, B. Optimized Thin Layers—Urban Roads, the Kastrupvej Experiment; Technical Note 66; Road Directorate, Danish Road Institute: Copenhagen, Denmark, 2008

201.   Trevino, M., & Dossey, T. (2009). On-board sound intensity testing of PFC pavements in Texas. *Noise Control Engineering Journal*, *57*(2), 94-103.

202.   Tschoegl, N. W. (1989). Representation of linear viscoelastic behavior by mathematical models. In The Phenomenological Theory of Linear Viscoelastic Behavior (pp. 314-364). Springer, Berlin, Heidelberg.

203.   Turner, J., & Pretlove, A. J. (1991). Acoustics for engineers. Macmillan International Higher Education.

204.   Uddin, W., & Garza, S. (2010). 3D-FE simulation study of structural response analysis for pavement-subgrade systems subjected to dynamic loads. In Pavements and Materials: Testing and Modeling in Multiple Length Scales (pp. 170-181).

205.   Valtanen, J., Hyyppä, I., & Sainio, P. (2002, August). Noise reduction vs wearing properties. In Ninth International Conference on Asphalt PavementsInternational Society for Asphalt Pavements.

206.   Van Poel, C. D. (1954). A general system describing the visco‑elastic properties of bitumens and its relation to routine test data. Journal of applied chemistry, 4(5), 221-236.

207.   Vázquez, V. F., Luong, J., Bueno, M., Terán, F., & Paje, S. E. (2016). Assessment of an action against environmental noise: Acoustic durability of a pavement surface with crumb rubber. *Science of the Total Environment*, *542*, 223-230.

208.   Venturini, Loretta & Giannattasio, Federica & Sangalli, Lorenzo. (2016). Anti-vibration pavement: Case of study Novara municipality. 10.14311/EE.2016.417.

209.   Vuye, C., Bergiers, A., & Vanhooreweder, B. (2016). The acoustical durability of thin noise reducing asphalt layers. Coatings, 6(2), 21.

210.   Wallman, C. G., & Åström, H. (2001). Friction measurement methods and the correlation between road friction and traffic safety: A literature review. Statens väg- och transportforskningsinstitut.

211.   Wang, B., & Yang, J. (2009). Analysis of the Dynamic Responses of CRCP and CRCP+ AC under the Vehicle Loading by FEM. Pavements and Materials: 131-139.

212.   Wang, J. C., Zeng, X., & Mullen, R. L. (2005). Three-dimensional finite element simulations of ground vibration generated by high-speed trains and engineering countermeasures. Modal Analysis, 11(12), 1437-1453.

213.   Wang, J., & Zeng, X. (2004). Numerical simulations of vibration attenuation of high-speed train foundations with varied trackbed underlayment materials. Modal Analysis, 10(8), 1123-1136.

214.   Wang, J., Zeng, X., & Gasparini, D. A. (2008). Dynamic response of high-speed rail foundations using linear hysteretic damping and frequency domain substructuring. Soil Dynamics and Earthquake Engineering, 28(4), 258-276.

215.   Wang, W., & Höeg, K. (2010). Cyclic behavior of asphalt concrete used as impervious core in embankment dams. Journal of Geotechnical and Geoenvironmental Engineering, 137(5), 536-544.

216.   Wang, Z. Y., Mei, G. X., & Yu, X. B. (2011). Dynamic shear modulus and damping ratio of waste granular rubber and cement soil mixtures. In Advanced Materials Research (Vol. 243, pp. 2091-2094). Trans Tech Publications.

217. Watson, D. E., & Heitzman, M. (2014). *Thin asphalt concrete overlays* (No. Project 20-05, Topic 44-07).

218. Wilcox, D., Dove, B., McDavid, D., & Greer, D. (2002). Image tool for Windows, version 3.0. The University of Texas, Health Science Center in San Antonio, Texas. USA.

219. Wozniak, R. (2001). Measurement of tyre/road noise in longitudinal slip conditions. In INTER-NOISE 2001-ABSTRACTS FROM INTERNATIONAL CONGRESS AND EXHIBITION ON NOISE CONTROL ENGINEERING.

220. Wozniak, R., & Taryma, S. (2004, August). Investigations in tyre/road noise in longitudinal slip conditions. In INTER-NOISE and NOISE-CON Congress and Conference Proceedings (Vol. 2004, No. 5, pp. 2300-2307). Institute of Noise Control Engineering.

221. Xiao, F., Amirkhanian, S., & Juang, C. H. (2007). Rutting resistance of rubberized asphalt concrete pavements containing reclaimed asphalt pavement mixtures. *Journal of Materials in Civil Engineering*, *19*(6), 475-483.

222. Xu, Q. (2014). Development of a computational method for inverting dynamic moduli of multilayer systems with applications to flexible pavements (Doctoral dissertation).

223. Ye, Q., Wu, S., & Li, N. (2009). Investigation of the dynamic and fatigue properties of fiber-modified asphalt mixtures. International Journal of Fatigue, 31(10), 1598-1602.

224. Yoo, P., & Al-Qadi, I. (2007). Effect of transient dynamic loading on flexible pavements. Transportation Research Record: Journal of the Transportation Research Board, (1990), 129-140.

225. Zelelew, H. M., Papagiannakis, A. T., & Masad, E. (2008, October). Application of digital image processing techniques for asphalt concrete mixture images. In The 12th International Conference of International Association for Computer Methods and Advances in Geomechanics (IACMAG) (pp. 119-24).

226. Zeng, X.(2005). Rubber-Modified asphalt concrete for high-speed railway roadbeds. Department of Civil Engineering, Case Western Reserve University.

227. Zeng, X., Rose, J. G., & Rice, J. S. (2001). Stiffness and damping ratio of rubber-modified asphalt mixes: Potential vibration attenuation for high-speed railway trackbeds. Journal of Vibration and Control, 7(4), 527-538.

228. Zhong, X. G., Zeng, X., & Rose, J. G. (2002). Shear modulus and damping ratio of rubber-modified asphalt mixes and unsaturated subgrade soils. Journal of Materials in Civil Engineering, 14(6), 496-502.

Appendix I: A_{RMS} results of Point A, C, E

Note:

*a "thickness10mm_distancetotop0cm_0.02" means:

1. The thickness of the damping layer is 10 mm.

2. The damping layer is layered 0 cm to the top.

3. The damping ratio of the material used in the damping layer is 0.02, similarly hereinafter.

*b "A$_{RMS}$" means the root-mean-square accelerations.

Conditions	A$_{RMS}$[b] of Point A [dm/s^2]	A$_{RMS}$ of Point B[dm/s^2]	A$_{RMS}$ of Point C[dm/s^2]
thickness10mm_distancetotop0cm_0.02[a]	22.27314556	1.14324267	0.106797689
thickness10mm_distancetotop0cm_0.05	22.15968956	1.129253244	0.105728304
thickness10mm_distancetotop0cm_0.1	22.0183615	1.106465705	0.103991421
thickness10mm_distancetotop0cm_0.15	21.90756855	1.084315859	0.102296078
thickness10mm_distancetotop0cm_0.2	21.81272223	1.062785252	0.100649397
thickness10mm_distancetotop10cm_0.02	23.40297712	1.162127011	0.109567995
thickness10mm_distancetotop10cm_0.05	23.35213692	1.14806958	0.108477508
thickness10mm_distancetotop10cm_0.1	23.26854681	1.125168186	0.106703173
thickness10mm_distancetotop10cm_0.15	23.18690909	1.102915232	0.10496944
thickness10mm_distancetotop10cm_0.2	23.10726646	1.081276103	0.103289663
thickness10mm_distancetotop15cm_0.02	23.05391815	1.161682764	0.109900482
thickness10mm_distancetotop15cm_0.05	23.00564753	1.147628532	0.108806231
thickness10mm_distancetotop15cm_0.1	22.8173461	1.124750421	0.10702987
thickness10mm_distancetotop15cm_0.15	22.74024072	1.102508404	0.105301053
thickness10mm_distancetotop15cm_0.2	22.66371567	1.080883491	0.103612857
thickness10mm_distancetotop20cm_0.02	23.05391815	1.162108784	0.110174513

thickness10mm_distancetotop20cm_0.05	23.00564753	1.147923699	0.109079267
thickness10mm_distancetotop20cm_0.1	22.92653867	1.124825174	0.107321749
thickness10mm_distancetotop20cm_0.15	22.84901668	1.1022525	0.105576897
thickness10mm_distancetotop20cm_0.2	22.7729988	1.080442018	0.103847601
thickness10mm_distancetotop5cm_0.02	23.26498523	1.163600258	0.109182591
thickness10mm_distancetotop5cm_0.05	23.21387814	1.149409748	0.108089029
thickness10mm_distancetotop5cm_0.1	23.12887675	1.126289909	0.106301652
thickness10mm_distancetotop5cm_0.15	23.04499563	1.103826379	0.104563234
thickness10mm_distancetotop5cm_0.2	22.96282079	1.081991353	0.102877442
thickness20mm_distancetotop0cm_0.02	22.95735501	1.161808406	0.106395136
thickness20mm_distancetotop0cm_0.05	22.74525598	1.13298983	0.104242009
thickness20mm_distancetotop0cm_0.1	22.47062392	1.087122944	0.100818029
thickness20mm_distancetotop0cm_0.15	22.25094809	1.04377457	0.097582302
thickness20mm_distancetotop0cm_0.2	22.08601836	1.002764362	0.094519861
thickness20mm_distancetotop10cm_0.02	23.56974258	1.153648759	0.10822863
thickness20mm_distancetotop10cm_0.05	23.46770986	1.126226955	0.10611072
thickness20mm_distancetotop10cm_0.1	23.30357186	1.082540314	0.102723939
thickness20mm_distancetotop10cm_0.15	23.14641525	1.041224777	0.09952563
thickness20mm_distancetotop10cm_0.2	22.99580375	1.002097113	0.096481346
thickness20mm_distancetotop15cm_0.02	23.25307636	1.152814067	0.108870373
thickness20mm_distancetotop15cm_0.05	23.15686144	1.125408274	0.106743124
thickness20mm_distancetotop15cm_0.1	23.00144734	1.081751888	0.103345779
thickness20mm_distancetotop15cm_0.15	22.85202328	1.040460549	0.100128526

thickness20mm_distancetotop15cm_0.2	22.70796339	1.001359701	0.097074653
thickness20mm_distancetotop20cm_0.02	22.89855586	1.153683277	0.109419283
thickness20mm_distancetotop20cm_0.05	22.80386668	1.125887945	0.107268833
thickness20mm_distancetotop20cm_0.1	22.65077769	1.081624322	0.103829477
thickness20mm_distancetotop20cm_0.15	22.50304725	1.039776915	0.100572307
thickness20mm_distancetotop20cm_0.2	22.36016076	1.000155987	0.097475414
thickness20mm_distancetotop5cm_0.02	23.40467306	1.156412493	0.107463384
thickness20mm_distancetotop5cm_0.05	23.29463821	1.128608971	0.105335982
thickness20mm_distancetotop5cm_0.1	23.11812893	1.084329718	0.101948252
thickness20mm_distancetotop5cm_0.15	22.949972	1.042458879	0.098743206
thickness20mm_distancetotop5cm_0.2	22.78935118	1.00281705	0.095702475
thickness30mm_distancetotop0cm_0.02	22.82579677	1.156875367	0.104127275
thickness30mm_distancetotop0cm_0.05	22.57478092	1.114030738	0.100991219
thickness30mm_distancetotop0cm_0.1	22.22962463	1.047343999	0.096121109
thickness30mm_distancetotop0cm_0.15	21.93962961	0.985990355	0.091647294
thickness30mm_distancetotop0cm_0.2	21.68318157	0.929408003	0.08754129
thickness30mm_distancetotop10cm_0.02	23.70676596	1.145128122	0.106904962
thickness30mm_distancetotop10cm_0.05	23.55549545	1.105013699	0.103819455
thickness30mm_distancetotop10cm_0.1	23.31600012	1.042481955	0.098994036
thickness30mm_distancetotop10cm_0.15	23.09055047	0.984838398	0.094545818
thickness30mm_distancetotop10cm_0.2	22.8772035	0.931571247	0.090428395
thickness30mm_distancetotop15cm_0.02	23.23133125	1.143981123	0.107847943
thickness30mm_distancetotop15cm_0.05	23.09068734	1.10389305	0.104740789

thickness30mm_distancetotop15cm_0.1	22.86671349	1.041390434	0.099881529
thickness30mm_distancetotop15cm_0.15	22.6541196	0.983780102	0.095390864
thickness30mm_distancetotop15cm_0.2	22.45150562	0.930537129	0.091225432
thickness30mm_distancetotop20cm_0.02	22.74591821	1.145372236	0.108671223
thickness30mm_distancetotop20cm_0.05	22.60672446	1.104510088	0.105503771
thickness30mm_distancetotop20cm_0.1	22.38443033	1.040840648	0.10055326
thickness30mm_distancetotop20cm_0.15	22.17282022	0.982199866	0.095976406
thickness30mm_distancetotop20cm_0.2	21.97066788	0.92805598	0.091727038
thickness30mm_distancetotop5cm_0.02	23.57878973	1.149097975	0.105770658
thickness30mm_distancetotop5cm_0.05	23.40850462	1.108277994	0.102675685
thickness30mm_distancetotop5cm_0.1	23.141178	1.044661127	0.097855304
thickness30mm_distancetotop5cm_0.15	22.89209883	0.986048447	0.093412391
thickness30mm_distancetotop5cm_0.2	22.65876	0.931905595	0.089311331

AAA